Electrical characterization of ion-beam induced damage in GaN

by

Phuti Ngako Mahloka Ngoepe

Submitted in partial fulfilment of the requirements for the degree

PhD (Physics)

in the Department of Physics

in the Faculty of Natural and Agricultural Science

University of Pretoria

PRETORIA

February 2019

Supervisor: Prof. W.E. Meyer

Co-supervisor: Prof. M. Diale

I, **Phuti Ngako Mahloka Ngoepe**, declare that the thesis/dissertation, which I hereby submit for the degree Philosophiae Doctor at the University of Pretoria, is my own work and has not previously been submitted by me for a degree at this or any other tertiary institution.

SIGNATURE:..……………………………....

DATE:…….………………………………......

Electrical characterization of ion-beam induced damage in GaN

by

Phuti Ngako Mahloka Ngoepe

Submitted in partial fulfilment of the requirement for the degree PHILOSOPHIAE DOCTOR in the Faculty of Natural and Agricultural Science, Department of Physics, University of Pretoria.

Supervisor: Prof. W. E. Meyer

Co-supervisor: Prof. M. Diale

SUMMARY

Ions with different energies have been used to modify the properties of semiconductors. In particular, these modifications have included altering the electrical properties of semiconductors. The ion-solid interactions during ion irradiation can induce electrically active defects in these materials. These defects can be beneficial or detrimental to the device, depending on the use of the device.

In this study, deep level transient spectroscopy (DLTS) was used to study electrically active defects in gallium nitride (GaN) after various ion-processing methods. These ion bombardment processes included ion implantation and irradiation. Low, medium, and high energy ions were used during these procedures. (In this study, ion implantation implies medium energy ion bombardment while ion irradiation implies high energy ion bombardment.)

Electron beam exposure (EBE) is a method that was used for exposing GaN to low ion energy conditions. In this method, GaN was exposed to metal evaporation conditions without evaporating the metal. In the second case GaN was exposed to 360 keV Cs ion implantation. Lastly, Xe ions with energy 167 MeV were irradiated onto GaN.

Different species of defects were observed in each case. Only one defect was observed in the EBE study and had an activation energy of 0.12 eV. This defect is similar to defects obtained in other studies, which used different irradiation methods, such as electron, proton and gamma irradiation. The Cs ion implantation yielded a defect with activation energy of

0.19 eV. A comparison was made to defects obtained using other processing techniques, which included electron beam deposition and various ion implantations. Lastly, Xe irradiation yielded two defects with activation energies of 0.07 and 0.48 eV. Both these defects were also compared with those obtained in other studies. The former was similar to a defect predicted by modelling while the latter was similar to a defect obtained by In doping.

It was found that all the processing techniques used in this study induced electrically active defects as measured by DLTS. It was found that the defects measured in this study had similar characteristics to those found in other studies, whereby different processing methods were used. It is therefore deduced that the defects are not related to the ion, but rather are intrinsic defects or defects related to impurities in the GaN. This shows that different energies of ions lead to different defects forming in GaN. This understanding will contribute to improved quality and reliability of devices fabricated on GaN in applications ranging from radiation detection to communications.

Keywords: deep level transient spectroscopy (DLTS), gallium nitride (GaN), swift heavy ion (SHI) irradiation, ion-beam induced damage, ion implantation

ACKNOWLEDGEMENTS

I would like to express my deep appreciation to the following:

- God the Father, the Son and the Holy Spirit for creating a reality to live in and a purpose for life.
- My supervisor Prof. Walter Meyer for the faith he has in me.
- My co-supervisor Prof. Mmantsae Diale for always pushing me to finish this project.
- Prof. Danie Auret for the good example that he sets with his hard work and incisive inputs.
- Staff of the physics department and members of the semiconductor group including Mr. Matshisa Legodi, Mr. Johan Janse van Rensburg, and Dr. Jackie Nel. Also included are Prof. Thulani Hlatshwayo and the physics head of department Prof. Chris Theron.
- My fellow colleagues Dr. Ezekiel Omotoso, Dr. Emmanuel Igumbor, Mr. Mmusi Gopane, Ms. Helga Danga, Dr. Shandarai.Tunhuma, Ms. Kelebogile Maabong, Mr. Fred-Joe Nambala, Mr. Ben Mwenkemwa, Mr. Meehleketo Mayimele, Mr. Kian Ostovar, Ms. Fatemeh Taghizadeh, Mr. Willem Barnard, and other colleagues in the physics department.
- My parents Tlabo and Mapula for their continuous and unconditional support and encouragement.
- My late grandfather J.D. Noko Ngoepe for his love and showing me the importance of God, family and education.
- My dear beloved siblings Amo, Noko and Magashe for always being there for me.
- My uncle Prof. Phuti Ngoepe for inspiring me to do physics.
- My extended family.
- My friends, most of whom I have not spent enough time with during my studies.
- The National Research Foundation for financial support.

TABLE OF CONTENTS

1 Introduction 1
2 Theoretical background 3
2.1. Introduction 3
2.2. Crystal structure 3
2.3. Semiconductor properties 4
2.3.1. Optical properties 4
2.3.2. Mechanical properties 5
2.4. Growth 6
2.5. Metal-semiconductor contacts 7
2.5.1. Schottky barrier formation 7
2.5.2. Schottky barrier height determination 12
2.5.3. Depletion width 13
2.5.4. Image force lowering 17
2.5.5. Ohmic contacts 20
2.6. Current transport mechanisms 22
2.6.1. Thermionic emission 23
2.6.2. Tunnelling 25
2.7. Ion-solid interaction 26
2.7.1. Introduction 26
2.7.2. Ion stopping 27
2.7.3. Nuclear stopping 28
2.7.4. Electronic stopping 28
2.7.5. Ion damage 29
References 30
3 Defect theory and characterization 33
3.1. Defect theory 33
3.1.1. Introduction 33
3.1.2. Point defects 34
3.1.3. Trapping and emission of carriers at deep energy levels 37

3.2. Defect characterisation 39
3.2.1. Introduction 39
3.2.2. DLTS description 40
3.2.3. DLTS principles 42
3.2.4. Rate window concept 45
3.2.5. Defect identification 49
3.2.6. Defects in GaN 50
References 51
4 Experimental techniques 53
4.1. Introduction 53
4.2. Sample preparation 53
4.3. Metal deposition 54
4.3.1. Electron beam deposition system 55
4.3.2. Resistive deposition system 56
4.4. Annealing 57
4.5. Irradiation and implantation 58
4.6. Devise Characterisation 60
4.6.1. Current and capacitance measurements 60
4.6.2. Deep Level Transient Spectroscopy (DLTS) 61
References 63
5 Results 64
5.1. Introduction 64
5.2. Electron beam exposure 65
5.3. Cs ion implantation 70
5.4. Xe ion irradiation 75
5.5. Summary of results 81
References 82
6 Conclusions 83
6.1. Introduction 83
6.2. Electron beam exposure 83
6.3. Cs ion implantation 83
6.4. Xe ion irradiation 84
6.5. Summary 84
6.6. Future work 84

Chapter 1

Introduction

Semiconductor technology has developed quite considerably in the past couple of decades and has become the foundation of the modern day electronics industry. These developments have led to reduction in size, increased power and greater reliability of semiconductor based devices. Gallium nitride (GaN), in particular, has emerged as a strong contender in the production of optoelectronic devices. This is due to its ability to operate at high temperatures, voltages and frequencies. It can also operate quite well in caustic environments. All these properties bode well for potential use of GaN in military, space, domestic and industrial applications.

Native defects and impurities can affect the electronic, mechanical, and optical properties of semiconductors. They can either enhance or degrade the material depending on the type of device being fabricated. Defects can enhance devices by acting as recombination centers which increase the switching speeds of diodes and for other high frequency devices. They can be detrimental by reducing the mobility of charge carriers and acting as traps, thus reducing carrier lifetimes. Defects can be introduced to the semiconductor either intentionally or unintentionally during growth, annealing, device fabrication, and other processing methods. In order to study defects and understand their origin, it is common to intentionally introduce them by processing methods such as ion implantation and irradiation.

One of the most important electrical characterisation techniques for studying defects in semiconductors is deep level transient spectroscopy (DLTS). Defects can be identified using this technique by a defect signature, which is composed of the activation energy and apparent capture cross section. DLTS is non-destructive, has a high sensitivity to defects, and can easily distinguish between majority and minority carriers. This makes it a suitable candidate for detecting electrically active defects in semiconductors.

In this study, defects in GaN were detected and characterised by DLTS after various processing techniques. These techniques included exposure of GaN to various radiation effects at low, medium and high energy, namely electron beam exposure, ion implantation

and ion irradiation respectively. Defects measured in this study were then compared to defects reported by other studies.

In Chapter 2 of this thesis the properties of GaN are discussed. This includes general properties such as the crystal structure, and optical and mechanical properties. Also, the evolution of the energy-band relationship between the contact of a metal and semiconductor is explained. A discussion on ion-solid interactions conclude the topics of this chapter. Chapter 3 explains general defect theory. The theory of the defect characterisation technique, namely DLTS, is also discussed in this chapter.

In Chapter 4 the experimental aspects of the study are explained. This includes the sample preparation method and the annealing procedure. The different metal deposition methods are discussed which include electron beam and resistive evaporation deposition. Also discussed is the annealing equipment and annealing technique used in the study. Since the samples were bombarded with ions, a brief section on ion implantation and irradiation is given. Lastly the electrical characterisation techniques (I-V, C-V and DLTS) are explained.

The results are presented as publications in Chapter 5. The first publication deals with electron beam exposure induced defects in GaN. The second publication is a study of the characterisation of GaN after the implantation of Cs ions into GaN. The last publication is the DLTS characterisation of defects in Xe irradiated GaN. After a presentation of all these publications, a brief summary of the defects obtained in all these studies is tabulated.

The final chapter gives a summary of the conclusions that were found in this study. Also included are possible future studies.

Chapter 2

Theoretical background

2.1. INTRODUCTION

This chapter gives an introduction to the characteristics of gallium nitride (GaN) and in general, the device that is formed when a metal comes into contact with a semiconductor. The first section looks at the crystal structure of GaN. The second section details the properties of GaN. These properties include both the optical and mechanical properties. In discussing these properties, examples of applications are also given. Section 2.4 looks at the growth of GaN wafers in particular the chemistry involved in the growth of the GaN samples used in this study. In Section 2.5, the relationship between a metal and semiconductor contact is discussed. This includes the evolution of the energy bands before and after contact, the electrical characterisation parameters which can be extracted from the newly formed diode, the depletion width of the metal-semiconductor contact, and factors which can cause the lowering of the barrier of the metal-semiconductor junction. Lastly, the transport mechanisms associated with a Schottky diode are explained.

2.2. CRYSTAL STRUCTURE

GaN is a binary semiconductor, which can crystallise in either the wurtzite, or zincblende crystal structures. The wurzite structure (with a hexagonal crystal system) is thermodynamically stable whereas zincblende is metastable. Fig. 2.1 shows the hexagonal wurzite crystal structure of GaN. Every Ga (cation) atom is surrounded by four N (anion) atoms and vice versa. The lattice constants of the wurtzite hexagonal structure are a = 3.189 Å and c = 5.185 Å for GaN [1]. The crystallographic orientation of faces in GaN is perpendicular to the c-axis. These faces are polar and are either nitrogen-terminated or gallium-terminated. It has been reported that the gallium-terminated faces are inert whereas the nitrogen-terminated faces are chemically active [2].

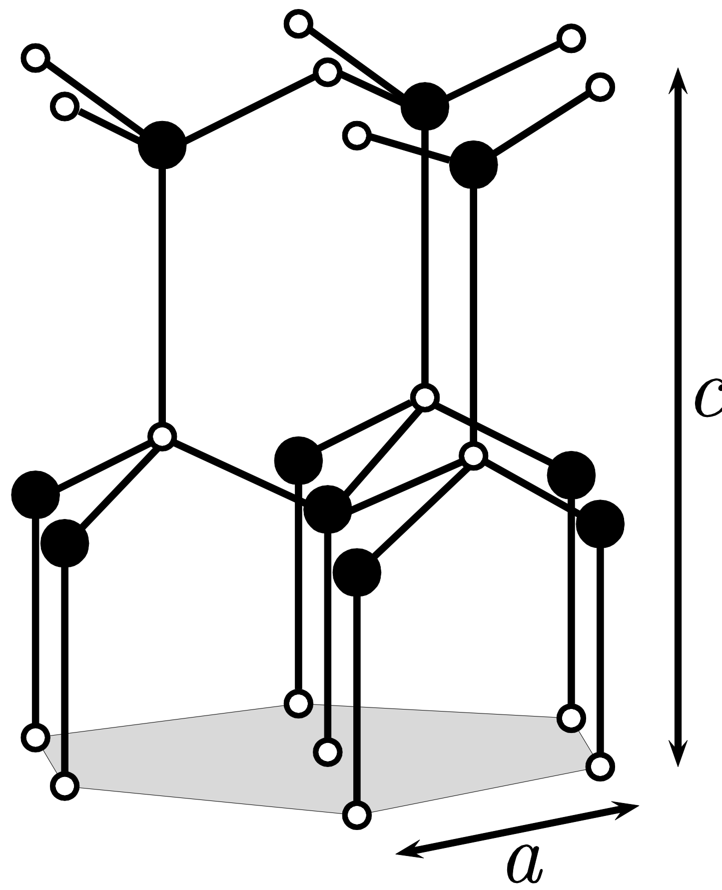

Fig. 2.1 Figure showing the hexagonal wurzite structure of GaN (dark spheres represent gallium, light spheres represent nitrogen) [3].

2.3. SEMICONDUCTOR PROPERTIES

This section gives a brief overview of the optical and mechanical properties of GaN. The applications relating to the properties are also given.

2.3.1. Optical properties

GaN is a wide, direct bandgap semiconductor, which has huge potential in optoelectronic applications. It is part of the III-nitrides, which also include indium nitride (InN) and aluminium nitride (AlN). The III-nitride semiconductors can be engineered in order to vary their bandgap from 0.7 to 6.2 eV. InN has a bandgap of 0.7 eV, GaN 3.4 eV, and AlN 6.2 eV [4]. By varying the bandgap, tertiary as well as quaternary structures can be formed. Examples of the former include aluminium gallium nitride (AlGaN), indium gallium nitride

(InGaN) and indium aluminium nitride (InAlN) while the latter include aluminium indium gallium nitride (AlInGaN). The variation in the bandgap implies that the wavelength range of the III-nitride semiconductors varies from 200 to 1770 nm, covering a wide spectral range, which includes the ultraviolet, visible and near infrared bands. This optical property makes III-nitrides suitable for a wide range of applications.

In addition, GaN has a large absorption coefficient due to its direct bandgap. This makes it suitable for use in detecting devices such as photodetectors, and chemical and biological sensors. It is also suitable for emitting devices such as laser diodes (LD's) and light emitting diodes (LED's). Due to its emission capacity, there is great interest in GaN and GaN related materials for general lighting applications, such as traffic lights, vehicle lighting, and full colour displays [5]. Other applications include fibre optic communication, optical data storage and other non-optoelectronic applications in the form of heterojunction emitters for transistors [6].

2.3.2. Mechanical properties

GaN has considerable mechanical strength. There are a number of factors to which this property may be attributed. Amongst these is the difference in the electronegativity of Ga and N, which is relatively high. The values of the former and the latter are 1.1 and 3.1 Pauling respectively [7]. This huge difference results in the high chemical stability and radiation hardness of GaN. It also leads to GaN being considered as an ionic compound.

The displacement threshold energy of GaN is high due to the difference in the bond strength of its constituent elements. The displacement energy for gallium is 19 eV while that for nitrogen is 22 eV [8,9]. This makes GaN significantly more radiation tolerant than semiconductors such as GaAs and Si. These exceptional qualities, therefore, make it a suitable candidate for space applications where devices, which are radiation resistant, are required. Table 2.1 gives several GaN parameters.

Table 2.1 The physical properties of GaN with a wurzite crystal structure.

Property	Value
Lattice constants (Å) [1]	a = 3.189
	c = 5.185
Dielectric constant [10]	8.9
Electron affinity (eV) [11]	4.1
Density (g/cm^3) [10]	6.07
Band gap @ 1.6 K (eV) [4]	3.5
Band gap @ 300 K (eV) [4]	3.4
Work function @ 300 K [4]	4.57
Effective electron mass (m_e) [12]	0.20
Breakdown field @ 300 K (V·cm^{-1}) [13]	$> 5 \times 10^6$

2.4. GROWTH

It has been challenging to grow GaN single crystals for device fabrication. This is due to a lattice mismatch between GaN and a suitable substrate. Sapphire (Al_2O_3) and silicon carbide (SiC) have been the primary substrates on which GaN has been grown. There are a number of factors, which contribute to the selection of a suitable substrate. These include, amongst others, coefficients of thermal expansion, lattice parameters, structural and chemical properties, thermal and electrical conductivity, cost and the crystal structure of the substrate. Cost has been one of the main reasons why sapphire is preferred over SiC.

A number of methods have been used to grow GaN. These methods are mainly epitaxial and include physical, liquid phase, and chemical vapour depositions. The term epitaxial means that the crystalline layer of the semiconductor is grown on a substrate in such a way that the crystalline layer has a similar lattice structure to the substrate. When the composition of a thin film is the same as that of the substrate, the deposition is called homoepitaxial. When the composition of the materials is different, the growth is heteroepitaxial. The different epitaxial growth methods used to grow GaN include reactive molecular beam epitaxy (RMBE) [14],

metal-organic vapour phase epitaxy (MOVPE) [15], epitaxial lateral overgrowth (ELOG) [16], and hydride vapour phase epitaxy (HVPE) [17]. In this study, samples grown by HVPE were investigated. This method is relatively inexpensive, has a high growth rate, and can be used on an industrial scale [18].

Ilegems reported in 1973 the growth of GaN by using the vapour phase method [19]. This was done by using NH_3 gas as a source for N and GaCl gas as a Ga source. The chemical reaction for HVPE grown GaN is as follows:

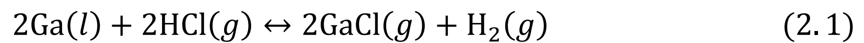

$$2\mathrm{Ga}(l) + 2\mathrm{HCl}(g) \leftrightarrow 2\mathrm{GaCl}(g) + \mathrm{H_2}(g) \qquad (2.1)$$

and

$$\mathrm{GaCl}(g) + \mathrm{NH_3}(g) \leftrightarrow \mathrm{GaN}(s) + \mathrm{HCl}(g) + \mathrm{H_2}(g) \qquad (2.2)$$

Liquid Ga reacts with HCl gas to form GaCl and hydrogen. The GaCl, which is stable above 600 °C, then reacts with ammonium gas to produce GaN [6]. The GaN is grown on a sapphire substrate. This substrate is an insulator thus confining the electrical characteristics to GaN. Also, wafers grown on a sapphire substrate usually have a diameter of 2 inches and are relatively cost effective to grow.

2.5. METAL-SEMICONDUCTOR CONTACTS

In this section a discussion is given of the energy relationship between a metal and a semiconductor when they come into contact with each other. Depending on the type of metal and semiconductor, the result of this contact can be a barrier called the Schottky barrier. From this barrier we can measure current and capacitance characteristics. From these characteristics, other electrical properties can be calculated. An Ohmic contact, which also forms as a result of the metal-semiconductor contact, is also discussed.

2.5.1. Schottky barrier formation

Energy bands can be used to explain the interaction between a metal and a semiconductor. These energy bands are useful in showing the electronic states that a charge carrier is allowed to occupy in a solid. The ideal energy band gap relationship between a metal and an n-type

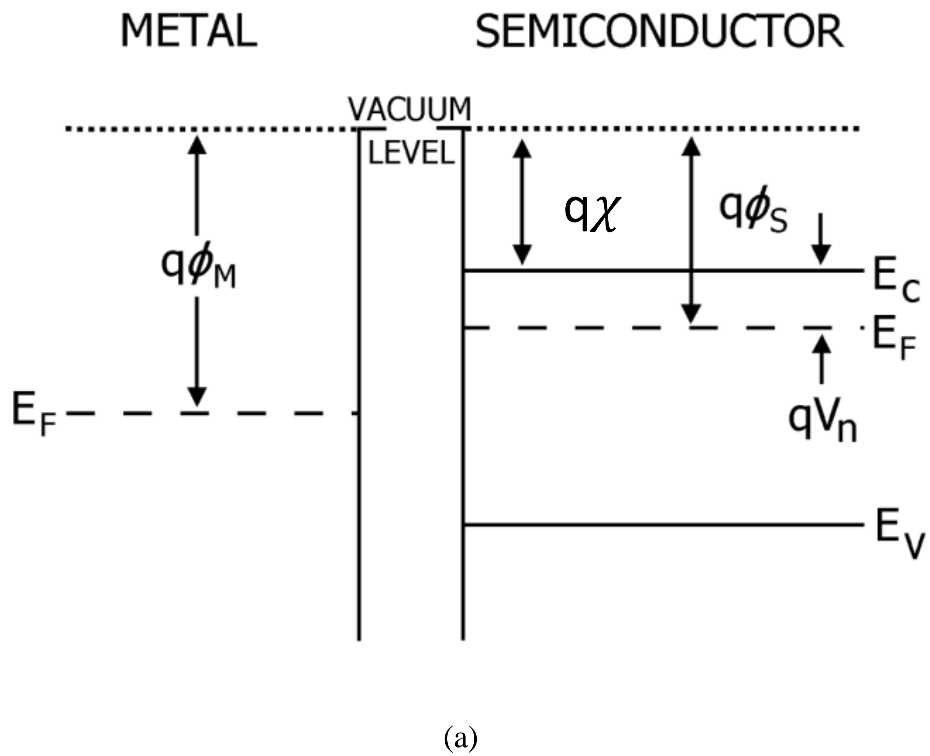

(a)

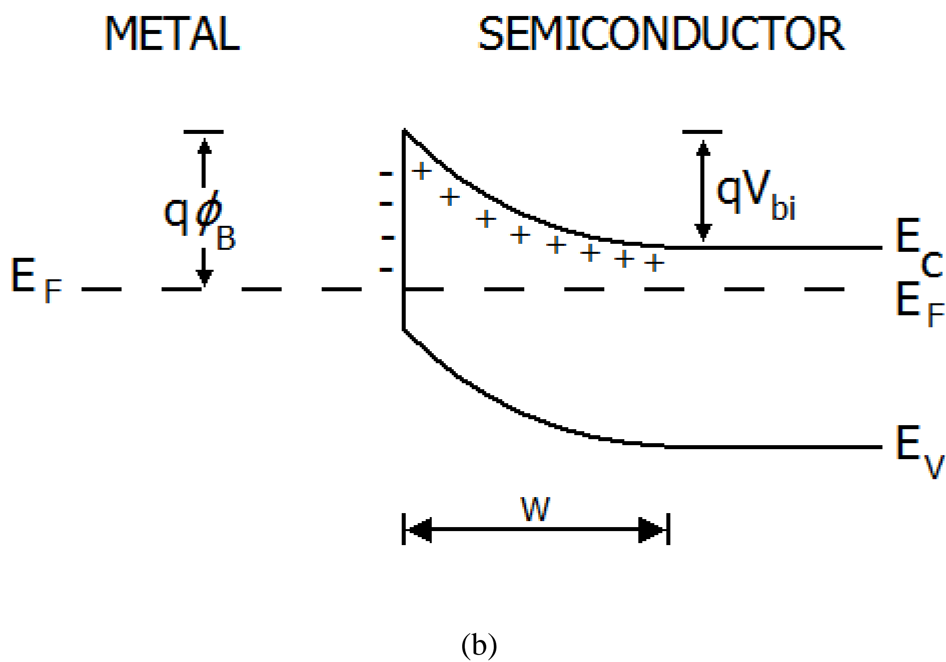

(b)

Fig. 2.2 Energy band diagrams of a metal and semiconductor (a) Before contact (b) After contact, which illustrate the formation of a Schottky barrier [20].

semiconductor is now explained. Fig.2.2 (a) shows the energy bands of an isolated metal and semiconductor, which are electrically neutral. When a metal and a semiconductor come into contact with each other, the electrons within the vicinity of the interface are affected. This is due to the difference in the work functions of the metal and the semiconductor. The work function is the difference between the vacuum level and the Fermi energy level. At absolute zero temperature, the work function is defined as the amount of energy required to remove an electron from a solid (in this case the metal or the semiconductor).

Since we consider a case in which the work function of the metal ($q\phi_M$) is larger than the work function of the semiconductor ($q\phi_S$), the energy bands of the semiconductor will bend upwards (as seen from the bulk of the semiconductor) because of the migration of electrons from the semiconductor to the metal after metal-semiconductor contact. This will cause a charge build up at the metal-semiconductor interface. On the metal surface the charge will be negative whilst on the semiconductor surface the charge will be positive. This charge build-up will cause an electric field to form which acts as a barrier to the flow of electrons between the metal and the semiconductor. The electrons in the semiconductor will flow into the metal until equilibrium. This equilibrium is reached when the Fermi levels of the metal and the semiconductor align. The Fermi level of the semiconductor is lowered by a value called the contact potential. This value is the difference between the work functions of the semiconductor and the metal.

A depletion region is realised as a result of the migration of electrons from the semiconductor to the metal. This region is depleted of electrons and the positive charge is due to uncompensated donor atoms remaining behind. The band bending of the conduction and valence bands is caused by the variation of the potential in the depletion region and is limited to this region. The variation of the potential steadily increases from within the semiconductor and reaches a maximum at the metal-semiconductor interface. At the interface, the barrier, which was alluded to earlier, is formed and prevents the flow of electrons across it. The height of this barrier, called the Schottky barrier height (SBH), is the distance between the Fermi level and the conduction band edge at the maximum. It is given by the following equation:

$$q\phi_B = q(\phi_M - \phi_S) + q(\phi_S - \chi) = q(\phi_M - \chi) \qquad (2.3)$$

where $q\phi_M$ is the metal work function, $q\phi_S$ is the semiconductor work function and $q\chi$ is the electron affinity. The electron affinity is the amount of energy released when an electron is added to the semiconductor. It is the difference between the vacuum level and the conduction band. The term $q(\phi_M - \phi_S)$ is the built in potential, qV_{bi}, and is the height of the barrier relative to the depth of the conduction band. The second term, $q(\phi_S - \chi)$, is the potential difference between the conduction band edge and the semiconductor Fermi level. The relationship is not so simple in practice due to factors such as metal-induced gap states, interface states, surface states and chemical reactions at the metal-semiconductor interface.

Under zero bias (equilibrium conditions) there is no net flow of electron over the barrier as the electrons moving across the barrier are balanced from both the metal and the semiconductor. A net flow of electrons occurs into either the metal or the semiconductor when a bias voltage is applied. The bias voltage applied can either be a forward or a reverse bias. This bias voltage influences the height of the barrier that the electrons have to surmount. Under forward bias conditions, a positive potential is applied to the metal (or a negative potential applied to the semiconductor). What this implies is that the Fermi level of the semiconductor is raised with respect to that of the metal and band bending is decreased. When this happens the potential that the electrons from the semiconductor "see" is decreased. The net flow of electrons under forward bias will be into the metal. Applying a forward bias decreases the depletion width.

When a reverse bias is applied to the metal-semiconductor contact, a negative potential is applied to the metal (or a positive potential is applied to the semiconductor). The Fermi level of the semiconductor is decreased with respect to that of the metal. This increases the depletion width. The electrons in the semiconductor will have to overcome a higher barrier to cross over into the metal. Under both reverse and forward bias, the barrier height, which the electrons from the metal experiences, remains constant. Fig. 2.3 illustrates the forward and reverse bias conditions.

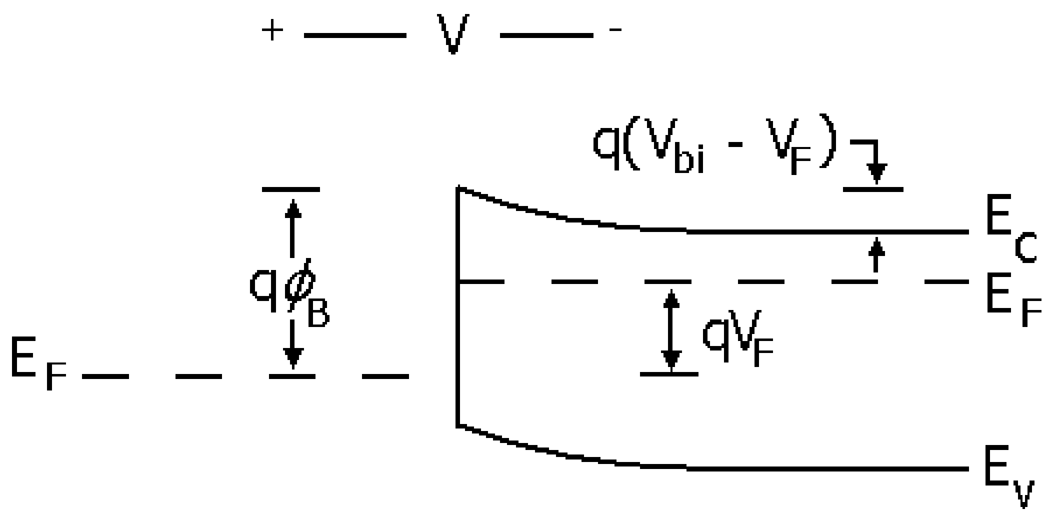

(a)

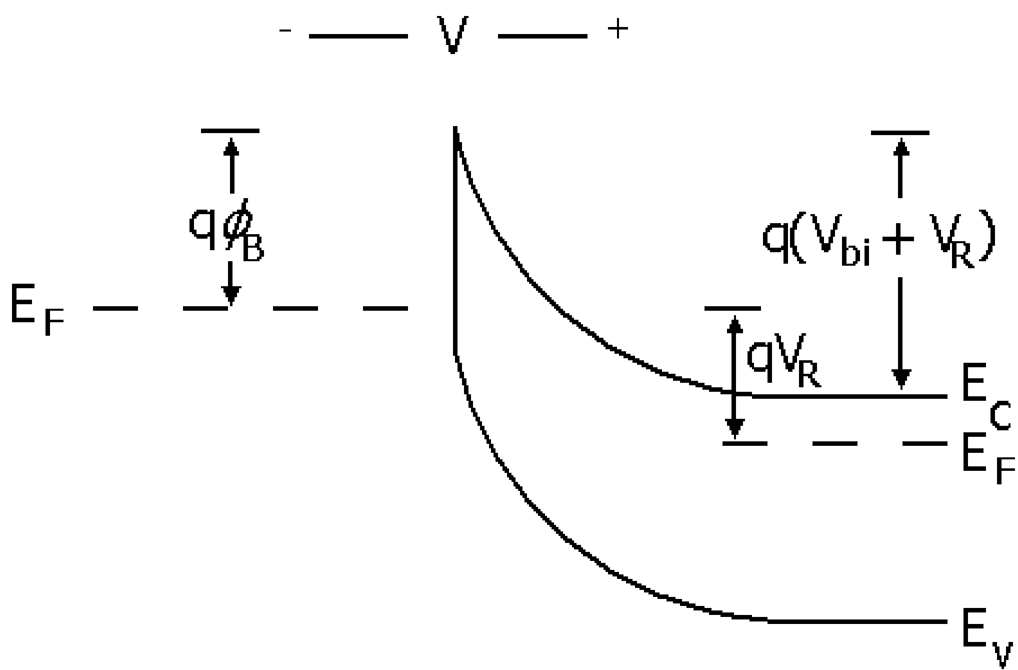

(b)

Fig. 2.3 Energy band diagram of a Schottky barrier illustrating the effects of applying (a) forward bias, V_F (b) reverse bias voltages, V_R [20].

2.5.2. Schottky barrier height determination

Current-voltage characteristics are mainly performed on Schottky diodes to assess the quality of the device. This is done by measuring the current under both reverse and forward bias conditions. From the forward bias characteristics, the barrier height, series resistance and ideality factor can be determined. From the reverse bias characteristics the rectifying capacity of the diode is determined. The current-voltage relationship is given by:

$$I = I_s\ [\exp(qV/nkT) - 1] \tag{2.4}$$

where I_s is the saturation current given by

$$I_s = AA^*T^2 \exp\left(-\frac{q\phi_B}{kT}\right), \tag{2.5}$$

A is the diode area and n is the ideality factor given by

$$\frac{1}{n} = \frac{kT}{q}\frac{d(\ln J)}{dV}, \tag{2.6}$$

where J is the current density. A^* in the above equation is the Richardson constant and is given by

$$A^* = \frac{4\pi m^* q k^2}{h^3} = 120\frac{m^*}{m}\left(\frac{AK^2}{cm^2}\right) \tag{2.7}$$

and the barrier height is given by the equation

$$\phi_B = \frac{kT}{q} ln\left(\frac{AA^*T^2}{I_s}\right). \tag{2.8}$$

The barrier height determined using this equation is so determined at zero bias. This barrier plays an important role when considering thermionic-emission conduction mechanism as will be considered in section 2.6.1.

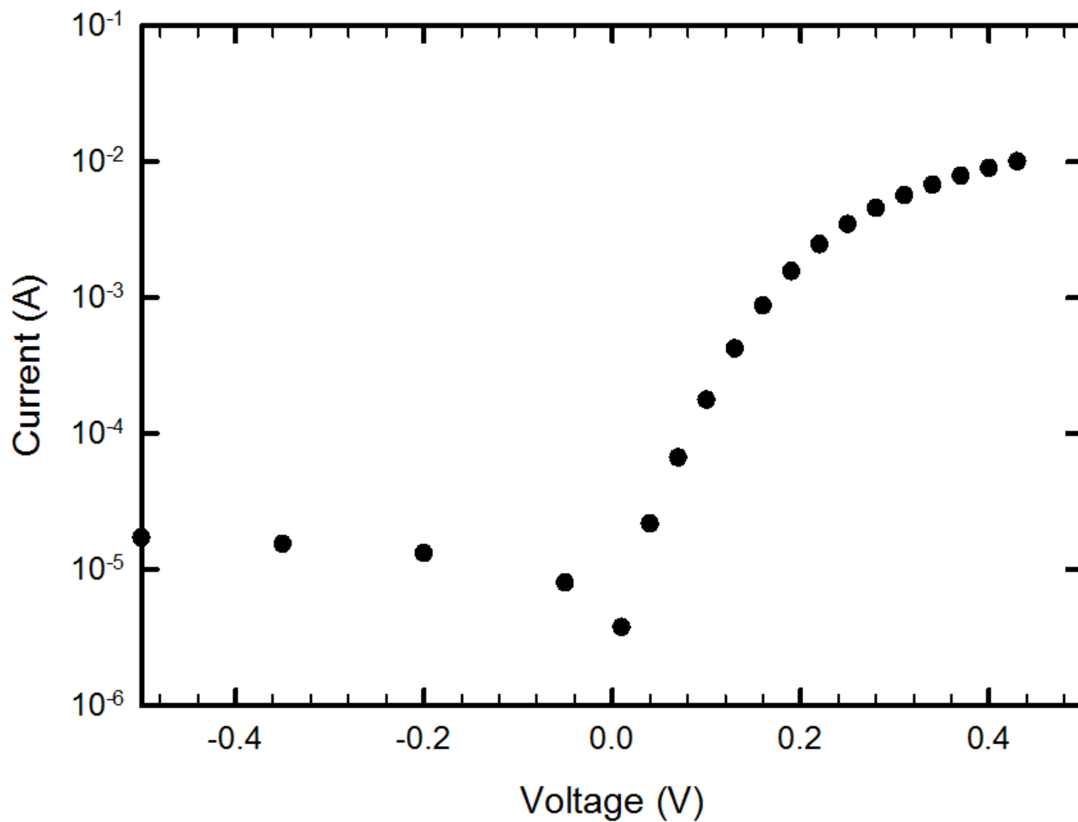

Fig. 2.4 *I-V* characteristics of a Schottky diode of Ni/Au deposited on GaN as used in this study.

The ideality factor is a measure of how much the forward voltage characteristics of a Schottky diode deviates from an ideal case. It incorporates all the unknown effects that make a device non ideal. The ideality factor of an ideal device is equal to unity whereas it is greater than unity for a non-ideal device. Factors which cause a device to deviate from ideality include damage to the metal-semiconductor interface, surface states, series resistance, variation in barrier height across the surface, bias dependent barrier height (field effect) and other current transport mechanisms (e.g. tunneling). Fig. 2.4 shows the *I-V* characteristics of a Ni/Au Schottky diode from which the various electrical parameters of a diode can be determined.

2.5.3. Depletion width

The details of what happens when a metal and a semiconductor come into contact have been explained in a previous section. When these come into contact, there are two boundary

conditions that can be considered. The first is due to the barrier height of the metal-semiconductor interface. The second boundary condition is to consider the electric field to be zero in the bulk of the semiconductor as there is charge neutrality in this region. The solutions to Poisson's equation in the one dimensional case can be written as

$$\frac{d^2V}{dx^2} = -\frac{1}{\varepsilon_s}\rho(x), \tag{2.9}$$

where $\rho(x)$ is the total charge density at a depth of x beneath the surface of the semiconductor and ε_s is the permittivity of the semiconductor. To simplify the total charge density, an abrupt approximation is made. The semiconductor is divided into two regions. The first region is called the depletion region and is closer to the metal-semiconductor contact. This region has no free carriers due to the high potential difference between the conduction band and the Fermi level in this region. The second region is the bulk of the semiconductor, in which no electric field exists and is electrically neutral. This therefore implies that the charge density can be written as

$$\rho(x) = \begin{cases} qN_D & \text{if } x \le w \\ 0 & \text{if } x > w \end{cases}, \tag{2.10}$$

where N_D is the doping density and q the electronic charge. By integrating equation (2.9) twice and applying the boundary conditions, the depletion width is given by the equation [20]

$$w = \sqrt{\frac{2\varepsilon_s V_{bi}}{qN_D}} \tag{2.11}$$

The electric field in the semiconductor is given by [20]

$$E(x) = -\frac{qN_D}{\varepsilon_s}(w - x) \tag{2.12}$$

The maximum electric field strength is obtained when $x = 0$. The electrostatic potential is given by [20]

$$V(x) = -\frac{qN_D}{2\varepsilon_s}(w - x)^2 \tag{2.13}$$

Fig. 2.5 shows the plots of the charge density, electric field and electric potential in the depletion width of a Schottky barrier diode.

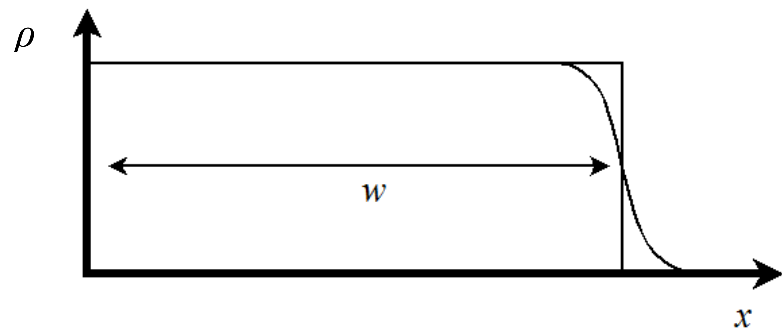

(a)

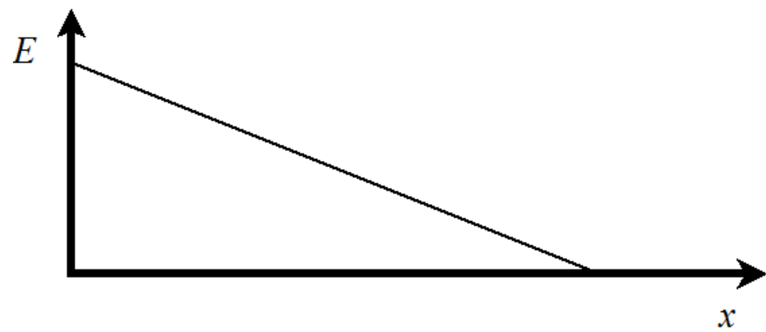

(b)

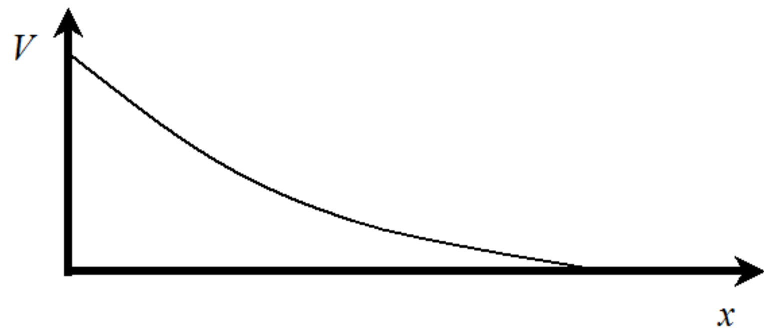

(c)

Fig. 2.5 Plots of the (a) charge density, (b) electric field, and (c) electric potential in the depletion region of a Schottky barrier diode.

The space charge per unit area of the depletion layer and semiconductor is given by

$$Q = qwN_D = \sqrt{2q\varepsilon_s N_D V_{bi}}\,, \tag{2.14}$$

while the capacitance per unit area of the depletion layer and semiconductor are given by

$$C = \frac{\partial Q}{\partial V_{bi}} = \sqrt{\frac{q\varepsilon_s N_D}{2V_{bi}}} = \frac{\varepsilon_s A}{w}\,, \tag{2.15}$$

This equation can be written in the form

$$\frac{1}{C^2} = \frac{2(V_{bi} - V_a - kT/q)}{q\varepsilon_s N_D}. \tag{2.16}$$

Equation (2.15) holds if we assume a parallel plate capacitance model where the edges of the space charge region act as the parallel plates. Two plots of the *C* vs. *V* and $1/C^2$ vs. *V* are respectively illustrated in Fig. 2.6 and Fig. 2.7 below. It follows from equation 2.16 that N_D can be calculated from the slope of the graph and V_{bi} calculated from the intercept with the *V*-axis.

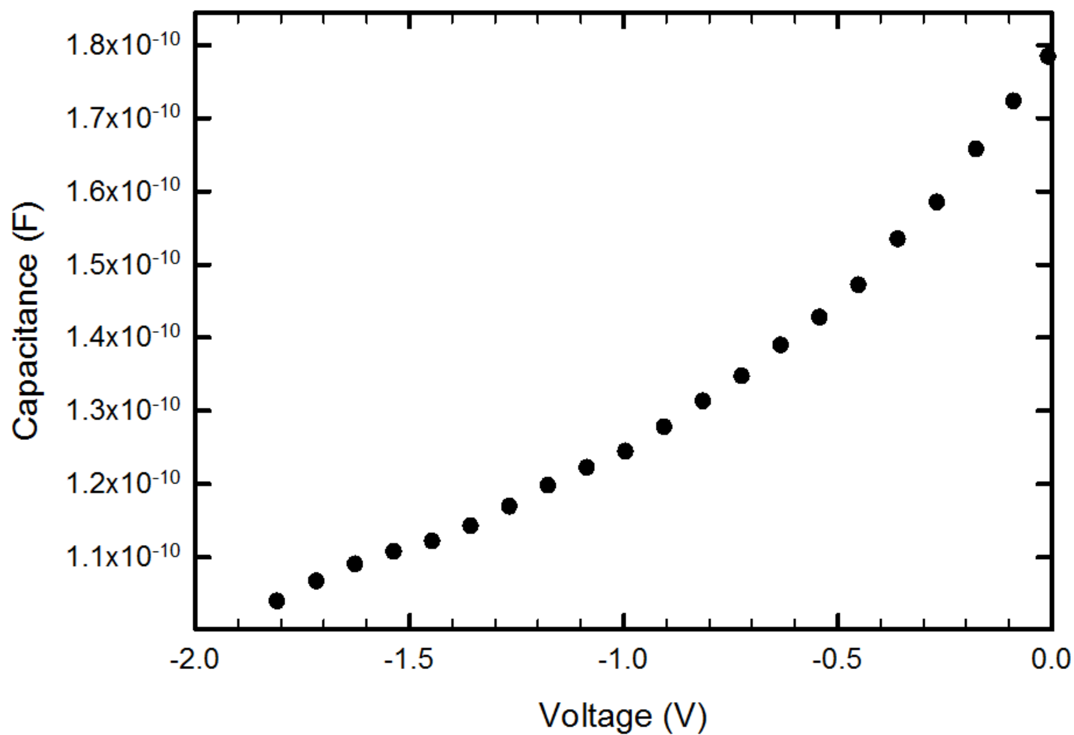

Fig. 2.6 Capacitance-voltage characteristics of a Ni/Au Schottky diode.

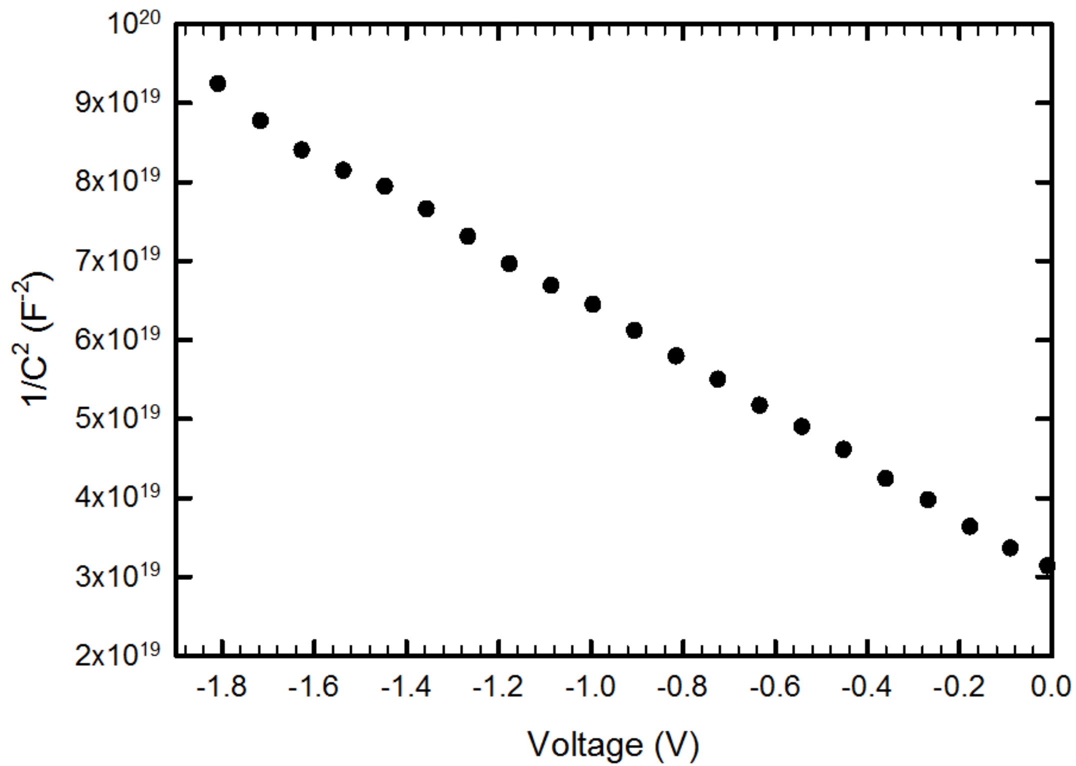

Fig. 2.7 Inverse of capacitance squared against the voltage of a GaN based Ni/Au Schottky diode.

2.5.4. Image force lowering

When a charge carrier (an electron) is brought close to the surface of a metal, it is attracted to the metal due to the electric field caused by the charge induced in the metal. This force is called image force and causes a lowering in the Schottky barrier, referred to as image force lowering. This is illustrated in Fig. 2.8. When the electron is brought close to the surface of the metal, the electric field can be calculated as if there was a positive charge in the metal which is the same distance behind the metal-semiconductor interface as the electron is in front of the interface.

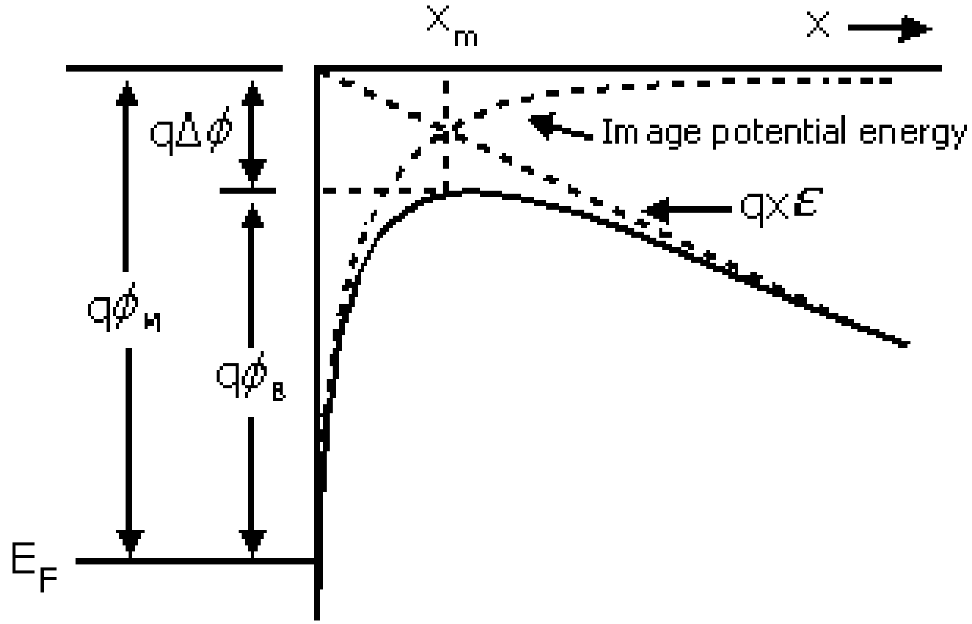

Fig. 2.8 Energy band diagram illustrating Schottky barrier lowering [20].

The force experienced by the electron as it approaches the metal can be written as

$$F = -\frac{q^2}{4\varepsilon_s\pi(2x)^2} = -\frac{q^2}{16\varepsilon_s\pi x^2} \tag{2.17}$$

where ε_s is the semiconductor permittivity which can be written as $\varepsilon_s = \kappa\varepsilon_o$, κ is the semiconductor dielectric constant while ε_o is the permittivity of the vacuum. The potential energy of an electron brought from infinity to a distance x from the metal surface is given by

$$U(x) = \int_{\infty}^{x} F\ dx = \frac{q^2}{16\varepsilon_s\pi x} \tag{2.18}$$

When an external electric field ξ is applied, the potential energy of the electron can be written as

$$P(x) = \frac{q^2}{16\varepsilon_s\pi x} + q\xi x\ . \tag{2.19}$$

To find the position where the electron will experiences the greatest potential energy, *P(x)* can be differentiated with respect to *x* and equated to zero such that the position is given by:

$$x_m = \sqrt{\frac{q}{16\varepsilon_s \pi \xi}}\,. \tag{2.20}$$

The Schottky barrier lowering can then be obtained by substituting x_m into *P(x)* which gives the Schottky barrier lowering [20]:

$$\Delta\phi = \sqrt{\frac{q\xi}{4\varepsilon_s \pi}} = 2\xi x_m \tag{2.21}$$

The barrier height determination using current measurements require that electrons surmount the barrier height. This implies that the movement of these electrons will be dependent on image force lowering. Since the capacitance is dependent on the width of the space charge region, they are not affected by image force lowering of the barrier height. Therefore image force lowering will lead to a lower barrier height for I-V measurements as compared to C-V measurements. The barrier height is affected by a bias voltage as shown in Fig. 2.9. The bias dependence of the image force lowering leads to an increase in *n* (as discussed in section 2.6.1) and an increase in the reverse leakage current. The image force lowering is more pronounced at higher carrier densities.

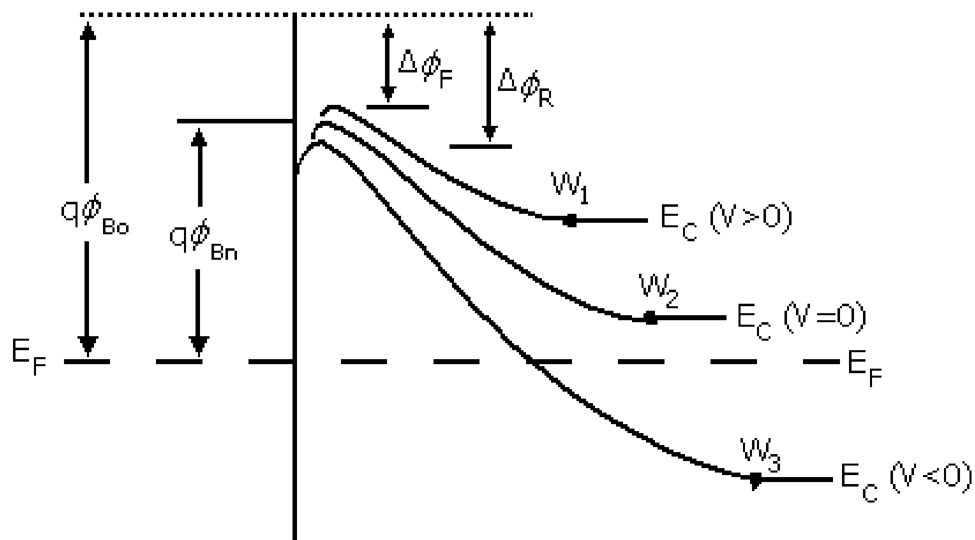

Fig. 2.9 Energy band diagram demonstrating Schottky lowering under different bias conditions [20].

2.5.5. Ohmic contacts

Ohmic contacts play a critical role in the performance of a device. It is important that the current linearly changes with the applied voltage (i.e. there is no asymmetry) and the contact resistance must be low. In order to have a low contact resistance, the Schottky barrier height must be very low and/or the semiconductor must be heavily doped to allow charge carriers to tunnel through the barrier. A low contact resistance is especially important for high frequency and high power devices. High contact resistance will cause excessive heat and ultimately lead to device failure [21].

Metals are selected for ohmic contacts depending on the type of semiconductor. This therefore means that the ohmic contact metals can be predicted by using the Schottky-Mott equation where $\phi_s < \chi$ (for n-type semiconductor). In some instances a metal might not be able to adhere well to the semiconductor, thus rendering it inappropriate for device fabrication. Also, a phenomenon, called Fermi level pinning, which involves surface states might occur. This can affect device performance. In the case of GaN the Fermi level is not pinned [22] and the barrier height of GaN is dependent on the work function of the metal used. Also, the type of bonding affects whether Fermi level pinning occurs. Ionically bonded semiconductors tend not to exhibit pinned surfaces. Semiconductors such as GaN which have a high electronegativity difference usually have these unpinned surfaces [23].

Fig. 2.10 shows the energy bands of a semiconductor before and after metal contact deposition on an n-type semiconductor. The work function of the semiconductor has to be larger than that of the metal for an Ohmic contact to form. When the metal and semiconductor come into contact, the electrons in the semiconductor will flow from the semiconductor to the metal. This is caused by the potential difference between the metal and the semiconductor due to the difference in the work functions. When the Fermi levels of the metal and the semiconductor align, the electrons will stop flowing into the metal as thermal equilibrium is reached. The alignment of these Fermi levels causes the conduction and valence bands to bend as shown in Fig. 2.10 (b). A good Ohmic contact should allow electrons to easily flow between the metal and the semiconductor when a potential is applied across the junction.

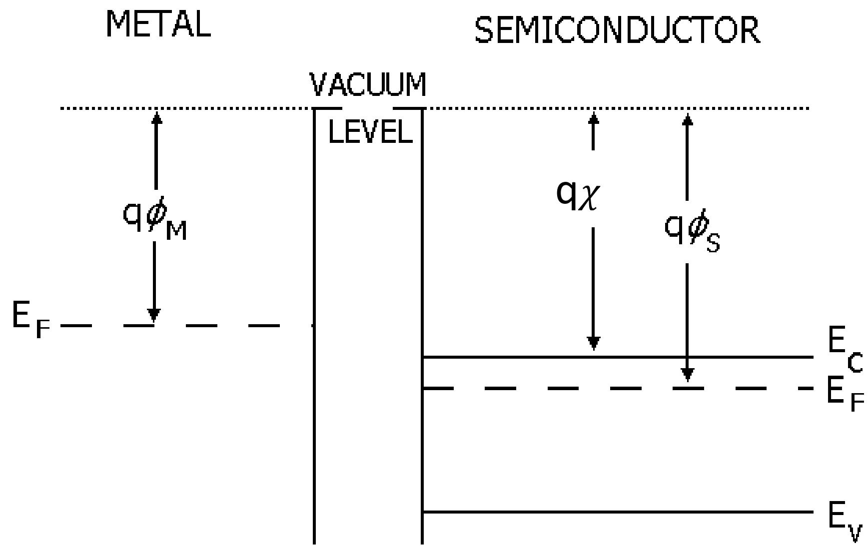

(a)

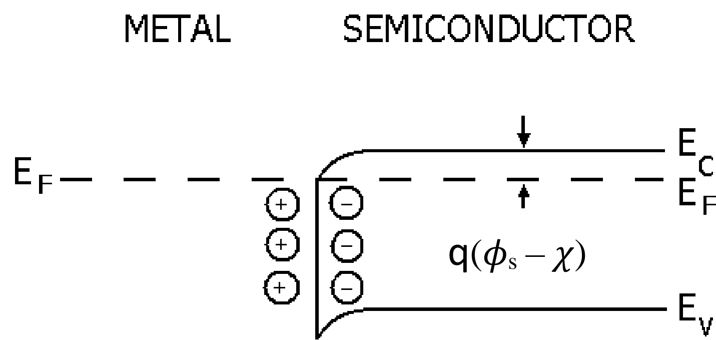

(b)

Fig. 2.10 Energy band diagrams of a metal and semiconductor forming an Ohmic contact: (a) before contact and (b) after contact.

2.6. CURRENT TRANSPORT MECHANISMS

There are a couple of mechanisms which govern the flow of current across a metal-semiconductor interface. This current is transported by majority carriers across the metal-semiconductor junction. Fig. 2.11 shows a diagram of four of these transportation mechanisms. In the diagram a forward bias is applied. These transportation mechanisms include [20,24]:

1. Electrons which surmount the Schottky barrier height from the semiconductor into the metal.
2. The quantum tunnelling of electrons through the Schottky barrier from the semiconductor into the metal
3. The recombination of electrons and holes in the space charge region (where the closed circles depicts an electron and the open circle a hole)
4. The recombination of electrons and holes in the neutral region. This is also known as hole injection.

Process 1 represents ideal conditions while processes 2, 3, and 4 represent a departure from ideal behaviour.

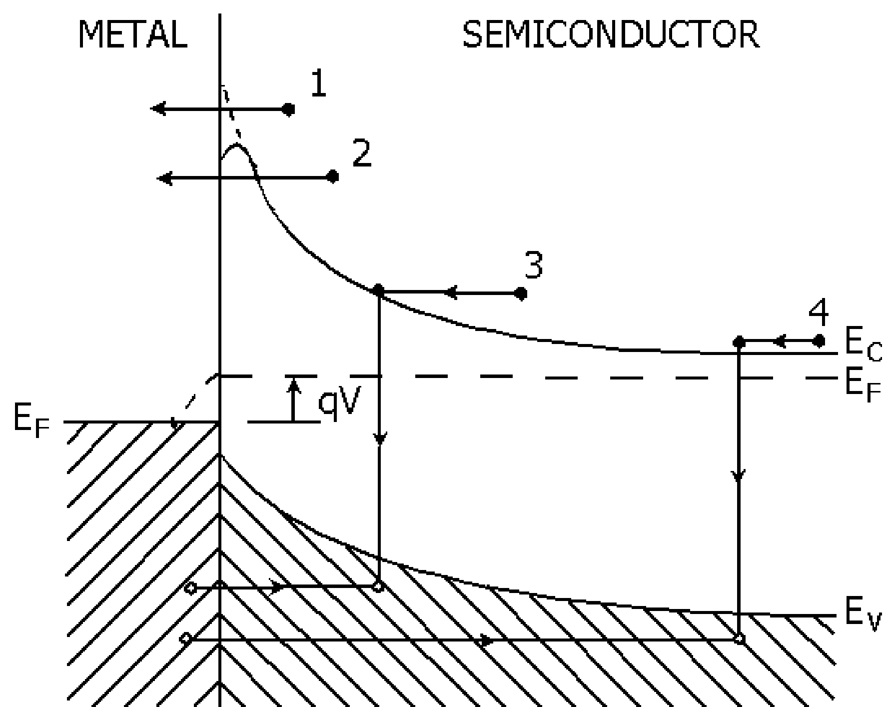

Fig. 2.11 Diagram showing different transportation mechanics of an electron across a metal-semiconductor contact [24].

2.6.1. Thermionic emission

Thermionic emission occurs for moderately doped semiconductors ($N_D < 10^{17}$ cm^{-3}). The depletion region in this case is relatively wide which make it difficult for charge carriers to tunnel through the barrier. Charge carriers have to surmount the barrier in this current transport mechanism. In most cases, the majority of the charge carriers do not cross the barrier. In the thermionic emission model, the flow of current from a semiconductor to a metal is only dependent on the barrier height. Electrons from the semiconductor have to overcome the barrier height in order to flow into the metal. The current density of those electrons which are able to overcome the barrier height and flow from the semiconductor into the metal is given by [20]:

$$J_{sm} = \int_{E_F + q\phi_B}^{\infty} qv_x \, dn \tag{2.22}$$

where $E_F + q\phi_B$ is the minimum energy required for electrons to overcome the barrier height and v_x is the carrier velocity in the direction of electron transport. The electron density in an incremental energy range is given by

$$\begin{aligned} dn &= N(E)F(E)dE \\ &= \frac{4\pi(2m^*)^{3/2}}{h^3}\sqrt{E - E_C}\exp\left[-\frac{E - E_C + qV_n}{kT}\right]dE \end{aligned} \tag{2.23}$$

where $N(E)$ is the density of states, $F(E)$ the Fermi-distribution function, m^* the effective mass of the electron in the semiconductor and qV_n is given by $E_C - E_F$. If we postulate that the energy of the electrons in the conduction band is kinetic energy, then

$$E - E_C = \frac{1}{2}m^*v^2$$

$$dE = m^*vdv$$

$$\sqrt{E - E_C} = v\sqrt{m^*/2} \tag{2.24}$$

After substituting equation (2.24) into (2.23), we get

$$dn = 2\left(\frac{m^*}{h}\right)^3 \exp\left(-\frac{qV_n}{kT}\right)\exp\left(-\frac{m^*v^2}{2kT}\right)(4\pi v^2 dv) \tag{2.25}$$

This equation gives the number of electrons per unit volume that have speeds between v and $v + dv$ distributed in different directions. If we were to resolve the speeds into different components, whereby the electrons are transported parallel to the x axis, then

$$v^2 = v_x^2 + v_y^2 + v_z^2 \tag{2.26}$$

Utilising the transformation $4\pi v^2 dv = dv_x dv_y dv_z$ and substituting it into the above equations (2.23) and (2.26) we get

$$J_{sm} = \left(\frac{4\pi q m^* k^2}{h^3}\right) T^2 \exp\left(-\frac{qV_n}{kT}\right) \exp\left(-\frac{m^* v_{ox}^2}{2kT}\right) \tag{2.27}$$

where v_{ox} is the minimum velocity required to overcome the Schottky barrier in the x direction. This velocity is given by

$$\frac{1}{2} m^* v_{ox}^2 = q(V_{bi} - V) \tag{2.28}$$

Substituting equation for v_{ox}^2 into J gives

$$J_{sm} = \left(\frac{4\pi q m^* k^2}{h^3}\right) T^2 \exp\left[-\frac{q(V_n + V_{bi})}{kT}\right] \exp\left(\frac{qV}{kT}\right)$$

$$= A^* T^2 \exp\left(-\frac{q\phi_B}{kT}\right) \exp\left(\frac{qV}{kT}\right) \tag{2.29}$$

where ϕ_B is the barrier height and A^* is the effective Richardson constant for thermionic emission. This effective Richardson constant does not take into account the effects of optical phonon scattering and quantum mechanical reflection.

Electrons surmounting the barrier height from the metal to the semiconductor do not see a varying barrier and this implies that the current flowing into the semiconductor is not affected by an applied voltage. At thermal equilibrium, the current flowing from the metal to the semiconductor should be the same as that flowing from the semiconductor to the metal, that is, when $V = 0$. Therefore setting $V = 0$ in the above equation

$$J_{ms} = -A^* T^2 exp\left(-\frac{q\phi_B}{kT}\right) \tag{2.30}$$

with the negative sign implying that the current is flowing from the metal to the semiconductor. The total current density flowing over the barrier is given by the sum of the current flow from the semiconductor into the metal and vice versa:

$$J_{tot} = \left[A^{*}T^{2}\exp\left(-\frac{q\phi_B}{kT}\right)\right]\left[\exp\left(\frac{qV}{kT}\right)-1\right]$$

$$= J_s\left[\exp\left(\frac{qV}{kT}\right)-1\right] \qquad (2.31)$$

where

$$J_s = \left[A^{*}T^{2}\exp\left(-\frac{q\phi_B}{kT}\right)\right] \qquad (2.32)$$

is the saturation current density [20].

In order to take the effects of image force lowering and other deviations from ideality into account, the ideality factor n is introduced. For an ideal Schottky diode $n = 1$ while deviations from ideality increase n.

2.6.2. Tunnelling

It is possible for electrons, which have energies below the barrier height to penetrate the barrier by tunnelling as illustrated in point 2 of Fig. 2.11. There are two possible cases to consider when this happens. In the first instance, at low temperatures and for heavily doped semiconductors ($N_D > 10^{18}$ cm^{-3}), when a forward bias is applied, the current emanates from the tunnelling of electrons from the semiconductor which are close to the Fermi level. This is known as field emission. The approach of using heavily doped semiconductors is usually used for ohmic contacts when a suitable metal-semiconductor contact is not found.

In the second case, if the temperature is raised, the kinetic energy of the electrons increases. When this occurs, there will be a significant number of electrons with an energy higher than the Fermi level. The probability of tunnelling will therefore increase as the electrons will see a thinner barrier. This increase in energy also implies that a larger fraction of electrons are emitted via thermionic emission, competing with the effects of tunnelling. This is known as thermionic field emission. This second process occurs for intermediately doped semiconductors ($10^{17} < N_D < 10^{18}$ cm^{-3}) [25].

If the temperature is raised even higher, all the electrons will have enough energy to surmount the barrier and tunnelling will become negligible. When this occurs, we then have pure thermionic emission.

For the case where tunnelling is the dominant mechanism for current flow, the transmission coefficient is given by [20]:

$$T(\eta) \sim \exp\left(-\frac{q\phi_B}{E_{00}}\right) \tag{2.33}$$

where

$$E_{00} = \frac{q\hbar}{2}\sqrt{\frac{N_D}{\epsilon_s m^*}} \tag{2.34}$$

Comparing the energy E_{00} to the thermal energy kT, for $E_{00} \ll kT$ thermionic emission dominates, for $E_{00} \approx kT$ thermionic-field emission, and for field emission $E_{00} \gg kT$ [26]. The tunnelling current density can be expressed as [20]:

$$J_t \sim \exp\left(-\frac{q\phi_B}{E_{00}}\right) \tag{2.35}$$

In the case where there are low doping levels in semiconductors, tunnelling becomes more significant under reverse bias than forward bias. This occurs because under large reverse bias voltages, the electrons in the semiconductor tunnel through the thin potential barrier into the metal [24].

2.7. ION-SOLID INTERACTION

2.7.1. Introduction

When an ion penetrates into a solid, it interacts with the target and suffers energy loss until it eventually comes to rest at a particular depth inside the material. The energy transfer of the ion to the solid is caused by elastic and inelastic collisions with the target. The interaction of these energetic ions and the target atoms are the basis of ion damage in solid materials. This can modify the structure and/or the properties of materials. A discussion of the related process is now discussed.

2.7.2. Ion stopping

There are two main processes of energy loss which are to be considered. These are elastic interactions with the target atoms called nuclear stopping and inelastic collisions with the target atoms due to the collision with the electrons of the target is called electronic stopping. The total stopping power is defined by the energy loss per unit distance of the matter traversed. It is the sum of the two energy loss components and is given by [27]:

$$S_{\text{total}} = \left(\frac{\mathrm{d}E}{\mathrm{d}x}\right)_{\text{nuclear}} + \left(\frac{\mathrm{d}E}{\mathrm{d}x}\right)_{\text{electronic}} \tag{2.36}$$

The E represents the ion projectile energy and x the path length. Each of these terms can be seen as a function of the ion velocity (which is proportional to the ion energy). Fig. 2.12 shows both these terms. It can clearly be seen from this figure that nuclear stopping dominates at low energies and electronic stopping dominates at higher energies.

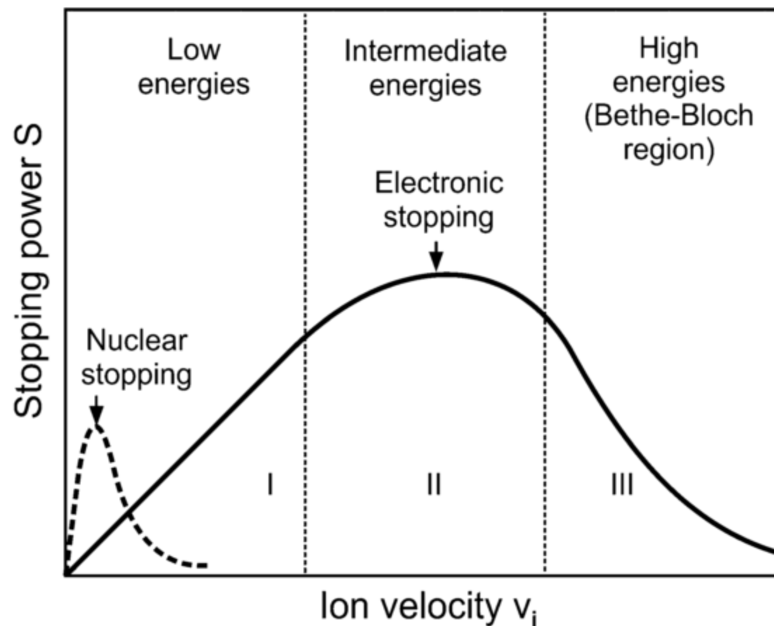

Fig. 2.12 Nuclear and electronic components of the stopping power as a function of ion velocity.

2.7.3. Nuclear stopping

When the charged ion collides with the nuclei of the target atoms, the process can be described in terms of a two body elastic collision model. Since this implies the conservation of momentum and kinetic energy, the kinetic energy transfer can be given as

$$T = \frac{2m_1 m_2}{(m_1 + m_2)^2} E_0 (1 - \cos\theta) \tag{2.37}$$

where m_1 is the mass of the incident ion, m_2 is the mass of the nucleus of the target atom, E_0 is the incident energy of the projectile, θ is the scattering angle in the centre of mass of the system. The maximum energy transfer is reached when $\theta = 180°$. And is given by

$$k = \frac{4m_1 m_2}{(m_1 + m_2)^2} \tag{2.38}$$

Incident ions can modify a crystal lattice by displacing a target atom when the projectile kinetic energy is larger than the threshold displacement energy E_d. This displacement energy is the minimum kinetic energy required to produce a permanent displacement.

2.7.4. Electronic stopping

Electronic stopping power is more complex than the two body interaction model of nuclear stopping power. The approaching ion has to interact with many electrons whereby the concentration is much denser than the nuclei. In addition, the electrons may be stripped form the ions as they traverse the target material. This leads to a continuous modification of the incident ion charge state. Various models, including the Bethe Bloch formula [28,29] therefore have to be used to obtain reasonable predictions.

Ion tracks can form in a material depending on the electronic deposition energy and the nature of the target material. The formation of these ion tracks can be inhibited in a material which has good thermal conductivity and a high melting point [27]. In a material with poor thermal conductivity and low melting point, the ion track may be formed by ions which have relatively low stopping power.

2.7.5. Ion damage

When light ions are implanted into a material, they are initially slowed down mainly by electronic stopping and the displacement damage that they cause is relatively small. Nuclear stopping ultimately becomes the dominant process and the damage caused at the end of the ion track is high. Heavy ions, by contrast may cause uniform damage along their path as they displace the target atoms from the surface of the solid. These ions experience a relatively higher degree of nuclear stopping compare to the light ions. Fig. 2.13 shows a schematic representation of this phenomenon.

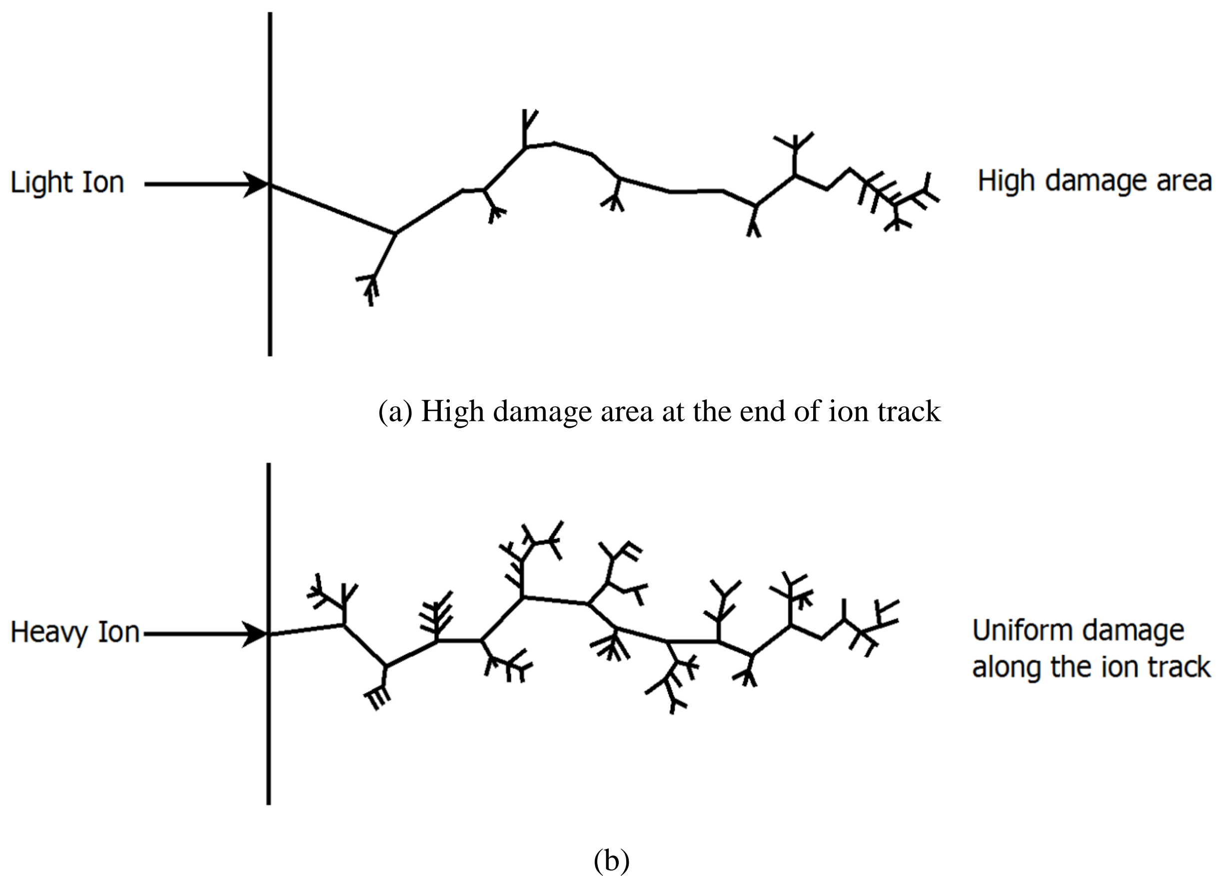

(a) High damage area at the end of ion track

(b)

Fig. 2.13 (a) Light and (b) heavy ion tracks formed in a solid.

REFERENCES

[1] O. Lagerstedt and B. Monemar, Variation of lattice parameters in GaN with stoichiometry and doping, Phys. Rev. B. 19 (1979) 3064. doi:10.1103/PhysRevB.19.3064.

[2] M. Leszczynski, Common crystal structures of group {III} nitrides, in: J.H. Edgar, S. Strite, I. Akasaki, H. Amano, and C. Wetzel (Eds.), Prop. Process. Appl. Gall. Nitride Relat. Compd., INSPEC, London, 1999: p. 3.

[3] T. Hanada, Basic properties of ZnO, GaN, and related materials, in T. Yao and S.-K. Hong, (Eds.), Oxide and Nitride Semiconductors Processing, Properties, and Applications, Springer-Verlag, Berlin Heidelberg, 2009: p. 3.

[4] S. Strite and H. Morkoç, GaN, AlN, and InN: A review, J. Vac. Sci. Technol. B Microelectron. Nanom. Struct. 10 (1992) 1237. doi:10.1116/1.585897.

[5] P. Kung, The Rise of III-nitrides : An Introduction, in: M. Razeghi and M. Henini (Eds.), Optoelectron. Devices III-Nitrides, 2004: pp. 11–15.

[6] O. Ambacher, Growth and applications of Group III-nitrides, J. Phys. D. Appl. Phys. 31 (1998) 2653–2710. doi:10.1088/0022-3727/31/20/001.

[7] M. Razeghi and M. Henini, Introduction, in: M. Razeghi and M. Henini (Eds.), Optoelectron. Devices III-Nitrides, Elsevier Ltd, Kidlington, 2004: p. 1.

[8] A. Ionascut-Nedelcescu, C. Carlone, A. Houdayer, H.J. Von Bardeleben, J.L. Cantin, and S. Raymond, Radiation hardness of gallium nitride, IEEE Trans. Nucl. Sci. 49 I (2002) 2733. doi:10.1109/TNS.2002.805363.

[9] J. Nord, K. Nordlund, and J. Keinonen, Molecular dynamics study of damage accumulation in GaN during ion beam irradiation, Phys. Rev. B. 68 (2003) 184104. doi:10.1103/PhysRevB.68.184104.

[10] W. Soluch, E. Brzozowski, M. Lysakowska, and J. Sadura, Determination of mass density, dielectric, elastic, and piezoelectric constants of bulk GaN crystal, IEEE Trans. Ultrason. Ferroelectr. Freq. Control. 58 (2011) 2469. doi:10.1109/TUFFC.2011.2103.

[11] J.I. Pankove and D. Shade, Photoemission from GaN, Appl. Phys. Lett. 25 (1974) 53. doi:10.1016/S0022-0248(97)00082-1.

[12] M. Suzuki, T. Uenoyama, and A. Yanase, First-principles calculations of effective-mass parameters of AlN and GaN, Phys. Rev. B. 52 (1995) 8132. doi:10.1103/PhysRevB.52.8132.

[13] H. Harima, Properties of GaN and related compounds studied by means of Raman scattering, J. Phys.: Condens. Matter 14 (2002) R967.

[14] Z. Fang, D.C. Look, W. Kim, and Z. Fan, Deep centers in n -GaN grown by reactive molecular beam epitaxy, Appl. Phys. Lett. 72 (1998) 2277.

[15] P. Hacke, A. Maekawa, N. Koide, K. Hiramatsu, and N. Sawaki, Characterization of the shallow and deep levels in Si doped GaN grown by metal-organic vapor phase epitaxy, Jpn. J. Appl. Phys. 33 (1994) 6443. doi:10.1143/JJAP.33.6443.

[16] I.-H. Lee, A.Y. Polyakov, N.B. Smirnov, A. V Govorkov, A. V Markov, and S.J. Pearton, Deep-level studies in GaN layers grown by epitaxial lateral overgrowth, Thin Solid Films. 516 (2008) 2035. doi:10.1016/j.tsf.2007.07.144.

[17] D.C. Look, Z.Q. Fang, and B. Claflin, Identification of donors, acceptors, and traps in bulk-like HVPE GaN, J. Cryst. Growth. 281 (2005) 143. doi:10.1016/j.jcrysgro.2005.03.035.

[18] P.R. Hageman, V. Kirilyuk, W.H.M. Corbeek, J.L. Weyher, B. Lucznik, M. Bockowski, S. Porowski, and S. Müller, Thick GaN layers grown by hydride vapor-phase epitaxy: hetero- versus homo-epitaxy, J. Cryst. Growth. 255 (2003) 241. doi:10.1016/S0022-0248(03)01259-4.

[19] M. Ilegems and H.C. Montgomery, Electrical properties of n-type vapor-grown gallium nitride, J. Phys. Chem. Solids. 34 (1973) 885.

[20] Sze, Physics of semiconductor devices, Second Edition, John Wiley & Sons, Inc., New York, 1981.

[21] S.J. Pearton, Processing of wide band gap semiconductors, First edition, Wlliam Andrew Publishing, Norwich, New York, 2000.

[22] H. Morkoç, S. Strite, G.B. Gao, M.E. Lin, B. Sverdlov, and M. Burns, Large bandgap SiC, III-V nitride, and II-VI ZnSe based semiconductor device technologies, J. Appl. Phys. 76 (1994) 1363. doi:10.1063/1.358463.

[23] S. Nakamura and G. Fasol, The blue laser diode: GaN based light emitters and lasers, First edition, Springer, Berlin, 1996. doi:10.1007/978-3-662-03462-0

[24] E.H. Rhoderick and R.H. Williams, Metal-semiconductor contacts, Second edition, Oxford University Press, New York, 1988. doi:10.1002/0470068329.

[25] H. Morkoç, Nitride semiconductors and devices, First edition, Springer, Berlin, 1999.

[26] D.K. Schroder, Semiconductor material and device characterization, Third Edition, John Wiley & Sons, Inc., Hoboken, 2006. doi:10.1063/1.2810086.

[27] W. Wesch and C.S. Schnohr, Swift heavy ion irradiation of Crystalline Semicondcutors, in W. Wesch and E. Wendler (Eds.), Ion Beam Modification of Solids: Ion-Solid Interaction and Radiation Damage, Springer, Switzerland, 2016: p. 367, 398-399.

[28] F. Bloch, Ann. Phys, Zur Theorie des Durchgangs schneller Korpuskularstrahlen durch Materie, (Leipzig) 16 (1933) 285.

[29] H. Bethe, Ann. Phys. (Leipzig), Zur Bremsung rasch bewegter Teilchen beim Durchgang durch Materie, 5 (1930) 324.

Chapter 3

Defect theory and characterization

3.1. DEFECT THEORY

3.1.1. Introduction

There are structural disorders and impurities which can be introduced in a semiconductor. These interruptions of the lattice periodicity of a crystal are commonly referred to as defects. They can primarily be introduced in two ways, namely growth and processing. The former includes the intentional or unintentional introduction of defects during the growth of the material. Doping is an example of this process. The latter is the post-growth introduction of defects in a material by different processes. These processes can include amongst others ion irradiation, different metal deposition methods, electron beam exposure (EBE), and inductively coupled plasma (ICP) processing.

A defect free semiconductor crystal is of little use in modern electronics. The presence of defects plays a significant role as states in the bandgap of a semiconductor can substantially alter the electronic properties of a semiconductor. The knowledge of the characteristics of defects is essential in designing and fabricating semiconductor based devices. These defects are important as they can either be beneficial or detrimental to a device depending on the application. In the case of fast switching devices, defects are beneficial whereas in light emitting devices they are detrimental [1].

Defects can be classified according to dimensionality as indicated by Yam et.al. [2]. The first are the zero dimensional defects. These point defects are the alteration of a lattice by just one atomic site. Examples include interstitials, vacancies, and substitutional atoms. The second type of defect is the one dimensional defect. These are defects which are associated with a direction. An example would be a dislocation, which is divided into screw and edge dislocations. The other two classifications include two dimensional (planar) and three dimensional (volume) defects. The former include grain boundaries and stacking faults while the latter includes voids and cracks. In this study the zero dimensional defects will be considered.

3.1.2. Point defects

Point defects can be classified into intrinsic and extrinsic defects. Intrinsic defects are formed as a result of a re-arrangement of the host atoms. Extrinsic defects, however, are formed due to the introduction of foreign defects. These foreign atoms can be introduced intentionally or unintentionally and are called solutes or impurities, respectively. The three primary types of point defects are now discussed. A vacancy defect occurs when a lattice has an unoccupied site. In a binary semiconductor like GaN, this can be due to a Ga atom not being on a Ga site and/or a N atom not being on a N site. An interstitial defect occurs when there are additional atoms in between the lattice sites. This type of defect can be divided into self and foreign interstitials. A self-interstitial arises when one of the native atoms lies between the lattice sites and a foreign-interstitial occurs when the interstitial atom is a different species from the host. A substitutional defect occurs when an impurity atom occupies the lattice site of a host atom. An antisite is a type of substitutional defect where, in the case of GaN, a Ga atom is on a N site or a N atom on a Ga site. Another point defect to consider is the Frenkel pair. This occurs when a self-interstitial atom is close to a vacancy. Fig. 3.1 shows a schematic representation of all these point defects.

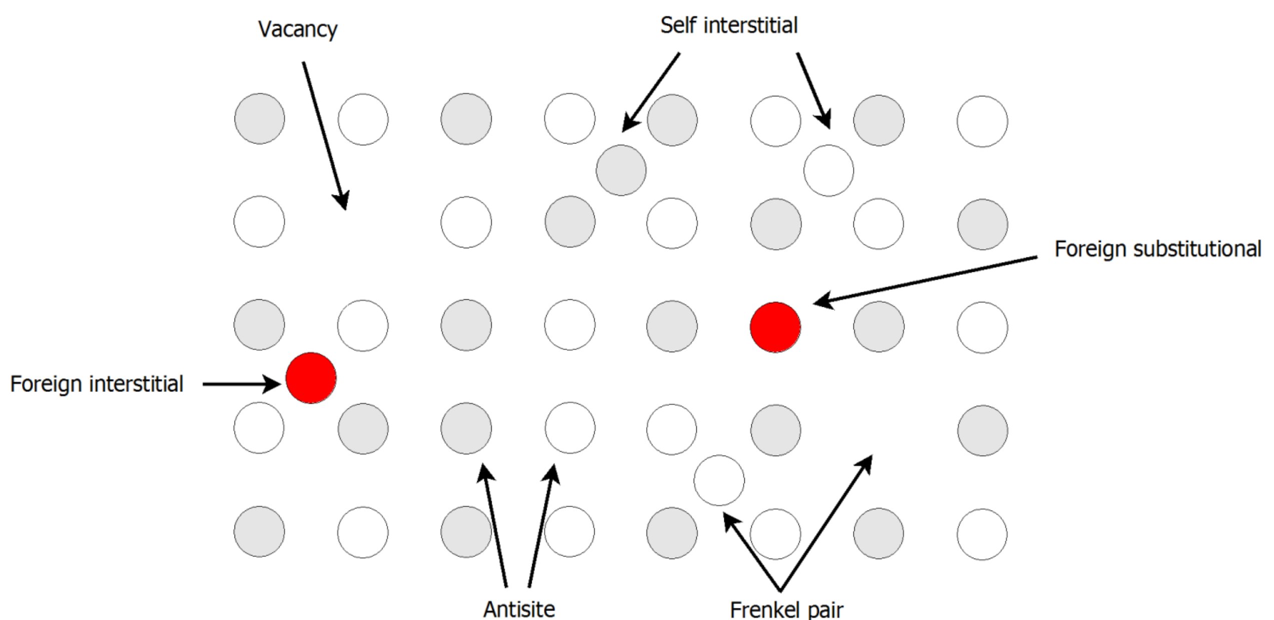

Fig. 3.1 A schematic representation of different point defects

3.1.2.1. Shallow levels

Shallow levels are point defects that bind to only one charge carrier. They can usually be treated by the hydrogen model of an atom. An excess or missing electron is bonded to the impurity atom in the same manner as in a hydrogen atom where an electron is bonded to a proton. A modified hydrogen model to predict the energy levels is given by the following equation:

$$E_n = \frac{m^*}{m_0 \varepsilon^2 n^2} E_H \tag{3.1}$$

where m^* is the electron or hole effective mass, m_0 is the electron rest mass, ε is the relative dielectric constant of the semiconductor, n is the number of the state, and E_H is the hydrogen atom ground state energy (13.6 eV). The Bohr radius is given by:

$$a_n = \frac{m_0 \varepsilon n^2}{m^*} a_H \tag{3.2}$$

where a_H is the Bohr radius (0.53 Å).

Shallow levels require little energy, typically thermal energy, to ionise. Their wave functions are spread out over several Bohr radii. They are formed by either an acceptor or donor atom which has been substituted for an atom which is intrinsic to a material. They are important to semiconductor materials as they can affect the conductivity or conduction (*n* or *p*) type of the semiconductor. When there are both acceptors and donors in the semiconductor, the carrier concentration can be calculated by the equation $|N_a - N_d|$ where N_a is the concentration of acceptors and N_d is the concentration of donors. The semiconductor will be *n*-type or *p*-type depending on which impurities are more numerous.

When an atom has an extra valence electron it is a donor and the conductivity is *n*-type. In this case the defect level will be close to the conduction band. If, however, an atom has one less valence electron than it should have, it is an acceptor and leads to *p*-type conductivity. A defect level formed by an acceptor will be closer to the valence band. In GaN, Ga is a group III element while N is group V. Thus if Si, which is a group IV element, is substituted for Ga, it will act as a donor. This will make the semiconductor *n*-type [3]. If, however, it is substituted for N, it will act as an acceptor, making the semiconductor *p*-type. If, however, Mg, which is a group II element, is substituted for Ga, the semiconductor will be *p*-type [4]. This is because Mg will act as an acceptor because it has one less electron than Ga.

The substitution of the host atoms with impurities in order to affect the conductivity of the material is referred to as doping. Doping in GaN usually occurs during growth. Doping can be intentional or unintentional. Intentional doping in GaN can be achieved by using dopants during the growth of the semiconductor [5]. In some semiconductors doping can be achieved after growth by ion implantation as well as the introduction of radiation induced defects [6]. Unintentional doping usually occurs during the growth of a semiconductor and is due to contaminants during growth. These contaminants can be either O or Si [7]. The growth of undoped GaN has largely resulted in *n*-type conductivity presumably due to contamination.

Fig. 3.2 illustrates the levels induced by impurities in the band gap of a semiconductor. The donor levels and acceptor levels are close to the band edges of the conduction and valence band, respectively. In order to maintain charge neutrality, the Fermi level shifts towards the conduction band when the material is *n*-type and towards the valence band when the semiconductor is *p*-type. Also illustrated are the electron and hole traps, which form part of the deep levels. These are now discussed in the next section.

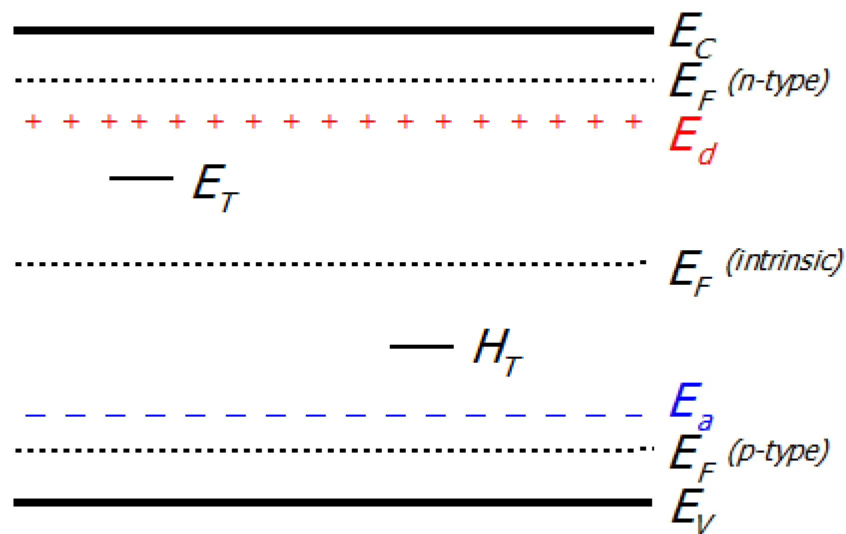

Fig. 3.2 A diagram illustrating the effects on the Fermi level by the acceptor E_a and donor E_d levels close to the band edges. Also shown are the positions of an electron and a hole trap.

3.1.2.2. Deep levels

Defects, which have properties that deviate significantly from those that are predicted by the hydrogen model, are called deep levels. They require great ionisation energies and contribute

minimally to the free carriers in a semiconductor. Deep levels will generally have a higher probability of capturing the majority charge carriers closer to their respective band edges. Those levels in the upper part of the band gap will have a high probability of capturing electrons from the conduction band. Similarly, levels in the lower part of the band gap will have a high probability of capturing holes from the valence band. Deep levels generally bind charge carriers more strongly than shallow levels. The wave function of a deep level is highly localised and thus has a high charge density.

3.1.3. Trapping and emission of carriers at deep energy levels

Discrete levels are created in the bandgap of a semiconductor when a foreign atom is added to a lattice. These discrete levels can also be created when there are crystal imperfections within the lattice. Defects act as generation centres when the carrier density is below its equilibrium value and as recombination centres when there are excess carriers in the semiconductor [8]. These levels affect the electrical and optical properties of a semiconductor by the capture and emission of charge carriers.

Fig. 3.3 outlines the processes which can occur between the conduction band, defect level and the valence band. Fig. 3.3 (a) shows a process in which the defect level first captures an electron from the conduction band and then captures a hole from the valence band. This process is referred to as recombination. In Fig. 3.3 (b), the electron is emitted to the conduction band followed by the hole being emitted to the valence band. This process is called generation. A defect level is defined as a trap if the charge carrier is captured by the defect level and then emitted from the defect level from which it came. This is illustrated in Fig. 3.3 (c) where the electron is captured and then emitted back to the conduction band and Fig. 3.3 (d) where the hole is captured and then emitted back into the valence band. There are a number of factors which can determine whether a defect level is a trap or a generation-recombination centre. These include the position of the Fermi level, the temperature, the defect energy level, and the capture cross sections of the defect.

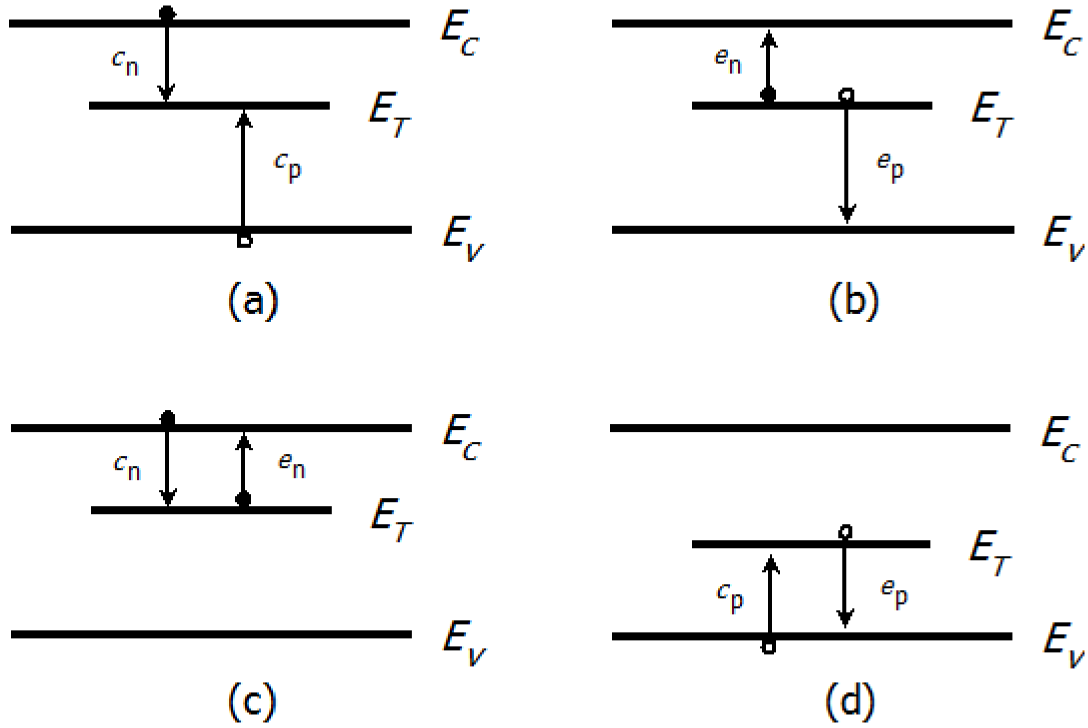

Fig. 3.3 Defect levels (a) recombination (b) generation (c) electron trap (d) hole trap.

The electron capture rate is defined as the number of electrons which are captured per second by the trap (G-R centre). The electron capture rate is given by the following equation:

$$c_n = \sigma_n \langle v_n \rangle n \tag{3.3}$$

where σ_n is the capture cross section (cm^2), $\langle v_n \rangle$ is the average electron thermal velocity (cm·s^{-1}) and n is the electron concentration in the conduction band. The capture cross section can vary in size depending on whether the G-R centre is neutral, positively, or negatively charged. The average thermal velocity is given by the equation

$$\langle v_n \rangle = \sqrt{3kT/m^*} \tag{3.4}$$

where k is the Boltzmann constant, T is the temperature (Kelvin), and m^* is the effective mass. The electron concentration can be defined as

$$n = N_C \exp\left[\frac{E_F - E_C}{kT}\right] \tag{3.5}$$

where N_C is the effective density of states (cm^{-3}) at the conduction band edge, E_F is the Fermi level (eV), and E_C is the conduction band energy. The thermal emission rate of electrons from a defect energy level E_T into the conduction band is given by

$$e_n = \frac{\sigma_n \langle v_n \rangle N_C}{g} \exp\left(-\frac{E_C - E_T}{kT}\right) \tag{3.6}$$

where g is the degeneracy of the defect level, E_T is the energy level of the defect below the conduction band minimum, and E_C - E_T is the activation energy of the deep level defect. The effective density of states can be expressed as

$$N_C = 2M_C \left(\frac{2\pi m^* kT}{h^2}\right)^{3/2} \tag{3.7}$$

where M_C is the conduction band minima and h is Planck's constant. Since $\langle v_n \rangle N_C$ is dependent on T^2, it follows that if e_n is measured as a function of temperature, E_T can be calculated from the Arrhenius plot of e_n/T^2 vs. $1/T$. It must be mentioned that the capture cross section calculated in this manner is referred to as the apparent capture cross section. This apparent capture cross section does not take into account temperature dependence. The true capture cross section, however, might depend on temperature. In the case of a capture barrier, the temperature dependence of the (true) capture cross section is given by

$$\sigma = \sigma_\infty \exp\left[-\frac{\Delta E_\sigma}{kT}\right] \tag{3.8}$$

Here σ_∞ is the capture cross section as T tends to ∞ and ΔE_σ is the thermal activation energy for a charge carrier to overcome the capture barrier.

3.2. DEFECT CHARACTERISATION

3.2.1. Introduction

There are different characterisation techniques that can be used to investigate defects in semiconductors. These techniques include optical (photoluminescence), structural (atomic force microscopy {AFM} and x-ray diffraction {XRD}) and electrical (deep level transient spectroscopy {DLTS} and Hall measurements) methods. In this study electrically active defects were investigated. Electrically active defects can be subdivided into shallow level and

deep level defects. Shallow level defects, such as dopants, affect the conductivity of a semiconductor. The type of conductivity can be obtained by Hall measurements. In an *n*-type semiconductor, shallow levels, as indicated in an earlier section, lie close to the conduction band. Deep level defects, however, lie towards the centre of the band gap. They can be detrimental or beneficial to a semiconductor depending on the application. The study of these electronic states in semiconductors therefore becomes imperative as semiconductors form the basis of the electronics industry.

Early methods, which were used to detect defects, were hampered by the low sensitivity of the equipment used. Space charge spectroscopy has proven to be quite useful in the characterisation of electrically active defects. In particular, DLTS has evolved as a powerful technique for the characterisation of deep level defects in semiconductors. It can be used to provide valuable information in order to improve various aspects of semiconductor devices. These include production and manufacturing of semiconductors, the examination of trace element contamination, process induced defects and analysis of the effect of deep levels on device performance [9]. A discussion of the importance of DLTS and a brief description of how it operates will now be given.

3.2.2. DLTS description

The DLTS technique was first introduced by D.V. Lang in 1974 [10]. It has provided a useful tool as it has been used to study electrically active defects in semiconductors. Also, earlier methods which were used to detect defects were hampered by, amongst others, the low sensitivity of the equipment used. With the DLTS technique, low concentration defects and deep electronic levels in semiconductors can be studied. It is one of the most sensitive defect detection techniques. At doping levels of 10^{17} cm^{-3} the DLTS technique has a defect concentration sensitivity of around 10^{12} defects cm^{-3}. This implies that in a semiconductor material it has a sensitivity factor of 10^{-5} of the free carrier concentration [10].

The DLTS technique probes the space charge region of a semiconductor to characterise electronically active defects. This is in contrast to some characterisation techniques, which are designed to characterise defects in bulk samples. DLTS measures deep levels, which are deeper in the energy band gap than those formed by dopants. The electronic transition of holes to the valence band and electrons to the conduction band is measured as a change in the

junction capacitance of a device. As defined in the previous chapter, the depletion width of Schottky barrier diodes is given by

$$w = \sqrt{\frac{2\varepsilon_s(V_{bi} + V)}{qN_D}} \tag{3.9}$$

where V is the applied voltage. The capacitance due to the depletion region is related to the depletion width by

$$C = \frac{\varepsilon_s A}{w} = \sqrt{\frac{q\varepsilon_s N_D}{2(V_{bi} + V)}} \tag{3.10}$$

where A is the area of the metal-semiconductor contact. From Equation 3.10 it can clearly be seen that if a change in the concentration of the trapped charge carriers in the depletion region occurs, there will be a change in the capacitance. The depletion width that is calculated in GaN used for this study is in the order of 10^{-7} m. Increasing the reverse bias voltage probes the semiconductor in the depletion region so that the lower this bias voltage the deeper the sampling depth.

DLTS is a powerful defect analysis technique from which one can calculate the concentration, the activation energy, the majority carrier capture cross-section and the depth distribution of the defect. A defect can be uniquely identified using the DLTS technique by simply calculating the activation energy and the carrier cross section. The combination of these two quantities is known as the DLTS "signature". There are a number of factors that make DLTS a choice technique for analysing defects. These include high sensitivity and non-destructive characterisation. One can also distinguish between majority and minority carriers. This can be identified by a positive or a negative peak.

The limitation of the DLTS characterisation technique is that it does not provide the physical structure of the defects measured. This makes it difficult to correlate the defect level to the defect itself. It is also difficult to correlate DLTS to other techniques. For example, when compared to RBS it is difficult to compare the concentration of impurities as these may or may not correspond to the number of electrically active defects measured.

3.2.3. DLTS principles

There are a number of steps which are taken to complete the DLTS measuring process. These are shown in Fig. 3.4. A reverse bias voltage is applied to the metal-semiconductor junction. This increases the depletion width. The reverse bias is applied long enough for steady state conditions to be reached. This is to ensure that all traps in the depletion region are empty i.e. that there are no carriers which are captured. A forward bias filling pulse is applied to the junction. This reduces the space charge region and therefore increases the capacitance of the depletion width. As the space charge region is decreased, the empty traps in this region are filled (the pulse has to be long enough that the traps are filled).

When the pulse is removed the reverse bias returns to its quiescent state. The space charge region increases but it becomes larger than it was to compensate for the electrons, which are trapped. The capacitance is also lower than it was under quiescent conditions. The electrons, above the Fermi level in the filled traps of the depletion region, are then emitted from these traps due to thermal processes. These electrons are rapidly swept out of the depletion region by the electric field in this region so that they are not able to be re-trapped. As the traps empty, the depletion width and the capacitance return to their quiescent values.

A series of capacitance transients can be measured if the voltage cycle is applied a number of times. If this is done at different temperatures then a number of these capacitance transients with different decay time constants will be realised. As a result, a DLTS spectrum can be obtained by analysing these capacitance transients.

The density of traps, assuming that the filing pulse is long enough such that they are all occupied by charge carriers at time t after removing the pulse width, is given by

$$N(t) = N_T \exp(-e_n t) \tag{3.11}$$

where N_T is the trap concentration and e_n is the thermal emission rate. From equations of e_n and $N(t)$ it can be shown that a change in the trap concentration will result in a change in the capacitance, which is dependent on time. If $N_T \ll N_D$, then the junction capacitance is given by

$$C(t) = C_0 - \Delta C_0 \exp(-e_n t) \tag{3.12}$$

where C_0 is the capacitance at equilibrium reverse bias voltage and ΔC_0 the change in capacitance directly after removing the filing pulse.

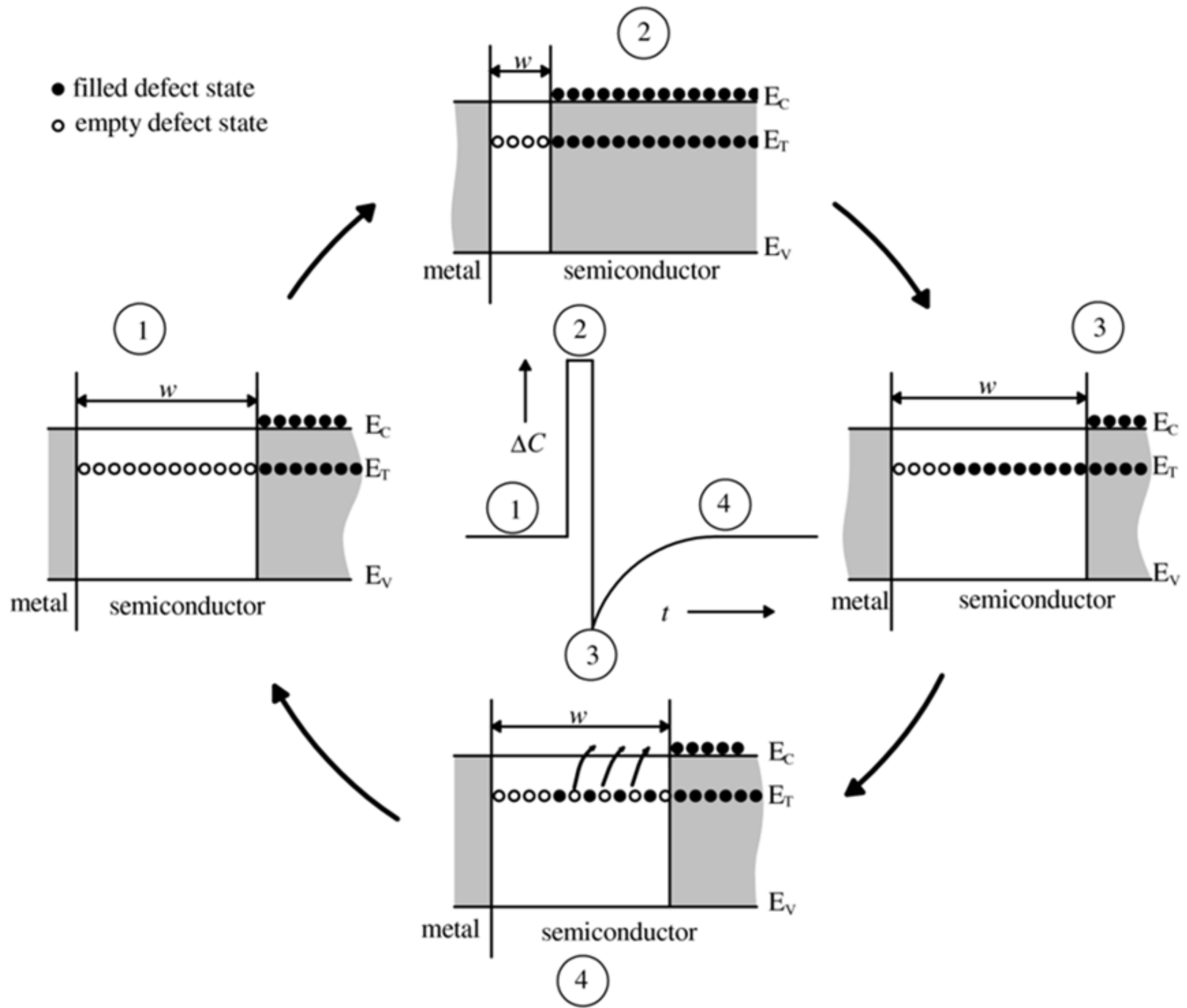

Fig. 3.4 A schematic showing the evolution of defect states within a space charge region in order to acquire a DLTS transient signal.

The DLTS signal is directly related to the defect concentration when the signal is small enough. This is the case where the number of defects is much smaller than the free carrier concentration, $N_T \ll N_D$. Thus the number of defects can be obtained by

$$N_T \approx 2N_D \frac{\Delta C}{C} \tag{3.13}$$

The sensitivity of the junction capacitance to trapped charges depends on the location of the charge in the depletion region. This sensitivity varies linearly from zero at the metal-semiconductor interface to a maximum at the depletion width. This implies that the capacitance measurements are insensitive to traps, which are located at the metal-semiconductor junction. Two regions can thus be considered within the space charge

region [11]. The first region is close to the metal-semiconductor junction. It consists of shallow donors and deep levels, which are above the Fermi level. The second region is called the transition region. The width of this region, which is independent of the depletion width, is given by

$$\lambda = \sqrt{\frac{2\varepsilon(E_F - E_T)}{q^2 N_D}} \tag{3.14}$$

This transition region is the distance from the depletion region edge to where the Fermi level intersects the defect level. Fig. 3.5 illustrates the relationship between the transition region and the depletion width of a band bending diagram of a Schottky barrier diode. The diagram shows the energy bands at zero bias and when a reverse bias is applied [11].

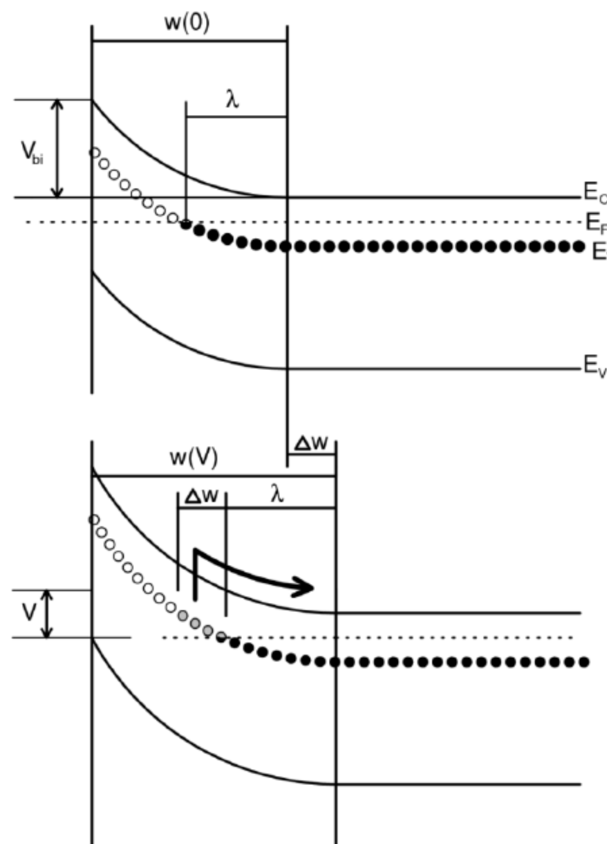

Fig. 3.5 Energy band diagram of the depletion width of a Schottky barrier diode showing the λ region and the change in the depletion width under zero bias (top) and reverse bias (bottom). (redrawn from [12])

3.2.4. Rate window concept

The DLTS system is designed to detect the maximum response within a preselected rate window. The system responds by giving a peak output associated with the rate window as shown in Fig. 3.6. The DLTS signal, which denotes a change in capacitance during different times, can be plotted as a function of increasing temperature. The rate-window concept is usually implemented by the DLTS system using a lock-in amplifier and a dual-gated integrator (also known as a double boxcar). These were originally attached by D.V. Lang in 1974 [10].

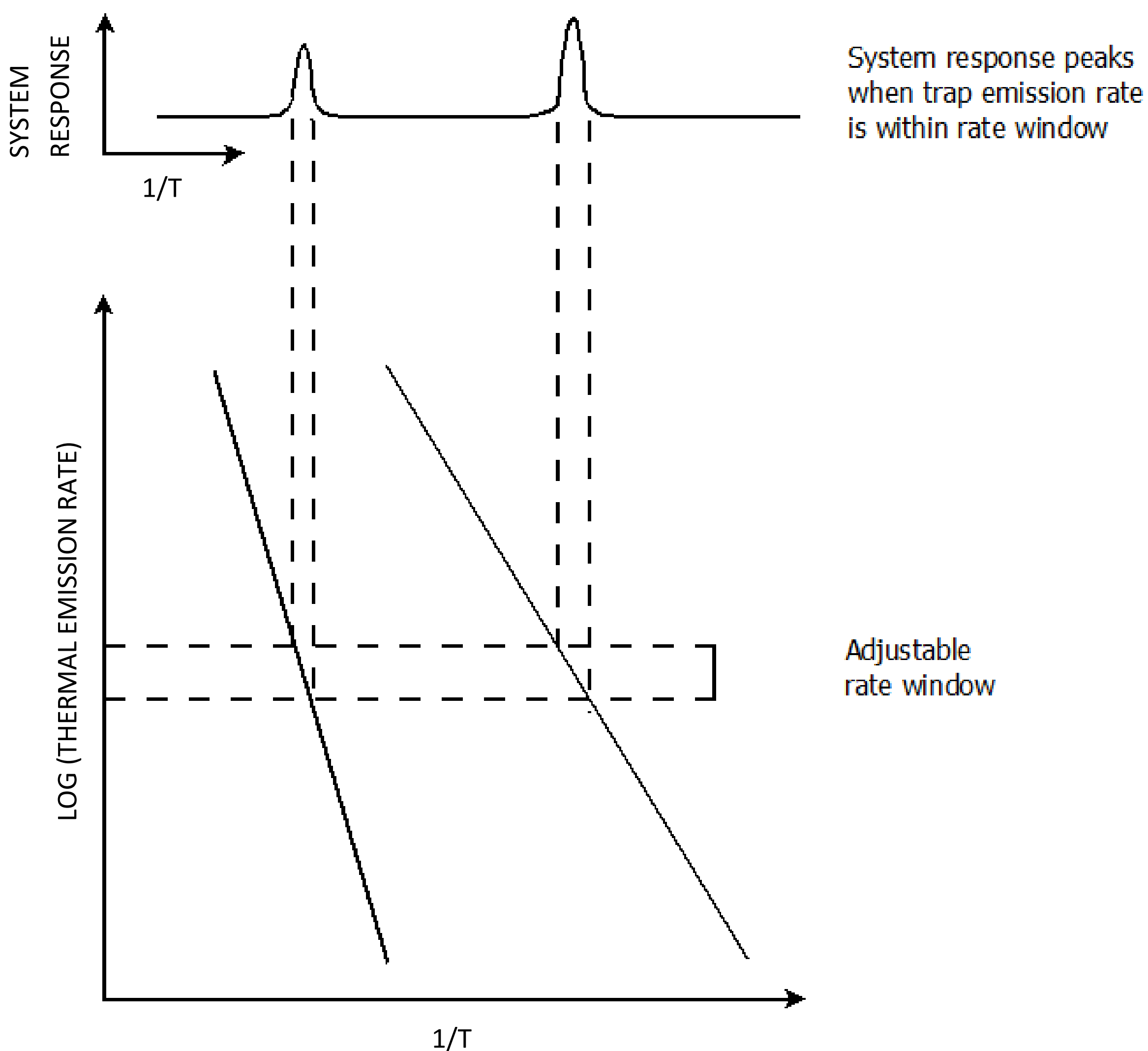

Fig. 3.6 This figure illustrates the peak in the output signal of a defect level when the decay component of the input signal corresponds with a pre-selected rate window [10]

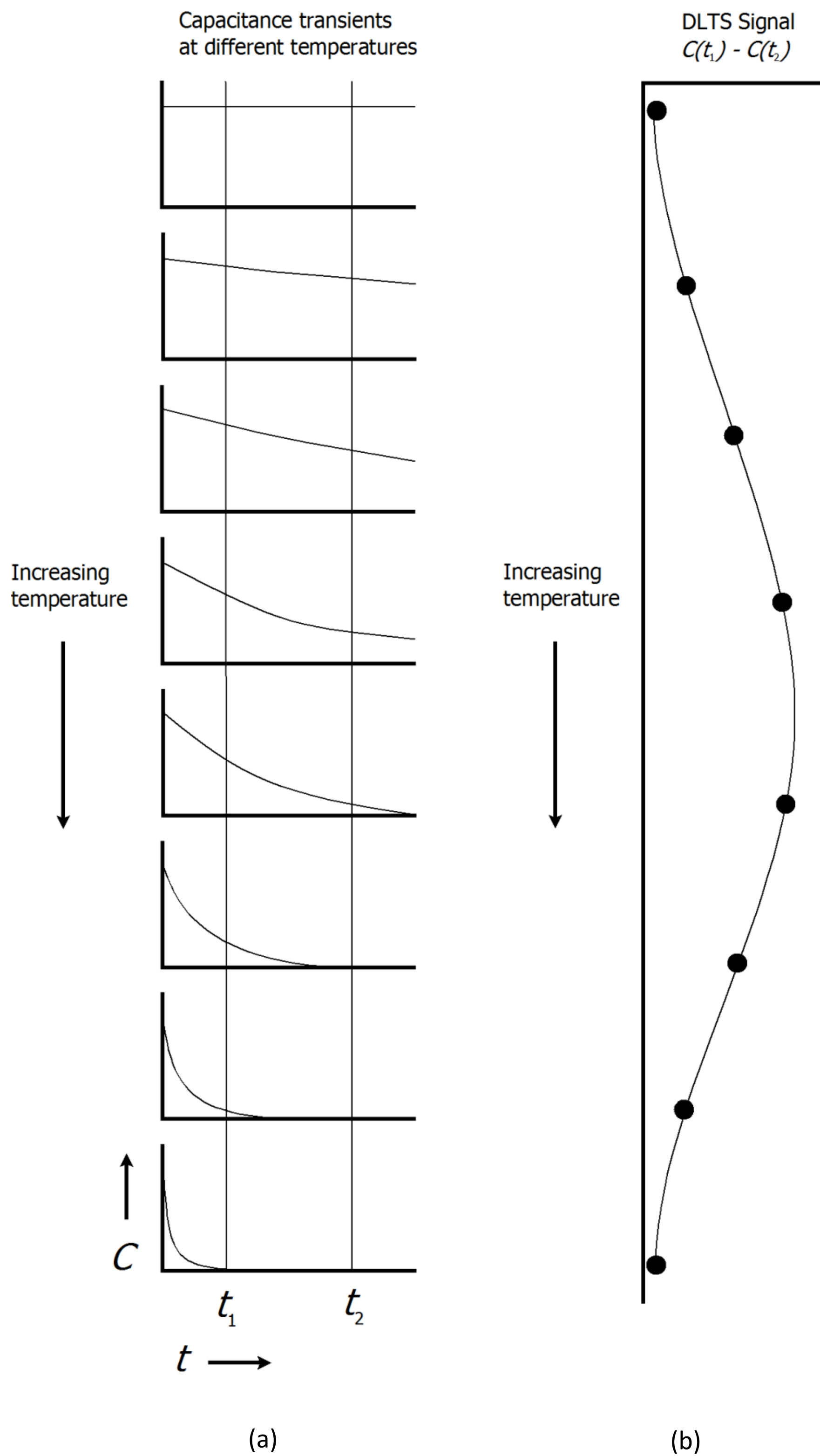

Fig. 3.7 A schematic diagram depicting how a DLTS spectrum is obtained from the rate window concept. (a) Various capacitance transients obtained at different times with increasing temperature and (b) the resulting spectrum from these transients.

The DLTS signal can be obtained by subtracting the capacitance measured at two different times namely t_1 and t_2. The difference in these two times, $t_1 - t_2$, is a time filter known as the rate window. The double boxcar calculates the difference in the capacitance $C(t_1) - C(t_2)$. This difference is converted into a DLTS signal of a thermally activated process and this signal is given by the equation

$$S(T) = \Delta C_0[exp(-t_1/\tau) - exp(-t_2/\tau)] \tag{3.15}$$

where ΔC_0 is the capacitance change due to the filling pulse at $t = 0$.

Fig. 3.7 shows how a DLTS spectrum is obtained. It can be observed from the diagram that at low temperatures, the DLTS signal is very low. This is caused by the small change in capacitance between t_1 and t_2 which is almost the same for both times. As the temperature increases the decay rate of the capacitance transient also increases. This causes the change in capacitance between t_1 and t_2 to increase, thus the DLTS signal increases up to a maximum at some temperature. As the temperature continues to increase, the decay rate of the transient also increases. At high temperatures the capacitance transient decays so fast that it decays before t_1. This implies that the DLTS signal will also be low at higher temperatures.

The peak of the DLTS signal will appear at different temperatures for different rate windows. If equation 3.15 is differentiated with respect to τ and the derivative set to equal zero, then the time constant at which the peak of the DLTS spectrum occurs is given by

$$\tau_{max} = \frac{t_1 - t_2}{\ln(t_1/t_2)} \tag{3.16}$$

This time constant is related to the peak emission rate such that $e_n = 1/\tau_{max}$. In order to calculate the activation energy of a defect level, several spectra are taken at different emission rates. Equation (3.6) can be written such that

$$\tau_{max} = \frac{1}{e_n(T)} = \frac{1}{(K_n T^2 \sigma_n)} e^{\frac{E_C - E_T}{kT}}$$

where

$$K_n = \frac{2(2\pi)^{\frac{3}{2}} 3^{\frac{1}{2}} m^* k^2 M_C}{g\hbar^3} \tag{3.17}$$

Take the natural log of both sides of the equation, the following equation can then be obtained:

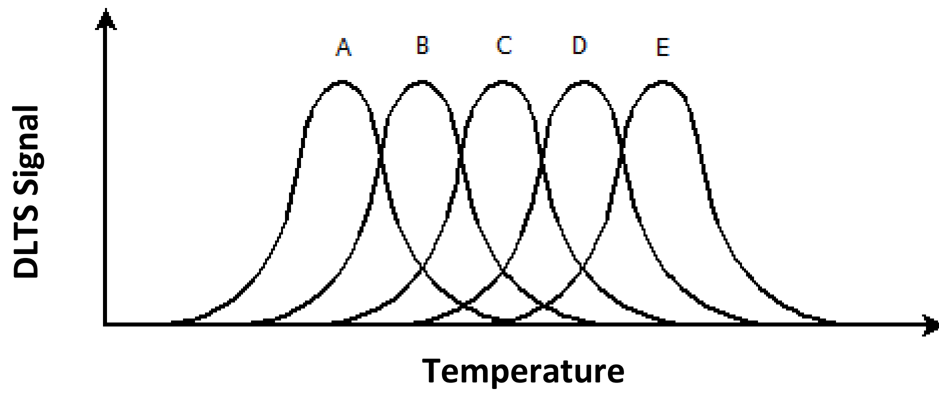

(a)

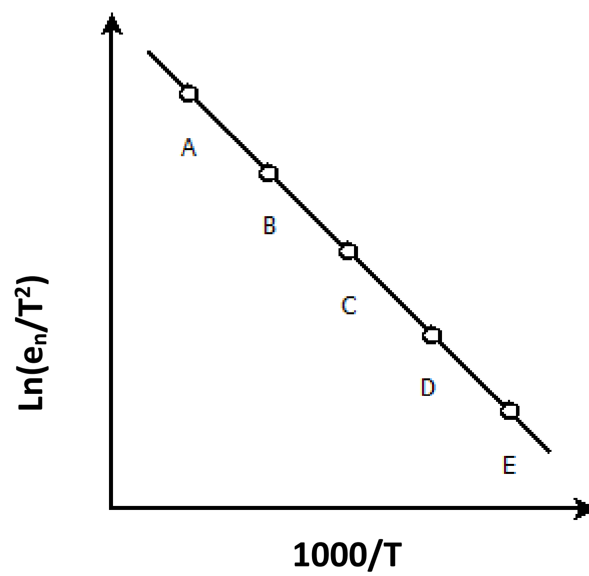

(b)

Fig. 3.8 Diagram of (a) the shift in peak position of the DLTS signal at various emission rates and (b) the Arrhenius plots obtained from the peak positions.

$$\ln(\tau_{max}T^2) = -\ln(K_n\sigma_n) + \frac{E_C - E_T}{1000k}\frac{1000}{T} \qquad (3.18)$$

This equation is a straight line graph called an Arrhenius plot and can be obtained by plotting $\ln(\tau_{max}T^2)$ versus $1000/T$. It contains the peaks of the spectra at different temperatures. The slope of the line $(E_C - E_T)/1000k$ gives the defect energy blow the conduction band and the y-axis intercept $-\ln(K_n\sigma_n)$ gives its capture cross section. T in this equation, is the temperature of the DLTS peak. An illustration is shown in Fig. 3.8.

When using conventional DLTS, states with similar emission rates can be separated if they have different activation energies. The separation of these states can be done by performing a DLTS scan at various rate windows. Doing this alone, however, will not be of any advantage if the activation energies are similar. It can occur that states, which have similar emission rates have different capture properties. In such instances, the deep state with the smaller capture cross section can be excluded from the measurement by reducing the filling pulse width. Another method would be to observe the peak shift as the electric field changes. It is also at times possible to separate a state which shows a strong Poole-Frenkel effect from one which does not.

3.2.5. Defect identification

The identification and mapping of defects are integral if defects in semiconductors are to be understood. Space charge spectroscopy assists in identifying defect parameters such as the energy, capture cross section and trap concentration of defects. They do not, however, give direct information about the chemical composition, which gives rise to the defect levels. A defect identification procedure has been proposed which can be used for identifying defects using DLTS [9]. When one has performed the experiment and analysed the results, there are couple of steps which can be taken to understand the results that have been found as outline by Benton et al [9]. A comparison of the DLTS signature can be made with the defects already identified in literature. This will be useful in compiling a defect library from which we can compare the different processes, such as irradiation and annealing, which introduce or induce defects.

The notation used for most defects in this thesis is $E_{0.xxx}$, where 0.xxx is the activation energy of the defect in eV. The activation energy is as determined by an Arrhenius plot. In order to compare defects, both activation energy and capture cross-section values should be

compared, taking uncertainties into account. Although the identity of a defect is often determined by comparing its capture cross section and activation energy with reference values, the most reliable method is to compare Arrhenius plots.

3.2.6. Defects in GaN

There are two peaks which are commonly observed by DLTS in GaN. The nature of the defects giving rise to these peaks is as yet unknown. The first of these has been observed by various authors in GaN layers which have been grown by MOCVD, HVPE and RMBE. The labels and activation energies of these defects have been reported as trap *D* (0.24 eV) [13], E_1 (0.264 eV) [14], DLN1 (0.25 eV) [15], and trap D (0.25 eV) [16,17]. It has been suggested by Fang *et al.* that trap D seems to be related to threading dislocations. As the epilayer thickness is decreased, the concentration of trap D increases with increasing threading dislocations [17].

The second defect, which has been a dominant defect in GaN, has also been reported by various authors. They have reported it as E_2 (0.58 eV) [14], *D*2 (0.60 eV) [18], DLN_3 (0.59 eV) [15], trap B (0.60 eV) [16], and trap B (0.61 eV) [17]. Haase *et. al.* have suggested that the *D*2 centre that they have observed is the N antisite [18]. This is based on the effects of 270 keV N^{2+} implantation and annealing.

It has been reported by Look *et al.* [16], however, that trap B is unchanged by either electron or plasma irradiation. This, they argue, suggests that it is either unrelated to simple point defects, or it is related to pre-existing defects such as the Ga vacancy. Trap B is often the dominant trap in material grown by different methods and therefore they suspect that it is related to either O, Si, C, or Ga vacancy as these are the most common defect species in *n*-GaN. It is, however, argued that it cannot be a simple shallow donor such as a Ga vacancy since it is an electron trap. This trap, they further argue, could be a complex arrangement of other impurities and defects [16].

REFERENCES

[1] M.A. Reshchikov, Point defects in GaN, in: L. Romano, V. Privitera, and C. Jagadish (Eds.), Semiconductors and semimetals: Defects in semiconductors, Academic Press, Waltham, 2015.

[2] F.K. Yam, L.L. Low, S.A. Oh, and Z. Hassan, Gallium nitride: An overview of structural defects, in: P. Predeep (Ed.), Optoelectron. - Mater. Tech., InTech, Rijeka, 2011: pp. 99–136. doi:10.1007/s12026-012-8302-x.GENETIC.

[3] W. Götz, N.M. Johnson, H. Amano, and I. Akasaki, Deep level defects in n-type GaN, Appl. Phys. Lett. 65 (1994) 463. doi:10.1063/1.112337.

[4] M.A. Reshchikov and H. Morkoç, Luminescence properties of defects in GaN, J. Appl. Phys. 97 (2005) 61301. doi:10.1063/1.1868059.

[5] S. Nakamura, T. Mukai, and M. Senoh, Si- and Ge-doped GaN films grown with GaN buffer layers, Jpn. J. Appl. Phys. 31 (1992) 2883. doi:10.1143/JJAP.31.2883.

[6] V.A. Kozlov and V. V Kozlovski, Doping of semiconductors using radiation defects produced by irradiation with protons and alpha particles, Semiconductors 35 (2001) 735.

[7] E.R. Weber, J. Kruger, and C. Kisielowski, New materials: Gallium nitride, in: K.A. Jackson, W. Schroter (Eds.), Handb. Semicond. Technol., Wiley-VCH, Weinheim, 2000: pp. 772–808.

[8] D.K. Schroder, Semiconductor material and device characterization, 3rd Edition, John Wiley & Sons, Inc., Hoboken, 2006. doi:10.1063/1.2810086.

[9] J.L. Benton, Characterization of defects in semiconductors by deep level transient spectroscopy, J. Cryst. Growth. 106 (1990) 116. doi:10.1016/0022-0248(90)90293-T.

[10] D.V. Lang, Deep-level transient spectroscopy: A new method to characterize traps in semiconductors, J. Appl. Phys. 45 (1974) 3023.

[11] M. Stavola, Identification of defects in semiconductors, Academic Press, San Diego, 1999.

[12] F.D. Auret and P.N.K. Deenapanray, Deep level transient spectroscopy of defects in high-energy light-particle irradiated Si, Crit. Rev. Solid State Mater. Sci. 29 (2004) 1. doi:10.1080/10408430490442458.

[13] Z-Q. Fang, D.C. Look, W. Kim, Z. Fan, A. Botchkarev and H. Morkoç, Deep centers in *n*-GaN grown by reactive molecular beam epitaxy, Appl. Phys. Lett. 72 (1998) 2277.

[14] P. Hacke, T. Detchprohm, K. Hiramatsu, N. Sawaki, K. Tadatomo, and K. Miyake, Analysis of deep levels in *n*-type GaN by transient capacitance methods, J. Appl. Phys. 76 (1994) 304.

[15] W. K. Götz, J. Walker, L. T. Romano, N. M. Johnson, and R. J. Molnar, Thickness dependence of electronic properties of GaN epi-layers, Mater. Res. Soc. Symp. Proc. 449 (1996) 525.

[16] D.C. Look, Z.-Q. Fang, and B. Claflin, Identification of donors, acceptors, and traps in bulk-like HVPE GaN, J. Crys Growth 281 (2005) 143.

[17] Z.-Q. Fang, D.C. Look, X.-L. Wang, J. Han, F.A. Khan and I. Adesida, Plasma-etching-enhanced deep centres in *n*-GaN grown by metalorganic chemical-vapor deposition, Appl. Phys. Lett. 82 (2003) 1562.

[18] D. Haase, M. Schmid, W. Kurner, A. Dörnen, V. Härle, F. Scholz, M. Burkard, and H. Scheizer, Deep-level defects and n-type-carrier concentration in nitrogen implanted GaN, Appl. Phys. Lett. 69 (1996) 2525.

Chapter 4

Experimental techniques

4.1. INTRODUCTION

This chapter will look at the experimental techniques, which were used in this study. It gives a general description while the specifics of each technique will be given in more detail in subsequent chapters as they relate to each relevant investigation. The first section deals with the preparation of the samples by giving details of the cleaning method. In the second section the metal deposition techniques are explained. Ohmic contacts were deposited using the electron beam deposition system while the Schottky contacts were deposited using the resistive deposition system. Section 4.4 elaborates on the thermal annealing of the samples and the equipment used. Since the samples were irradiated with ions, a brief explanation of the ion implantation and irradiation conditions is given in section 4.5. The electrical characterisation of the samples is described in the last two sections. The *I-V* and *C-V* characterisation measurement techniques and equipment are explained in section 4.5. The DLTS setup, used to characterise electrically active defects, is described in the last section.

4.2. SAMPLE PREPARATION

The purpose of cleaning a sample prior to metal deposition is to remove surface oxides and other contaminants, which can affect the operation of a fabricated device. A well-cleaned surface will result in a relatively intimate metal-semiconductor contact, which can lead to thermally stable contacts. There are three primary semiconductor cleaning methods, namely dry (physical), wet (chemical) and vapour (phase) [1]. In this study, wet cleaning was used on Si-doped GaN. The method for cleaning this semiconductor by wet chemical treatment is well-established [2]. There are two primary processes for cleaning a semiconductor wafer using this method, namely degreasing and etching. Firstly, the sample had to be degreased in order to remove any organic impurities that were on the surface of the GaN sample. These were boiled in trichloroethylene and isopropanol for 3 minutes each. The samples were then rinsed in de-ionised water to prepare them for etching. The etching process included placing

the samples in boiling aqua regia ($HCl:HNO_3$ of 3:1) for 10 minutes and then dipping them in an $HCl:H_2O$ solution for 1 minute. After each etching step, the samples were rinsed in deionised water. In all the rinsing steps, the beaker containing the deionised water was placed in an ultrasonic bath for 2 minutes. Nitrogen gas was used to blow dry the samples to remove any liquid from the samples.

4.3. METAL DEPOSITION

There are a number of methods, which can be used to deposit metals on semiconductors. These include electroplating, alloying, sputtering and evaporation. In this study, only the evaporation techniques were used. These included both resistive (thermal) and electron beam depositions. The resistive evaporation system was used to deposit Schottky contacts while the electron beam system was used for the ohmic contacts. Both these metal contacts were deposited on one side of the GaN substrate as shown in Fig. 4.1. The reason for this is that GaN is grown on a sapphire (Al_2O_3) substrate which is an insulator, thus leaving only one side of the GaN sample to be electrically active. The ohmic contacts were the first metal contacts to be deposited on this active side. A thin glass slide was cut in a rectangular shape and the GaN substrate covered in such a way that only the ohmic contacts could be deposited. Once the ohmic contacts had been deposited, the GaN was placed on a mask in order to deposit the Schottky contacts.

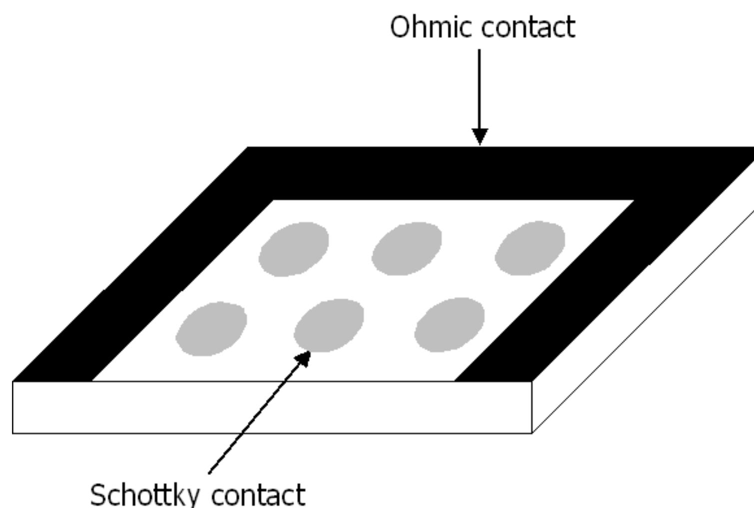

Fig. 4.1 A diagram showing Schottky and ohmic contacts on a GaN substrate.

4.3.1. Electron beam deposition system

The electron beam system employs a physical vapour deposition technique whereby electrons are accelerated onto a source metal with enough energy to evaporate the metal. This system was used in this study as it has the ability to deposit four metals without breaking vacuum. This particular system was installed with an air interlock system, which also allowed samples to be loaded into the system without breaking vacuum. A picture of the deposition system is shown in Fig. 4.2. The electron beam system can reach pressures of as low as 10^{-7} mbar due to a turbo pump that is connected in series with a roughing pump. This vacuum is essential to prevent the reaction of the evaporant with background gases as it traverses the vacuum chamber to the target substrate. The electron beam system was also used because it can melt metals with high melting points such as Ti (1668 °C) and W (3422 °C).

Fig. 4.2 A picture of the electron beam system used for ohmic contact deposition.

4.3.1.1. Ohmic contacts

The electron beam system was used to deposit ohmic contacts on GaN. These contacts consisted of Ti (150 Å)/ Al (2200 Å)/ Ni (400 Å)/ Au (500 Å). The thicknesses of the deposited metals were measured by an Inficon thickness monitor. When choosing an ohmic contact metal for an *n*-type semiconductor, the work function of the metal must be close to or smaller than the electron affinity of the semiconductor. Due to this factor Ti (4.33 eV) and Al

(4.28 eV) are good candidates for ohmic contact formation on *n*-GaN. These contacts have good thermal stability and the contact resistance decreases when annealed at temperatures of up to 700 ℃ [3]. The reaction between Ti and GaN should ideally make an ohmic contact. It has also been argued that when Al is deposited on Ti, the reaction between Ti and Al form a stable and reliable contact [3]. Ti and Al oxidise easily therefore Au is used as a capping layer because it is oxidation resistant. Ni is used as a diffusion barrier to reduce the interaction of Ti/Al with Au [4].

4.3.1.2. Electron Beam Exposure

The electron beam system was also used for the exposure of samples to electron beam deposition conditions without deposition. This experimental technique was carried out in order to investigate the defects, which would be induced under deposition conditions. It was first explored by Coelho *et al.* to investigate the prolonged exposure of Ge to electron beam deposition conditions without deposition [5]. Details of the experiment, as it applies to GaN, will be explained in the results and discussion chapter of the electron beam exposure study.

4.3.2. Resistive deposition system

The resistive evaporation system that was used in this study can reach a vacuum of as low as 10^{-5} mbar. The system has a rough pump in series with a turbo pump, similar to the electron beam system. A glass bell jar was used to enclose the system. In the resistive evaporation system, a crucible made out of a refractory metal was used. The refractory metal was heated by passing a current through it. The amount of current that was used depended on the metal being deposited as metals with a high melting point require a higher current. The resistive evaporation system was used to deposit the Schottky contacts onto the GaN substrate. The deposition rate was between 0.5 and 1 Å/s and this was monitored by an Inficon thickness monitor. A picture of the electron beam system is shown in Fig. 4.3.

A metal with a large work function is required to form a Schottky barrier on GaN. The Schottky contacts for the EBE experiment had thicknesses of Ni (250 Å)/ Au (650 Å) whereas the Cs implantation and Xe irradiation had thicknesses of Ni (200 Å)/ Au (600 Å). The differences in these thicknesses do not considerably affect the electrical properties required for this study. Ni was chosen not only because of its large work function but also because it has good adhesion to GaN. Au was used as a cap layer as it adhered well to Ni, was resistant to oxidation and is a good conductor of electricity.

Fig. 4.3 A picture of the resistive evaporation system used to deposit Schottky contacts.

4.4. ANNEALING

The annealing in this study was performed by a Lindberg annealing furnace. Fig. 4.4 shows a diagram of this system. It has the capability of reaching temperatures of up to 1200 °C. A thermocouple was attached to this system in order to measure the temperature. The annealing furnace had refractory bricks in order to contain the heat within the system. Ohmic contacts formed on GaN were annealed at temperatures of up to 500 °C. This was performed for 5 minutes in an Argon gas ambient. The gas flow rate was set to 2 litres per second.

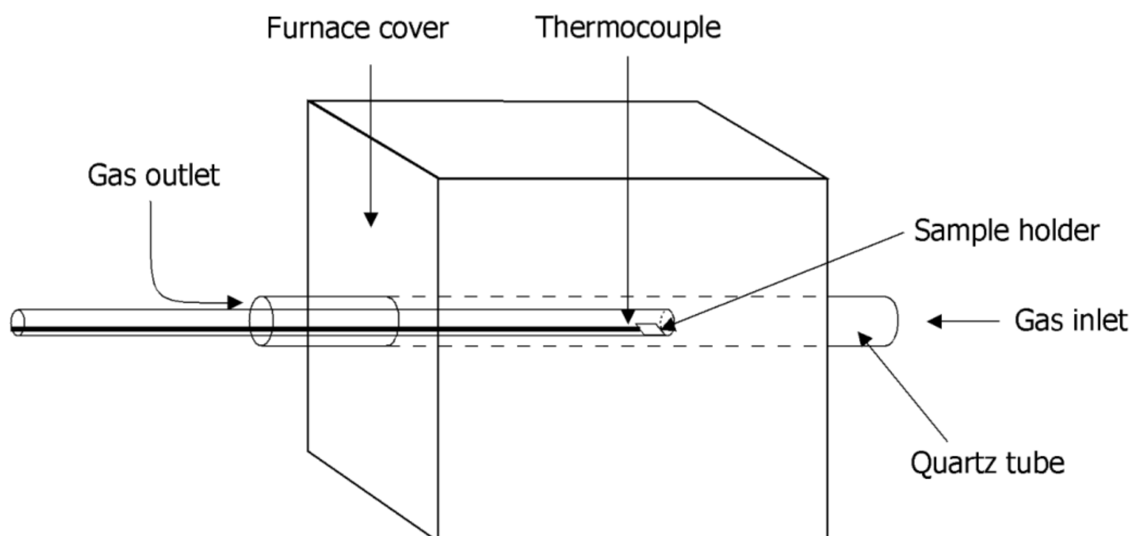

Fig. 4.4 A diagram of the Lindberg annealing system.

4.5. IRRADIATION AND IMPLANTATION

GaN was irradiated with Xe^{+26} ions of 167 MeV with fluence of up to 10^{10} cm^{-2} at room temperature using the IC-100 FLNR JINR cyclotron in Dubna, Russia. A two dimensional beam scanning system was used over the whole sample in order to achieve ion beam homogeneity. A low flux was use to minimise heating the samples. Fig. 4.5 shows the trim profiles which were used for calculations relating to the Xe^{+26} ions [6]. These calculations included the depth of the irradiated ions, and nuclear and electronic stopping loss.

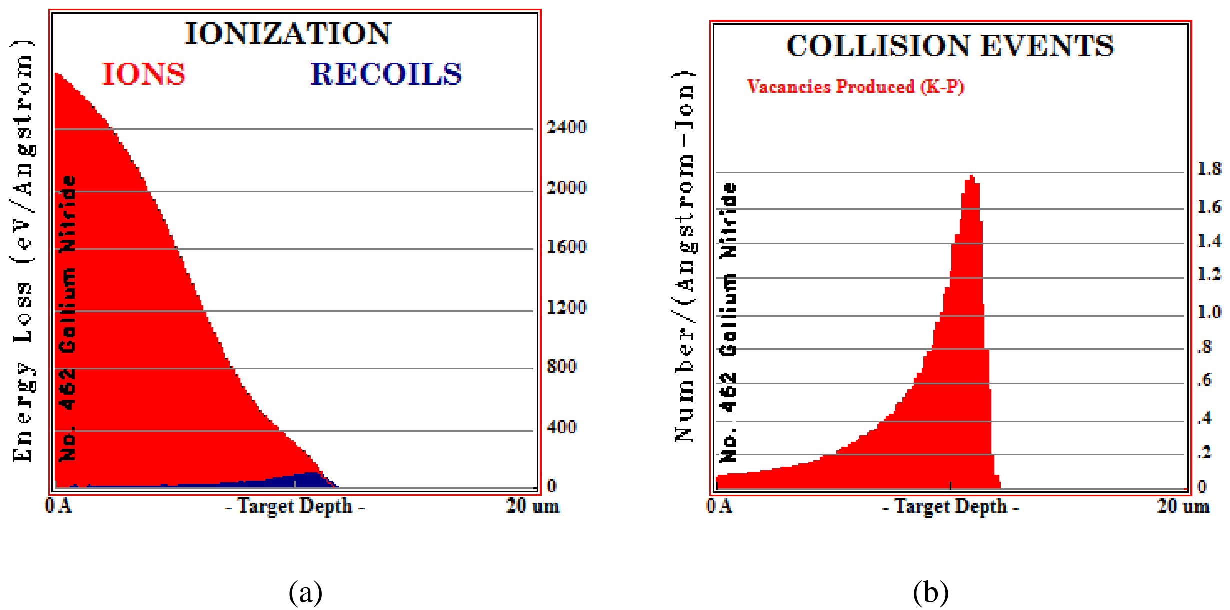

(a) (b)

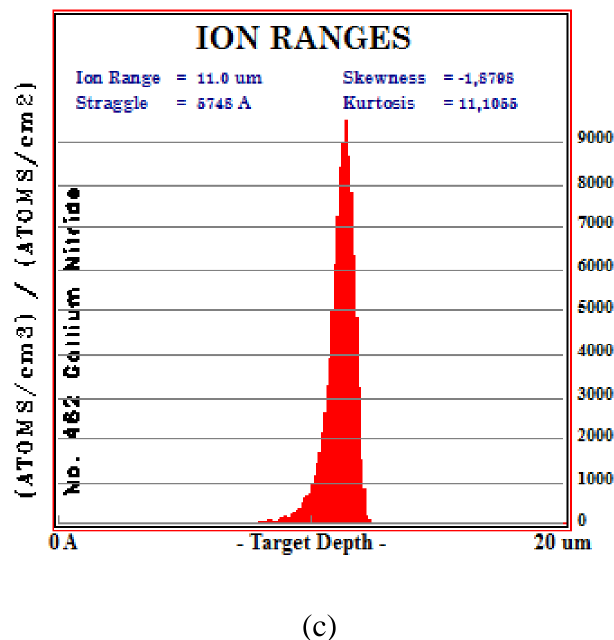

(c)

Fig. 4.5 TRIM profiles of Xe^{26+} irradiated GaN which consist of the (a) energy loss (b) nuclear loss and (c) ion range.

Cs^+ ions of 360 keV were implanted at room temperature with a fluence of up to 10^{11} cm^{-2}. The ion beam was scanned over the whole sample. The implantation was performed at the Institut für Festkörperphysik, Friedrich-Schiller-Universität, Jena, Germany. A low flux was also used during implantation to minimize heating the samples. Fig. 4.6 shows the TRIM profiles which were utilised for Cs^+ ion related calculations [6].

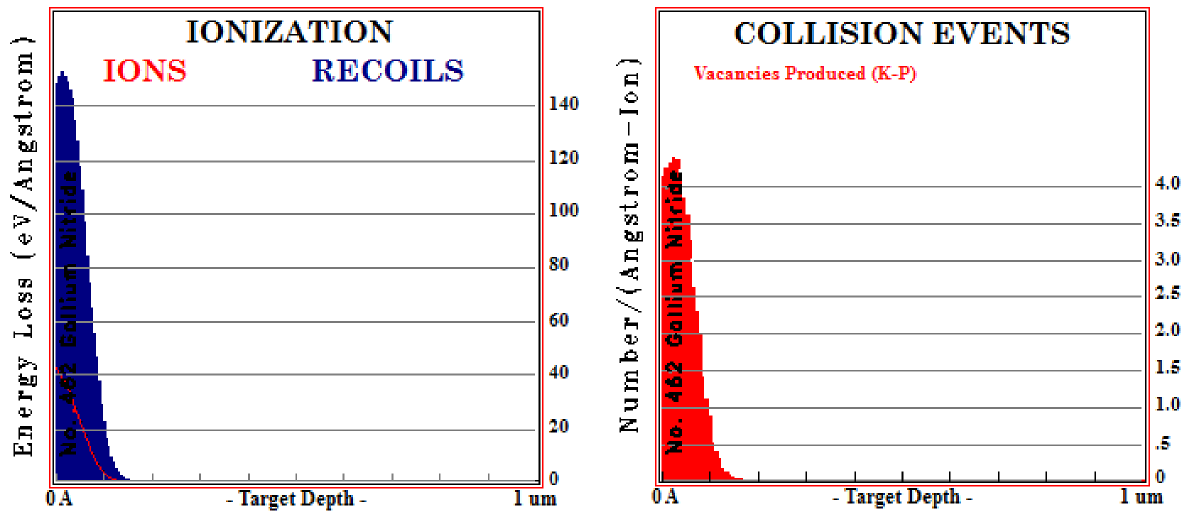

(a) (b),

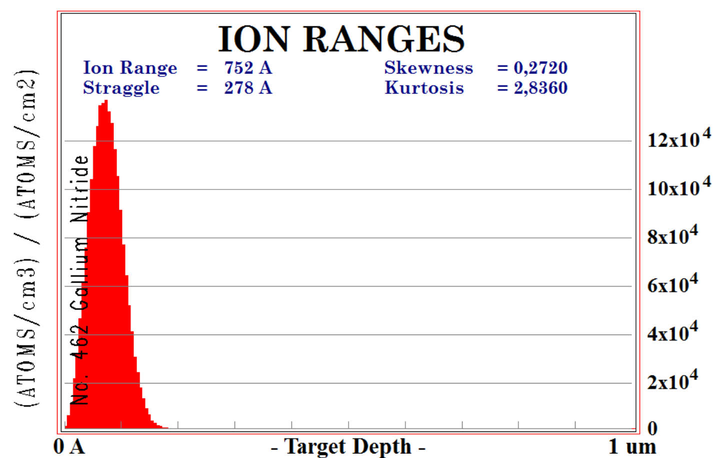

(c)

Fig. 4.6 TRIM profiles of Cs^+ irradiated GaN which consist of the (a) energy loss (b) nuclear loss and (c) ion range.

4.6. DEVISE CHARACTERISATION

4.6.1. Current and capacitance measurements

Electrical characterisation involving both current-voltage (*I-V*) and capacitance-voltage measurements (*C-V*) were performed on the samples. The measurements were done in a dark enclosure to minimise the influence of light on the results obtained. The *I-V* measurements were performed by using an HP 4140B pA Meter/DC Voltage Source. The *I-V* meter has the ability to take current measurements of as low as 10^{-14} A. The *I-V* measurements were performed to ascertain the quality of the Schottky prior to the DLTS measurements. Parameters that can be extracted from the *I-V* measurements include the Schottky barrier height, ideality factor and the series resistance.

The *C-V* measurements were done using an HP 4192 A LF Impedance Analyser. These measurements can be performed to obtain parameters such as the Schottky barrier height, the built-in voltage and the free-carrier concentration. These measurements can also be performed to obtain the uniformity of the doping profile. A LabView™ routine was used to collect data from both the *I-V* and *C-V* measurements. A schematic of the electrical connections of the *I-V* and *C-V* setup up is shown in Fig. 4.7.

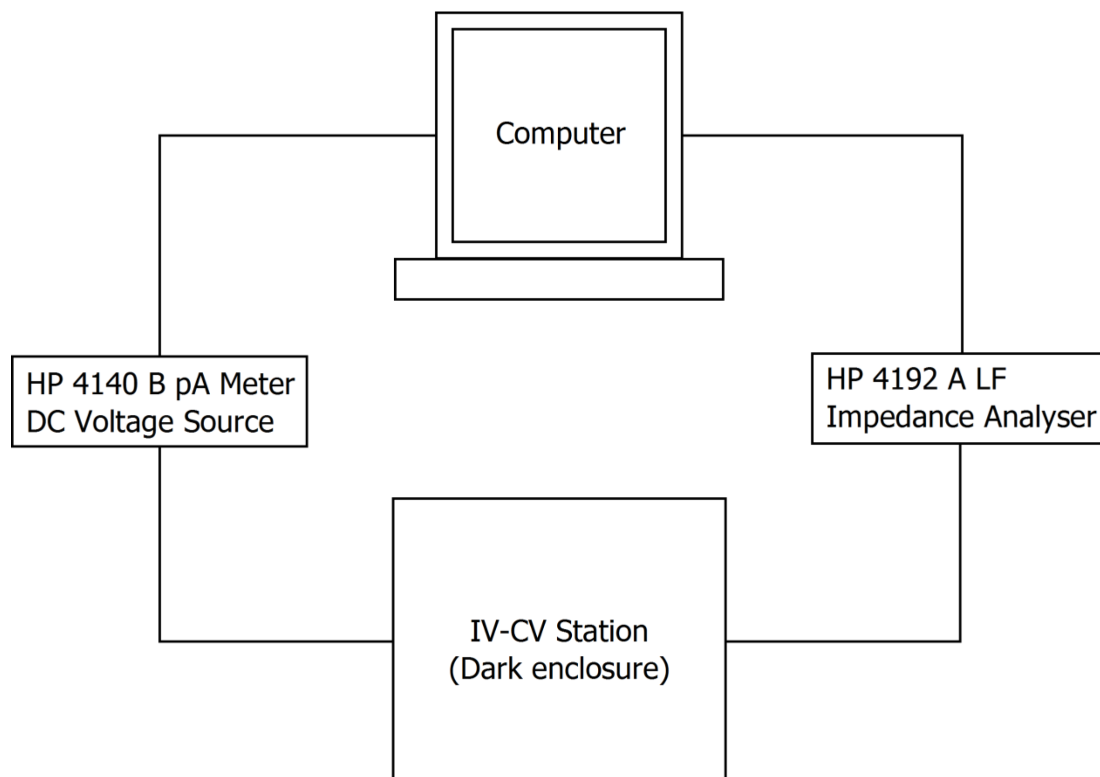

Fig. 4.7 Schematic diagram of the electrical wire connection of the *I-V* and *C-V* station setup.

4.6.2. Deep Level Transient Spectroscopy (DLTS)

The DLTS measurements were performed by a computer controlled system with a closed cycle helium cryostat. The program used for controlling this system was also used to collect the measured data. Measurements were performed in the 16 to 380 K temperature range as this was also the limit of the DLTS system. Fig. 4.8 shows a schematic diagram of the DLTS system used for the experiments in this study. The temperature was controlled by a Lakeshore 332 temperature controller. A thermocouple was connected to the cryostat close to where the sample was placed in order to measure the temperature at the sample. A 1 Mhz Boonton 7200 capacitance meter with 100 mV was used to measure the capacitance from the thermal emission caused by excitation of charge carriers due to the voltage change by the pulse generator. The pulse generator was an HP 33120A 15 MHz arbitrary waveform generator. It was controlled by a Labview^{TM} routine. The capacitance meter, pulse generator and temperature controller were all controlled by a National Instruments GPIB interface card.

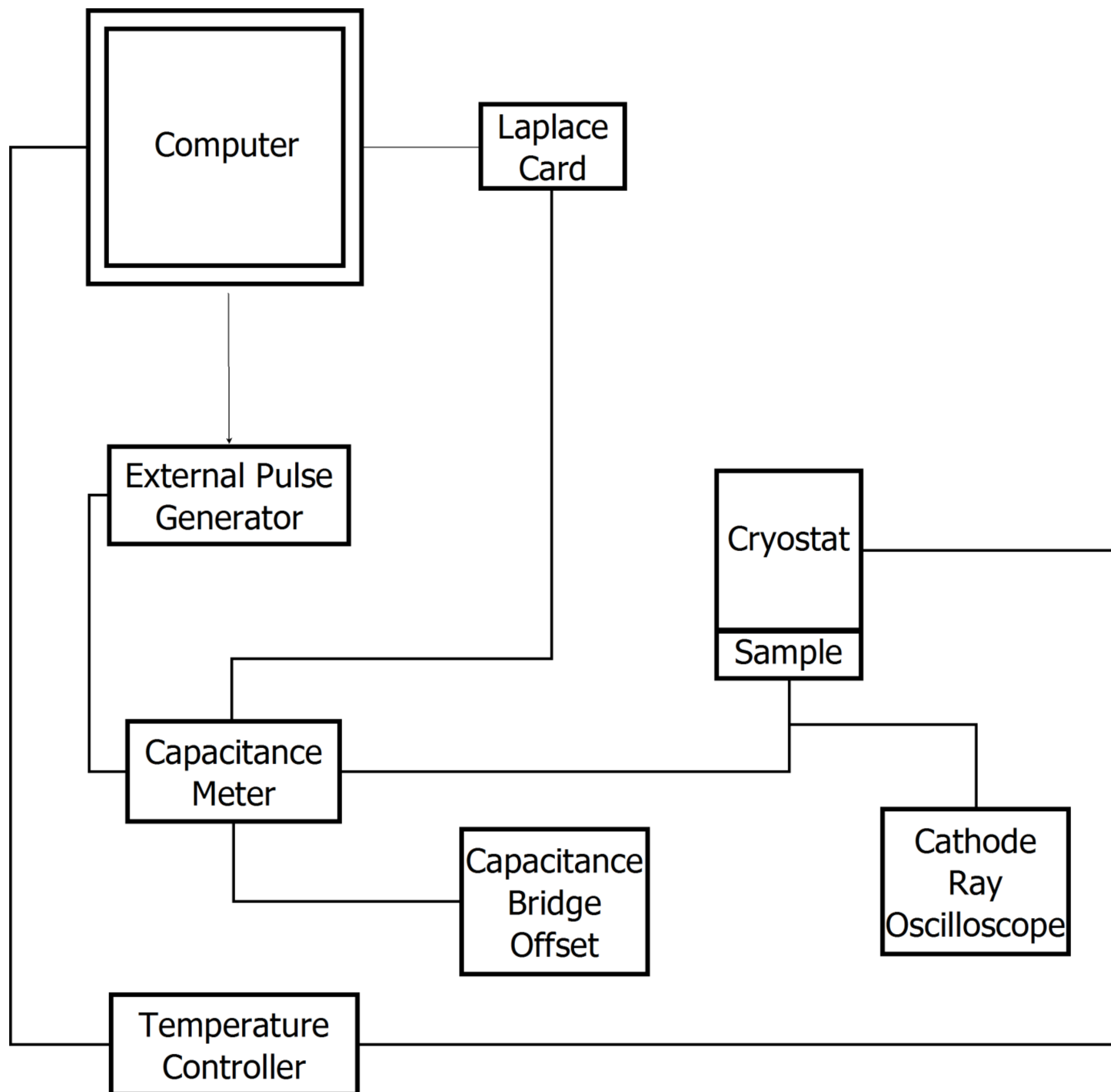

Fig. 4.8 A schematic diagram of the DLTS setup.

REFERENCES

[1] W. Kern, Handbook of semiconductor wafer cleaning technology: science, technology and applications, Noyes Publications, Westwood, 1993.

[2] P. Hacke, T. Detchprohm, K. Hiramatsu, and N. Sawaki, Schottky barrier on n-type GaN grown by hydride vapor phase epitaxy, Appl. Phys. Lett. 63 (1993) 2676.

[3] Q.Z. Liu and S.S. Lau, A review of the metal–GaN contact technology, Solid. State. Electron. 42 (1998) 677. doi:10.1016/S0038-1101(98)00099-9.

[4] S. Ruvimov, Z. Liliental-Weber, J. Washburn, K.J. Duxstad, E.E. Haller, and L. Berkeley, Microstructure of Ti / Al and Ti / Al / Ni / Au Ohmic contacts for n -GaN, Appl. Phys. Lett. 69 (1996) 1556.

[5] S.M.M. Coelho, F.D. Auret, P.J. Janse van Rensburg, J.M. Nel, Electrical characterization of defects introduced in n-Ge during electron beam deposition or exposure, J. Appl. Phys. 114 (2013) 173708. doi:10.1063/1.4828999.

[6] J.F. Ziegler, M.D. Ziegler, and J.P. Biersack, SRIM – The stopping and range of ions in matter (2010), Nucl. Instrum. Meth. B. 268 (2010) 1818.

Chapter 5
Results

5.1. INTRODUCTION

The results of this study will be presented in the form of articles which have been published in internationally recognised, peer reviewed journals. The study consists of the post growth introduction of defects in GaN by various processes. These processes include electron beam exposure, ion implantation and swift heavy ion irradiation. The electrically active defects were characterised by DLTS. The first section is a report on a technique called electron beam exposure. This is a novel method in which a semiconductor is exposed to deposition conditions without deposition. The second section is a study of the defects induced by Cs ions implanted at room temperature. The last section investigates the defects induced by swift heavy ion irradiation.

5.2. ELECTRON BEAM EXPOSURE

Paper 1: DLTS characterization of defects in GaN induced by electron beam exposure

During previous studies [1,2] it was found that electron beam deposition caused damage to samples that was observable by means of DLTS. This damage was found to be removed by shielding the sample from the electron gun. This can have an effect on the electrical properties of the semiconductor, including the introduction of electrically active defects. Therefore, although it is not common practice, it became standard practice in this laboratory to install such a shield. Since the electrons do not have enough energy to cause displacement damage, it is assumed that the damage caused is due to low energy ions accelerated towards the sample from the electron gun, either directly or possibly by collisions with electrons [3]. In order to have a better understanding of this damage, a procedure was developed by means of which a high melting point metal (tungsten) was heated (but not evaporated) by an electron beam while all the shields were removed. This therefore leads to exposure of the semiconductor substrate to deposition conditions (without deposition) for a prolonged period of time during which an easily measureable concentration of defects may be produced. This technique, where GaN was exposed to metal deposition conditions without deposition, was termed electron beam exposure (EBE) [4].

In order to gain deeper insight into the cause of these defects, this study compares the defects induced during EBE to defects caused by other device processing methods such as electron, proton, and gamma irradiation. In the case of Si, GaAs and Ge, it was found that EBE induced some defects different to those induced by particle irradiation. Since the electron beam system is used for metal deposition, a comparison was made to defects obtained after electron beam metal deposition. Lastly a brief summary is given of the results obtained during EBE on various semiconductors such as Ge, Si, and SiC.

It was found that, in contrast to the case of Si, Ge and SiC, EBE in GaN introduced a single defect with an energy 0.12 eV and apparent capture cross section 8.0×10^{-16} cm^2 with properties similar to those of a radiation induced defect previously observed after proton, electron and gamma radiation.

The present author performed the experiments and wrote the publication with input from the co-authors.

Due to space limitations, some relevant information could not be included in the papers, it is therefore included below.

Table 5.1 Electrical properties of the control and EBE processed GaN samples which were extracted from current voltage and capacitance voltage measurements.

	Control	EBE
Current-voltage		
Schottky Barrier Height, ϕ_B (eV)	0.719	0.646
Ideality factor, n	2.01	2.67
Series resistance, R_s (Ω)	20	255
Current at -2 V (A)	3.2×10^{-7}	4.11×10^{-6}
Capacitance-voltage		
Schottky Barrier Height, ϕ_B (eV)	1.01	1.24
Built-in voltage, V_{bi} (V)	0.842	1.08
Free carrier concentration, N_d (cm^{-3})	1.3×10^{17}	3.6×10^{16}

As shown in Table 5.1, the current voltage properties of the fabricated diode deteriorated after EBE processing of the GaN sample. The rectifying properties of the diodes were however still in a good enough condition to perform DLTS measurements.

Publication details

P.N.M. Ngoepe, W.E. Meyer, F.D. Auret, E. Omotoso, and M. Diale, "DLTS characterization of defects in GaN induced by electron beam exposure", Mat. Sci. Semicon. Proc. **64** (2017) 29-31. http://dx.doi.org/10.1016/j.mssp.2017.03.008

Materials Science in Semiconductor Processing 64 (2017) 29–31

Contents lists available at ScienceDirect

Materials Science in Semiconductor Processing

journal homepage: www.elsevier.com/locate/mssp

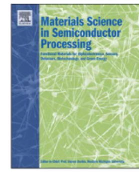

DLTS characterization of defects in GaN induced by electron beam exposure

P.N.M. Ngoepe*, W.E. Meyer, F.D. Auret, E. Omotoso, M. Diale

Department of Physics, University of Pretoria, Private bag X20, Hatfield 0028, South Africa

ARTICLE INFO

Keywords:
GaN
DLTS
Electron beam exposure
Defect

ABSTRACT

The deep level transient spectroscopy (DLTS) technique was used to investigate the effects of electron beam exposure (EBE) on *n*-GaN. A defect with activation energy of 0.12 eV and capture cross section of 8.0×10^{-16} cm^2 was induced by the exposure. The defect was similar to defects induced by other irradiation techniques such as proton, electron, and gamma irradiation. In comparison to GaN, the EBE induced defects in other materials such as Si and SiC are similar to those induced by other irradiation methods.

1. Introduction

GaN is a wide bandgap (≈3.4 eV) binary semiconductor which has been used in various applications because of its optical and electrical properties. These applications include detecting and emitting devices. The resistance to radiation damage has been one of the key factors in making it a suitable candidate for amongst other applications space applications. High energetic particles are known to induce electrically active defects in semiconductors. In particular, different processes, which are known to induce defects, have been investigated in a controlled environment. Doping is a process by which Cho et al. investigated the behavior of defects in intentionally and unintentionally doped *n*-GaN [1]. Various growth methods have been used to investigate deep levels in GaN. These include reactive molecular beam epitaxy (RMBE) [2], metal-organic vapour phase epitaxy (MOVPE) [3], hydride vapour phase epitaxy (HVPE) [4], and epitaxial lateral overgrowth (ELOG) [5]. A study of defects induced by etching using inductively coupled plasma (ICP) was performed by Nakamura et al. [6]. Auret et al. [7] investigated the introduction of defects by different metal deposition techniques. These included electro-deposition, sputter deposition, and electron beam deposition. It was reported by these authors that the deposition of metals using the electron beam deposition system induces defects in GaN. During metal deposition, the semiconductor is usually shielded until the metal is evaporated. In industrial applications, however, it may be difficult to shield the samples until just before evaporation. A novel method, termed electron beam exposure (EBE), has been explored by Coelho et al. [8] whereby Ge was exposed to electron beam deposition conditions without depositing the metals. This was with the view of investigating the effect that prolonged exposure of the samples to deposition conditions would have on the defect properties of the sample. In this study, we investigate the effect of electron beam exposure on GaN using DLTS.

2. Experimental

The study was performed on a Si doped *n*-type GaN wafer which was grown by HVPE. This wafer had a carrier concentration of 1×10^{17} cm^{-3}. The GaN wafer was degreased by boiling in trichloroethylene and isopropanol for 3 min each. Boiling aqua regia was used to etch the sample for 10 min. After each cleaning step, the sample was rinsed 3 times in de-ionised water. An HCl:H_2O solution was then used as the last etching step. Thereafter the sample was blown dry with N_2. Ohmic contacts consisting of Ti (150 Å)/Al (2200 Å)/Ni (400 Å)/Au (500 Å) were deposited using the electron beam evaporation system. The ohmic contacts were annealed for 5 min in flowing Ar. Prior to loading the sample in the electron beam system, the sample was dipped in an HCl:H_2O solution to remove contaminants that might have formed on the surface. The sample was then placed in the electron beam chamber. There are two main sources of particles in an electron beam system. These included particles that are released from the filament from which the electrons are accelerated onto the target metal and also particles which are evaporated from the metals being deposited. The electron gun was shielded from the target sample. This was done to reduce stray particles from the electron gun that might impinge on the sample. Whilst in the electron beam system chamber, the sample was exposed to electron beam conditions without evaporating any metals. A crucible containing tungsten was heated at a current of 100 mA for exposure times of 50 and 80 min. Tungsten was used as a target metal due to its high melting point (3422 °C). It can simulate electron beam deposition conditions of metals with lower melting points without evaporation. Ni (250 Å)/ Au (650 Å) Schottky contact was deposited using a resistive evaporation system, a process that is known not to

* Corresponding author.
E-mail address: phuti.ngoepe@up.ac.za (P.N.M. Ngoepe).

http://dx.doi.org/10.1016/j.mssp.2017.03.008
Received 11 October 2016; Received in revised form 8 February 2017; Accepted 7 March 2017
1369-8001/ © 2017 Published by Elsevier Ltd.

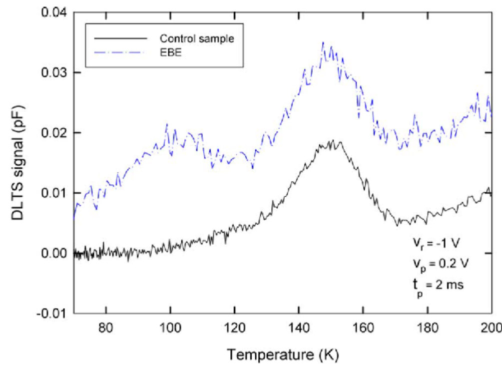

Fig. 1. DLTS spectra comparing the control sample spectrum to the EBE spectrum.

introduce electrically active defects in measurable quantities. One sample was subjected to EBE while another sample was used as a reference. Current-voltage characteristics were performed in order to verify the suitability of the Schottky contact for deep level transient spectroscopy (DLTS) measurements. Conventional DLTS was then employed to measure the defects before and after exposure. The DLTS measurements were performed by a computer controlled system with a closed cycle helium cryostat and a 1 MHz Boonton 7200 capacitance meter.

3. Results and discussion

The DLTS spectra of the control and EBE samples are compared in Fig. 1. The DLTS spectra were measured using a reverse bias voltage of −1 V, a filing pulse height of 0.2 V and a filing pulse width of 2 ms. The reverse bias voltage was relatively small in order to probe the space charge region close to the surface of the metal-semiconductor contact. The rate window of the measured spectra was 80 s^{-1}. A comparison is made for a temperature range of 70 and 200 K as the spectra beyond these temperatures are the same. The DLTS spectrum shows that a defect is induced at a peak temperature of 100 K after EBE. The Arrhenius plot of the defects before and after exposure is shown in Fig. 2. Table 1 compares the EBE induced defect to other irradiation induced defects. The activation energy of the EBE induced defect and the apparent capture cross section are 0.12 eV and 8.0×10^{-16} cm^2 respectively. These parameters were extracted from a multirate window scan of the DLTS spectra.

The EBE induced defect is a bulk defect in the semiconductor near the surface of the metal-semiconductor interface. The distinction

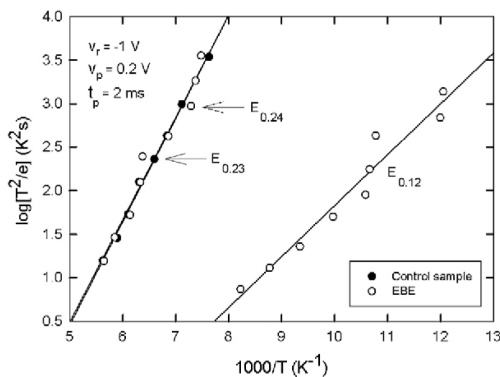

Fig. 2. Arrhenius plots of Ni/Au diodes which were resistively evaporated on GaN. One sample was subjected to EBE while the other was used as a control sample.

between bulk traps and interface states is that the peak maximum of the DLTS signal of bulk traps does not move or moves towards lower temperatures whereas the peak maximum of interface states moves towards higher temperatures with increasing pulse height. In our study we observed that the peak maximum of the DLTS signal does not move with respect to the temperature when we increase the pulse height by changing the reverse bias voltage.

The activation energy of the EBE defect is similar to the activation energy of the ER1 defect reported by Goodman et al. [9]. In their study they irradiated GaN with electrons and protons. Zhang *et al.* and Castaldini et al. also irradiated GaN with protons [10,11]. The activation energies of the induced defects in their studies were 0.13 and 0.12 eV respectively. The proton irradiation was done with different irradiation energies namely 1.8 MeV and 24 GeV. Umana-Membreno et al. subjected undoped *n*-type GaN to ^{60}Co gamma irradiation and also found a defect similar to the EBE induced defect [12]. The gamma irradiation induced defect had activation energy of 0.13 eV. In their study, Umana-Membreno *et al.* also observed that the defect is significantly insensitive to fluence rate. This observation was comparable to gamma particle radiation investigated by Shmidt et al. [13]. The concentration of the defect induced by EBE was not affected by exposure time beyond 50 min. The sample was first exposed to electron beam conditions for 50 min. After exposure for an additional 30 min, the concentration of the defect remained relatively unchanged. It seems that saturation is reached after 50 min exposure. We speculate that the defect might be a complex between a mobile irradiation induced defect and an immobile as-grown defect, that might not be electrically active. One would therefore expect the concentration of the complex to increase until all as-grown defects have reacted, after which the concentration will level off. The concentration of the EBE induced defect was 2.6×10^{13} cm^{-3}.

A comparison of different metallisation techniques is tabulated in Table 2. The activation energy of the EBE induced defect is smaller than the activation energies of the defects induced by electron beam and sputter deposition. These two deposition techniques induced defects with activation energies of 0.19 eV [14] and 0.22 eV [15] respectively. Other defects induced by these two methods had higher activation energies.

In the electron beam deposition (EBD) study, Auret et al. speculated that some ionised atoms, possibly from the evaporated metal and residual gasses in the vacuum chamber, reached the surface of the semiconductor with sufficient energy to damage the sample [14]. During the EBE method, W was heated but not deposited onto the semiconductor. This produced the conditions under which the radiation induced damage occurred for long enough to ensure that a measureable concentration of defects was formed before a metal layer was deposited (effectively screening the semiconductor from further damage). Since metals were evaporated during EBD, the ionised atoms from these metals and other atoms with which subsequent collisions occurred, could gain sufficient energy to cause more damage on the EBD samples than the EBE samples.

The as grown defect increased in concentration by approximately a factor of 2 from 2.4×10^{13} cm^{-3} to 4.5×10^{13} cm^{-3}. The activation energies of the control and EBE sample of this defect are 0.23 and 0.24 eV respectively. This defect has been reported by various authors. It has been observed in GaN grown with different methods such as HVPE, MOVPE, ELOG, and RMBE [16].

Other DLTS studies have been performed on different semiconductor materials using the EBE method. Danga et al. reported that in Si, the defect induced was similar to defects induced by proton and alpha particle irradiation [17]. In 4H-SiC, Omotoso *et al.* observed that the defects induced by EBE are similar to those induced by alpha particle and high-energy electron irradiation [18]. Coelho et al. reported that to the best of their knowledge, none of the EBE induced defects in Ge had been reported before [8]. It is interesting to note that apart from Ge, the defects induced by EBE in other semiconductor materials are similar to

Table 1
Comparison of defects induced by the EBE technique and different irradiation methods.

Process	Defect label	Defect level (eV)	Apparent capture cross section (cm^2)	Peak Temperature (K)	Similar defects/Ref.
Electron beam exposure	$E_{0.12}$	0.12	8.0×10^{-16}	100	
0.2–2.4 MeV electron irradiation	ER1	0.13	–	98	[9]
2.0 MeV proton irradiation	ER1	0.13	–	98	[9]
1.8 MeV proton irradiation	–	0.13	1×10^{-17}	100	[10]
24 GeV proton irradiation	T1	0.12	1.3×10^{-17}		[11]
^{60}Co gamma irradiation	G_A	0.13	4.9×10^{-18}		[12]

Table 2
Comparison between the defect induced by the EBE and different metallisation techniques.

Process	Defect label	Defect level (eV)	Apparent capture cross section (cm^2)	Peak Temperature (K)	Similar defects/ Ref.
Electron beam exposure	$E_{0.12}$	0.12	8.0×10^{-16}	100	
Electron beam deposition	Ee1	0.19	1.2×10^{-15}	120	[14]
Sputter deposition	ES1	0.22	6.5×10^{-16}	120	[15]

defects induced by different irradiation methods. This is also consistent with the findings performed on GaN in this study.

4. Conclusion

Electron beam exposure induced a defect with activation energy of 0.12 eV in GaN. This defect is similar to other defects induced by different irradiation methods including electron, proton and gamma particle irradiation. The activation energy of the EBE induced defect was much lower than other defects induced by different metal deposition techniques. EBE can thus be another method of introducing the 0.12 eV defect. The as grown defects in the sample were not significantly affected by EBE. A comparison of different semiconductors subjected to EBE indicates that, except for Ge, the EBE induced defects are similar to other irradiation induced defects.

Acknowledgements

The authors would like to acknowledge the South African National Research Foundation (NRF) (Grant No. 99861) for the financial support during this study.

References

[1] H.K. Cho, C.S. Kim, C.-H. Hong, J. Appl. Phys. 94 (2003) 1486.
[2] Z.-Q. Fang, D.C. Look, W. Kim, Z. Fan, A. Botchkarev, H. Morkoc, Appl. Phys. Lett. 72 (1998) 2277.
[3] P. Hacke, A. Maekawa, N. Koide, K. Hiramatsu, N. Sawaki, Jpn. J. Appl. Phys. 33 (1994) 6443.
[4] D.C. Look, Z.-Q. Fang, B. Claflin, J. Cryst. Growth 281 (2005) 143.
[5] In-Hwan Lee, A.Y. Polyakov, N.B. Smirnov, A.V. Govorkov, A.V. Markov, S.J. Pearton, Thin Solid Films 516 (2008) 2035.
[6] W. Nakamura, Y. Tokuda, H. Ueda, T. Kachi, Physica B 376–377 (2006) 516.
[7] F.D. Auret, S.A. Goodman, G. Myburg, S.E. Mohney, J.M. de Lucca, Mater. Sci. Eng. B82 (2001) 102.
[8] S.M.M. Coelho, F.D. Auret, P.J. Janse van Rensburg, J.M. Nel, J. Appl. Phys. 114 (2013) 173708.
[9] S.A. Goodman, F.D. Auret, F.K. Koschnick, J.M. Spaeth, B. Beaumont, P. Gibart, Mater. Sci. Eng. B71 (2000) 100.
[10] Z. Zhang, E. Farzana, W.Y. Sun, J. Chen, E.X. Zhang, D.M. Fleetwood, R.D. Schrimpf, B. McSkimming, E.C.H. Kyle, J.S. Speck, A.R. Arehart, S.A. Ringel, J. Appl. Phys. 118 (2015) 155701.
[11] A. Castaldini, A. Cavallini, L. Polenta, J. Phys.: Condens. Matter 12 (2000) 10161.
[12] G.A. Umana-Membreno, J.M. Dell, T.P. Hessler, B.D. Nener, G. Parish, L. Faraone, U.K. Mishra, Appl. Phys. Lett. 80 (2002) 4354.
[13] N.M. Shmidt, D.V. Davydov, V.V. Emtsev, I.L. Krestnikov, A.A. Lebedev, W.V. Lundin, D.S. Poloskin, A.V. Sakharov, A.S. Usikov, A.V. Osinsky, Phys. Stat. Sol. (b) 216 (1999) 533.
[14] F.D. Auret, S.A. Goodman, G. Myburg, F.K. Koschnick, J.M. Spaeth, B. Beaumont, P. Gibart, Physica B 273–274 (1999) 84.
[15] F.D. Auret, W.E. Meyer, S.A. Goodman, F.K. Koschnick, J.M. Spaeth, B. Beaumont, P. Gibart, Physica B 273–274 (1999) 92.
[16] F.D. Auret, S.A. Goodman, G. Myburg, W.E. Meyer, J.M. Spaeth, P. Gibart, B. Beaumont, Radiat. Eff. Defects Solids 156 (2001) 255.
[17] H.T. Danga, F.D. Auret, S.M.M. Coelho, M. Diale, Physica B 480 (2016) 206.
[18] E. Omotoso, W.E. Meyer, F.D. Auret, S.M.M. Coelho, P.N.M. Ngoepe, Solid State Phenom. 242 (2016) 427.

5.3. Cs ION IMPLANTATION

Paper 2: Characterisation of Cs ion implanted GaN by DLTS

The study of the effects of implantation of ions in semiconductors gives a clue of the nature of defects, which are in these semiconductors. Ion implantation has been used for, amongst other applications, device isolation. This section is a study of defects induced in GaN after Cs ion implantation. The implantation energy was 360 keV with a fluence of up to 10^{11} cm^{-2}. The implantation was performed at room temperature. After Cs ion implantation, the sample was characterised using DLTS. A defect level with an energy level of 0.19 eV and an apparent capture cross section of 1.1×10^{-15} cm^2 was observed. In this study, a comparison was made to various processing methods used in other studies, which obtained defects with similar defect energy. These methods included electron beam deposition, rare earth element implantation, and proton and electron implantation.

Table 5.2 below which was not included in the paper compares the quality of the diodes before and after irradiation. The current voltage properties of the fabricated diode deteriorated after Cs ion implantation of the GaN sample. The rectifying properties of the diodes were however still in a good enough condition to perform DLTS measurements.

Table 5.2 Electrical properties of the control and Cs ion implanted GaN samples, which were extracted from current voltage and capacitance voltage measurements.

	Control	Cs ion implantation
Current-voltage		
Schottky Barrier Height, ϕ_B (eV)	0.97	0.57
Ideality factor, n	2.14	3.38
Series resistance, R_s (Ω)	100	26
Current at -2 V (A)	4.8×10^{-14}	9.1×10^{-5}
Capacitance-voltage		
Schottky Barrier Height, ϕ_B (eV)	0.86	0.91
Built-in voltage, V_{bi} (V)	0.699	0.725
Free carrier concentration, N_d (cm^{-3})	1.4×10^{17}	5.5×10^{16}

Publication details

P.N.M. Ngoepe, W.E. Meyer, F.D. Auret, E. Omotoso, T.T. Hlatshwayo, and M. Diale, "Characterisation of Cs ion implanted GaN by DLTS", Physica B **535** (2018) 96-98. http://dx.doi.org/10.1016/j.physb.2017.06.064

Physica B 535 (2018) 96–98

Contents lists available at ScienceDirect

Physica B

journal homepage: www.elsevier.com/locate/physb

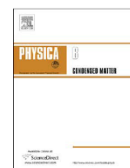

Characterisation of Cs ion implanted GaN by DLTS

P.N.M. Ngoepe*, W.E. Meyer, F.D. Auret, E. Omotoso, T.T. Hlatshwayo, M. Diale

Physics Department, University of Pretoria, Pretoria, South Africa

ARTICLE INFO

Keywords:
GaN
Cs implantation
Defect
DLTS

ABSTRACT

Deep level transient spectroscopy (DLTS) was used to characterise Cs implanted GaN grown by hydride vapour phase epitaxy (HVPE). This implantation was done at room temperature using energy of 360 keV to a fluence of 10^{-11} cm^{-2}. A defect with activation energy of 0.19 eV below the conduction band and an apparent capture cross section of 1.1×10^{-15} cm^2 was induced. This defect has previously been observed after rare earth element (Eu, Er and Pr) implantation. It has also been reported after electron, proton and He ion implantation.

1. Introduction

Gallium nitride (GaN) is a binary semiconductor with a direct bandgap of 3.4 eV. GaN based devices have promising prospects in military, satellite and commercial applications. This is due to the optical, electronic and mechanical properties of GaN. Devices which can be fabricated from GaN include both light detecting and emitting devices, such as solar-blind detectors and light emitting diodes (LED's) respectively [1].

An important mechanical characteristic of GaN is its radiation hardness. It has a strong resistance to radiation damage due to its high bond strength. The density of GaN is 6.10 g/cm^3 and the displacement energies of gallium and nitrogen are 19 and 22 eV respectively [2]. This makes GaN more radiation resistant than GaAs for instance. Moreover, the radiation hardness of GaN makes it more suitable for higher irradiation doses as the amorphisation threshold is much higher. Ion implantation has been employed in various studies for different purposes in GaN. It has been utilised for doping using rare earth elements and transition metals [3,4] and for processing GaN-based devices such as LED's and field effect transistors [1]. Material damage caused by ion implantation and the effect of this damage on material properties have also been investigated by Ronning et al. [5].

Of particular interest is the growing research related to ion irradiation of GaN and the effect of the induced defects on its electrical properties. These defects can have a detrimental or beneficial effect on the fabricated device depending on its application. Defects induced in GaN by different particles such as protons, electrons, and numerous ions have been studied by various authors. A variety of ions have been implanted in GaN at various energies, including the several hundred keV range, in order to study the effect on its electrical and optical properties [3,4]. To the best of our knowledge no studies have been done on Cs ion implanted GaN.

Cs is an alkali metal that has been utilised in photo sensitive applications. It has been used in the synthesis of highly spectrally sensitive photocathodes to produce GaN based photodetectors. Kampen et al. [6] are among the few authors who have investigated the adsorption of Cs on *n*-GaN [6]. Also, Ji et al. used density functional theory (DFT) calculations to investigate the effects of Ga and N shallow vacancy defects on the adsorption of Cs on GaN [7]. In this study GaN was implanted with Cs ions with the view of studying the defects induced by this implantation process. The electrically active defects were measured *ex situ* using deep level transient spectroscopy (DLTS).

2. Experimental

In this study Si doped GaN grown by hydride vapour phase epitaxy (HVPE) was utilised. The samples had a free carrier density of 1×10^{17} cm^{-3}. The cleaning of the samples involved degreasing and etching. Firstly, the samples were submerged for 3 min in boiling TCE and for another 3 min in boiling isopropanol. They were then rinsed 3 times in de-ionised water. The samples were etched in boiling aqua regia for 10 min. This was followed by another etching process whereby the samples were dipped in $HCl:H_2O$ solution for 60 s. Between each of the etching steps de-ionised water was used to rinse the samples. The samples were then blown dry with nitrogen prior to metal deposition. An ohmic contact consisting of Ti (150 Å)/ Al (2200 Å) / Ni (450 Å) / Au (550 Å) was then deposited onto the GaN using an electron beam system. The samples were later annealed at 500 °C in a furnace for 5 min in an argon ambient with the argon gas flowing at 2 l per minute. Annealing was done in order to minimise contact resistance. Schottky diodes with a diameter of 0.6 mm were

* Corresponding author.
E-mail address: phuti.ngoepe@up.ac.za (P.N.M. Ngoepe).

http://dx.doi.org/10.1016/j.physb.2017.06.064
Received 21 April 2017; Received in revised form 19 June 2017; Accepted 22 June 2017
Available online 23 June 2017
0921-4526/ © 2017 Elsevier B.V. All rights reserved.

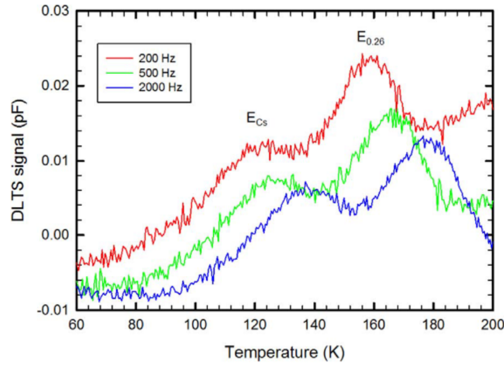

Fig. 1. DLTS signals of Cs implanted GaN measured at different rate windows.

then evaporated through a mask onto the GaN samples using a resistive evaporation system. The Schottky contact consisted of Ni (200 Å) as the first layer and Au (600 Å) as a cap layer. The characterisation of the samples involved measuring the current-voltage (*I-V*) response to assess whether the diodes were good enough to characterise electrically active defects using DLTS. The defect characterisation was performed in the 80–200 K temperature range. The measurements were taken before and after processing the samples. The samples were implanted with Cs ions at 360 keV to a fluence of 10^{11} cm^{-2} at room temperature. To determine the DLTS signature, the spectra were measured at different emission rates ranging from 5 to 2000 s^{-1}. The DLTS measurements were performed by a computer controlled system with a closed cycle helium cryostat and a 1 MHz Boonton 7200 capacitance meter.

3. Results and discussion

The DLTS spectra of Cs implanted GaN are shown in Fig. 1. The measurements were performed at a reverse bias voltage of −1 V, a filling pulse amplitude of 0.5 V and a filling pulse width of 1 ms. The DLTS signature, namely the defect energy level and apparent capture cross section, was determined from the Arrhenius plots shown in Fig. 2. The defect with activation energy of 0.26 eV is a common as grown defect in GaN. The calculated apparent capture cross section was 9.4 × 10^{-16} cm^2. This defect was observed by Hacke et al. in HVPE grown GaN [8].

A new defect, which we have labelled E_{Cs}, was observed after Cs ion implantation at peak temperature of 119 K using a rate window of 80 s^{-1}. This defect has an energy level of 0.19 eV and an apparent capture cross section of 1.1 × 10^{-15} cm^2.

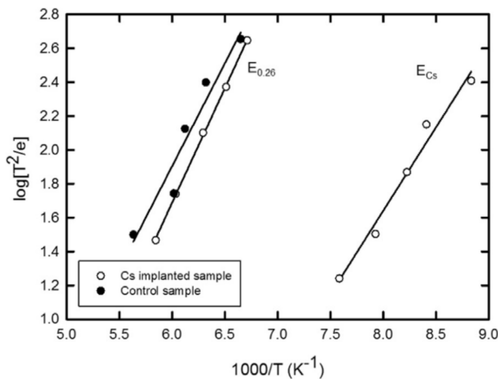

Fig. 2. Arrhenius plots of Ni/Au diodes which were resistively evaporated on GaN. One sample was subjected to Cs implantation while the other was used as a control sample.

Table 1 contains defects which are similar to this defect. Auret et al. reported a defect with activation energy of 0.19 eV below the conduction band [9]. This defect was induced after the electron beam deposition of a Schottky contact consisting of Ru. They compared their findings to those of Fang et al. [10] and Auret et al. [11]. The former obtained a defect with activation energy of 0.18 eV after electron irradiation while the latter observed a defect with activation energy of 0.20 eV after both proton and He ion irradiation. In their study, Fang et al. noted that should the capture cross section that they obtained be temperature dependent, the 0.18 eV defect could be compared to the E_C − 0.07 eV defect observed by Look et al. [12]. They used Hall measurements to study electron irradiated GaN. In their investigation they attributed the defect they had characterised to a nitrogen vacancy.

Janse van Rensburg et al. also observed a defect with activation energy of 0.19 eV [3]. They implanted GaN with Xe and Eu ions. Song et al. implanted GaN with 2 rare earth elements, namely Er and Pr [13]. They also obtained defects for both the Er and Pr implanted GaN with activation energy of 0.19 eV. They then compared their results to those obtain by Filhol et al. who used density functional theory (DFT) calculations to investigate doping of GaN with rare earth elements (Eu, Er, and Tm) [14]. Janse van Rensburg et al. also compared their results to those obtained by Filhol et al. By introducing rare earth dopants to GaN, Filhol et al. concluded from their studies that rare earth substitutional Ga sites, RE_{Ga}, bound more strongly with a nitrogen vacancy. Since in their investigation Janse van Rensburg et al. compared the implantation of Xe to the implantation of Eu, the latter being a rare earth element, and found the same activation energies for both defects, they concluded that the 0.19 eV defect is not just a rare earth element related defect. This defect, they added, was more of a general structure in which the Ga could have been substituted by another implanted species to form a defect complex with the nitrogen vacancy.

From transport of ions in matter (TRIM) calculations [15], the penetration depth of 360 keV Cs ions in GaN is 73 nm with a straggle of 30 nm and a fluence of 1 × 10^{11} cm^{-2} leading to a peak concentration of about 1 × 10^{16} cm^{-3} Cs atoms. From depletion width calculations, the depletion depth was 80 nm during the pulse bias and 160 nm during the quiescent reverse bias conditions. It is therefore expected that the DLTS measurements would probe a region with significant Cs concentration and that any electrically active defects directly related to Cs would be detected by DLTS. Since no unique DLTS peaks were observed, it is concluded that no Cs related peaks were observed, and that Cs probably does not lead to electrically active defects in GaN.

4. Conclusion

Cs ion implantation in GaN at room temperature induces a defect with energy level of 0.19 eV below the conduction band. Defects with this energy level have been observed using different processing methods including the deposition of Ru using electron beam deposition and Xe and Eu ion implantation. Other rare earth elements which have induced this defect after implantation include Er and Pr. This defect has also been observed after proton, He and electron irradiation. In comparison to defects obtained in other studies, it has become apparent that the E_{Cs} defect is not just a defect related to the implantation of Cs ions. It is therefore not an intrinsic defect but a defect related to irradiation effects.

Acknowledgements

This work is based on research supported by the National Research Foundation of South Africa (Grant No. 98961). Opinions, findings and conclusions or recommendations are the authors, and the NRF accepts no liability whatsoever in this regard.

Table 1
Comparison of defects with similar activation energies.

Process	Defect label	Defect level (eV)	Apparent capture cross section (cm^2)	Peak temperature (K)	Reference
Cs implantation	E_{Cs}	0.19	1.1×10^{-15}	119	This study
Electron beam deposition	Ee1	0.19	1.2×10^{-15}	120	[9]
Xe implantation	E_{Xe1}	0.19	1.2×10^{-15}	–	[3]
Eu implantation	E_{Eu1}	0.19	2.6×10^{-16}	–	[3]
Er implantation	Er15/900	0.19	5.6×10^{-16}	–	[13]
Pr implantation	Pr15/1050	0.19	5.6×10^{-16}	–	[13]
Proton and He ion irradiation	ER3	0.20	4.0×10^{-15}	121	[11]
Electron irradiation	–	0.18	2.5×10^{-15}	118	[10]

References

[1] S.J. Pearton, F. Ren, E. Patrick, M.E. Law, A.Y. Polyakov, Review — Ionizing radiation damage effects on GaN devices, ECS J. Solid State Sci. Technol. 5 (2016) Q35–Q60. http://dx.doi.org/10.1149/2.0251602jss.

[2] A.Y. Polyakov, S.J. Pearton, P. Frenzer, F. Ren, L. Liu, J. Kim, Radiation effects in GaN materials and devices, J. Mater. Chem. C 1 (2013) 877–887. http://dx.doi.org/10.1039/c2tc00039c.

[3] P.J. Janse Van Rensburg, F.D. Auret, V.S. Matias, A. Vantomme, Electrical characterization of rare-earth implanted GaN, Phys. B 404 (2009) 4411–4414. http://dx.doi.org/10.1016/j.physb.2009.09.018.

[4] A.Y. Polyakov, N.B. Smirnov, A.V. Govorkov, N.V. Pashkova, A.A. Shlensky, S.J. Pearton, M.E. Overberg, C.R. Abernathy, J.M. Zavada, R.G. Wilson, Electrical and optical properties of Cr and Fe implanted n-GaN, J. Appl. Phys. 93 (2003) 5388. http://dx.doi.org/10.1063/1.1565677.

[5] C. Ronning, E.P. Carlson, R.F. Davis, Ion implantation into gallium nitride, Phys. Rep. 351 (2001) 349–385. http://dx.doi.org/10.1016/S0370-1573(00)00142-3.

[6] T.U. Kampen, M. Eyckeler, W. Mönch, Electronic properties of cesium-covered GaN (0001) surfaces, Appl. Surf. Sci. 123–124 (1998) 28–32.

[7] Y. Ji, Y. Du, M. Wang, Influence of vacancy defect on surface feature and adsorption of Cs on GaN (0001) surface, Sci. World J. (2014) 1–7.

[8] P. Hacke, T. Detchprohm, K. Hiramatsu, N. Sawaki, K. Tadatomo, K. Miyake, Analysis of deep levels in n-type GaN by transient capacitance methods, J. Appl. Phys. 76 (1994) 304–309.

[9] F.D. Auret, S.A. Goodman, G. Myburg, F.K. Koschnick, J.-M. Spaeth, B. Beaumont, P. Gibart, Defect introduction in epitaxially grown n-GAN during electron beam deposition of Ru schottky contacts, Phys. B 273–274 (1999) 84–87. http://dx.doi.org/10.1016/S0921-4526(99)00412-3.

[10] Z. Fang, J.W. Hemsky, D.C. Look, M.P. Mack, Electron-irradiation-induced deep level in n -type GaN, Appl. Phys. Lett. 72 (1998) 448–449.

[11] F.D. Auret, S.A. Goodman, F.K. Koschnick, J.-M. Spaeth, B. Beaumont, P. Gibart, Proton bombardment-induced electron traps in epitaxially grown n-GaN, Appl. Phys. Lett. 74 (1999) 407–409.

[12] D.C. Look, D.C. Reynolds, J.W. Hemsky, J.R. Sizelove, R.L. Jones, R.J. Molnar, Defect donor and acceptor in GaN, Phys. Rev. Lett. 79 (1997) 2273–2276.

[13] S.F. Song, W.D. Chen, C. Zhang, L. Bian, C.C. Hsu, L.W. Lu, Y.H. Zhang, J. Zhu, Electrical characterization of Er- and Pr-implanted GaN films, Appl. Phys. Lett. 86 (2005) 152111. http://dx.doi.org/10.1063/1.1901828.

[14] J.-S. Filhol, R. Jones, M.J. Shaw, P.R. Briddon, Structure and electrical activity of rare-earth dopants in GaN, Appl. Phys. Lett. 84 (2004) 2841–2843. http://dx.doi.org/10.1063/1.1710710.

[15] J.F. Ziegler, M.D. Ziegler, J.P. Biersack, SRIM – The stopping and range of ions in matter (2010), Nucl. Instrum. Methods B 268 (2010) 1818–1823. http://dx.doi.org/10.1016/j.nimb.2010.02.091.

5.4. Xe ION IRRADIATION

Paper 3: Deep level transient spectroscopy characterisation of Xe irradiated GaN

GaN is a radiation hard semiconductor. This is one of the properties that make it suitable for, amongst others, space applications. The bombardment of a device by particles can affect its operation. It thus becomes important to study the effect of such particles on the semiconductors on which the devices are based. In this study, swift heavy ions were irradiated into GaN with the intention of studying the defect levels induced in them. The irradiation energy of the ions was 167 MeV with fluence of up to 10^{10} cm^{-2}. The current-voltage characteristics before and after irradiation were compared. Deep level transient spectroscopy was then used to characterise the defect levels induced by the irradiation. The defects were then compared to those reported by other studies. The processing methods in other studies included thermal annealing and In doping. Some authors also obtained similar defect by modelling. SRIM calculations were also performed to calculate the penetration depth of the Xe ions.

Table 5.3 summarizes the quality of the Schottky diodes before and after irradiation. The current voltage properties of the fabricated diode deteriorated after Xe ion irradiation of the GaN sample. The rectifying properties of the diodes were however still in a good enough condition to perform DLTS measurements.

Fig.5.1 contains the DLTS spectra for the un-irradiated and Xe ion irradiated GaN. The DLTS spectra have been included in this section to highlight the 0.58 eV defect, which was not observed after Xe irradiation. This defect, it seems, was suppressed by Xe irradiation.

Table 5.3 Electrical properties of the un-irradiated and Xe ion irradiated GaN samples, which were extracted from current voltage and capacitance voltage measurements.

	Un-irradiated	Xe ion irradiation
Current-voltage		
Schottky Barrier Height, ϕ_B (eV)	1.15	0.507
Ideality factor, n	1.84	2.03
Series resistance, R_s (Ω)	156	44
Current at -2 V (A)	8.0×10^{-15}	1.9×10^{-4}
Capacitance-voltage		
Schottky Barrier Height, ϕ_B (eV)	0.93	1.1
Built-in voltage, V_{bi} (V)	0.771	0.899
Free carrier concentration, N_d (cm^{-3})	1.3×10^{17}	3.3×10^{16}

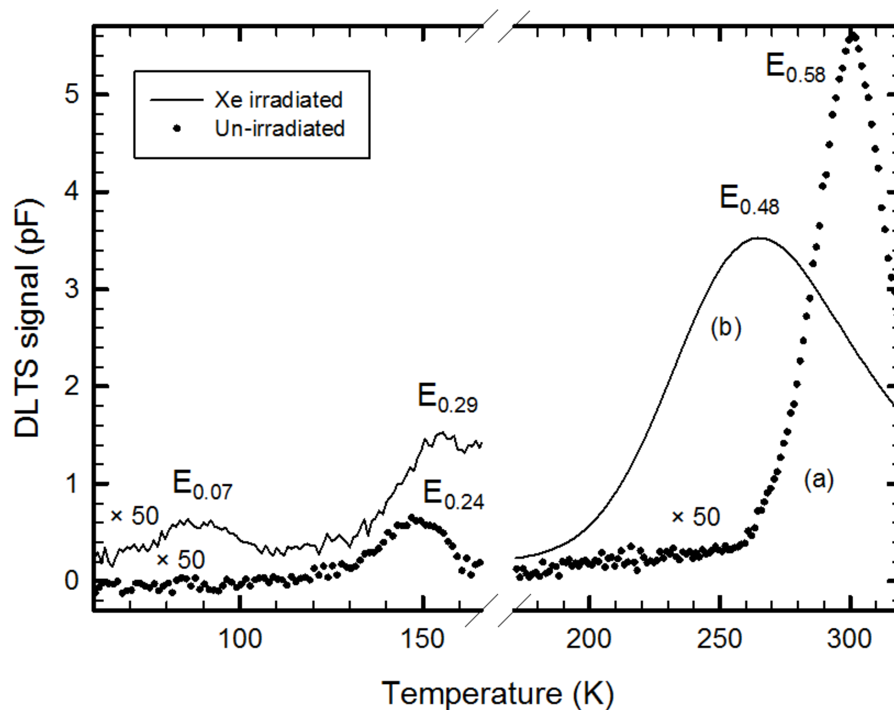

Fig. 5.1 DLTS spectra of un-irradiated and Xe irradiated GaN. Where indicated, the spectra have been increased by a factor of 50 for clarity. The spectra were recorded using a reverse bias of -2 V, filling pulse of 0V, filling pulse width of 2ms and emission rate window of 80 s^{-1}.

Publication details

P.N.M. Ngoepe, W.E. Meyer, F.D. Auret, E. Omotoso, T.T. Hlatshwayo, V.A. Skuratov, and M. Diale, "Deep level transient spectroscopy characterisation of Xe irradiated GaN", Nucl. Instrum. Meth. B **409** (2017) 69-71. http://dx.doi.org/10.1016/j.nimb.2017.05.032

Nuclear Instruments and Methods in Physics Research B 409 (2017) 69–71

Contents lists available at ScienceDirect

Nuclear Instruments and Methods in Physics Research B

journal homepage: www.elsevier.com/locate/nimb

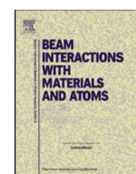

Deep level transient spectroscopy characterisation of Xe irradiated GaN

P.N.M. Ngoepe [a,*], W.E. Meyer [a], F.D. Auret [a], E. Omotoso [a], T.T. Hlatshwayo [a], V.A. Skuratov [b], M. Diale [a]

[a] Department of Physics, University of Pretoria, Private Bag X20, Hatfield 0028, South Africa
[b] Joint Institute for Nuclear Research, Joliot-Curie 6, 141980 Dubna, Moscow Region, Russia

ARTICLE INFO

Article history:
Received 10 December 2016
Received in revised form 15 May 2017
Accepted 15 May 2017
Available online 2 June 2017

Keywords:
DLTS
GaN
Defects
SHI irradiation

ABSTRACT

In this study *n*-type GaN was subjected to irradiation. This irradiation was performed by Xe^{+26} of 167 MeV to a fluence of 10^{10} cm $^{-2}$ at room temperature. Irradiation resulted in an increase in the reverse current by about 10 orders of magnitude. This has been explained by the generation/recombination centers formed during irradiation. Using the deep level transient spectroscopy (DLTS) technique, two defects were identified after irradiation with activation energies of 0.07 and 0.48 eV below the conduction band. These defects have similar signatures to other defects observed after electron irradiation, thermal annealing and In doping.

© 2017 Published by Elsevier B.V.

1. Introduction

Gallium nitride (GaN) is a wide direct bandgap semiconductor with a hexagonal wurzite crystal structure. GaN based material systems have been studied for various optoelectronic applications. These include absorbing devices such as detectors and emitting devices such as light emitting diodes (LED's) [1]. The bandgap of GaN based materials can be varied from 1.9 eV (InN) to 6.3 eV (AlN). This property makes these materials good candidates for fabrication of devices in a wide spectral range. In addition, the low thermal carrier generation rates and high breakdown fields of GaN make it a good candidate for high temperature and high power electronics.

GaN is a radiation hard material, thus devices based on this material can operate under chemically harsh conditions. The displacement energies of gallium and nitrogen in GaN are 19 and 22 eV respectively [2,3]. Defects can be induced in materials by ion bombardment in outer space or by nuclear applications. Therefore, it is important to simulate similar conditions in a controlled environment in order to understand the defects formed in these materials.

The irradiation of protons, electrons and various ions has been performed on GaN with the aim of understanding defects induced in these materials [4–8]. In particular, defects induced in GaN after swift heavy ion (SHI) irradiation have been studied using various techniques [9,10]. Ion irradiation has the advantage that uniform spatial tailoring can be readily achieved. The effects of ion beams on materials are dependent on a number of factors including ion energy, ion species, fluence and the irradiation temperature [10,11]. It is therefore important to understand the effect of these parameters on the properties of semiconductor materials. Irradiation on GaN by 92 MeV Xe ions has previously been studied [9]. In this study the deep level transient spectroscopy (DLTS) technique was used to investigate defects induced in GaN by 167 MeV Xe ion irradiation.

2. Experimental

Hydride vapour phase epitaxy (HVPE) grown GaN was used in this study. The *n*-type conductivity of GaN was formed by Si doping. The GaN samples were prepared using a well-established cleaning recipe. The samples were first degreased in boiling trichloroethylene and then isopropanol for 3 min. Thereafter, they were etched in boiling aqua regia for 10 min. Nitrogen was lastly used to blow dry the samples. Ohmic contacts consisting of Ti (150 Å)/Al (2200 Å)/Ni (450 Å)/Au (550 Å) [12] were evaporated onto the samples using an electron beam deposition system. The samples were shielded from the trajectory of electrons from the e-beam gun system to minimize the impact of these electrons on the material. The samples were then annealed for 5 min in an argon ambient. Ni (200 Å)/Au (600 Å) Schottky contact with a diameter of 0.6 mm was deposited using a resistive deposition system. This deposition system is less likely to induce defects in measurable quantities as no energetic particles and high accelerating potentials are present when compared to an e-beam system. The

* Corresponding author.
E-mail address: phuti.ngoepe@up.ac.za (P.N.M. Ngoepe).

http://dx.doi.org/10.1016/j.nimb.2017.05.032
0168-583X/© 2017 Published by Elsevier B.V.

samples were then irradiated with Xe^{+26} ions of 167 MeV to a fluence of 10^{10} cm^{-2} at room temperature. Current-voltage (*I-V*) measurements of the samples were performed, at room temperature, in order to determine the quality of the Schottky diode. The *I-V* characteristics indicated that the diodes were suitable for DLTS measurements. The DLTS system was used to electrically characterize the defects in the samples. The DLTS "signature", which consists of the defect energy level and the apparent capture cross section, was determined from DLTS spectra measured at different rate windows. The measured rate windows varied from 5 to 2000 s^{-1}. The DLTS spectra were acquired at a reverse bias voltage of −2 V, filling pulse amplitude of 0 V, and a filing pulse width of 2 ms. A SRIM code was used to estimate the depth of the irradiated ions, and the nuclear and electronic stopping loss [13].

3. Results and discussion

Fig. 1 compares the un-irradiated and Xe irradiated *I-V* characteristics of GaN based Schottky diodes. There was an increase in the reverse leakage current of the diodes after Xe irradiation. The reverse bias leakage current of the diode at −2 V increased from 1.1×10^{-14} to 1.9×10^{-4} A. This signaled a degradation of the diode after irradiation. Defect traps in the depletion region may serve as generation/ recombination centers, causing high leakage currents.

Fig. 2 is a comparison of the DLTS spectra of the un-irradiated and Xe irradiated GaN. The temperature range of the measurement was 60 to 290 K. Prior to Xe irradiation there were 2 as-grown defects which have been widely reported, with energy levels at 0.24 and 0.58 eV below the conduction band. These have apparent capture cross sections of 1.9×10^{-16} and 1.2×10^{-15} cm^2, respectively. These defects are growth related and have been reported for different growth techniques such as HVPE, metal-organic vapour phase epitaxy (MOVPE) and reactive molecular beam epitaxy (RMBE) and epitaxial lateral overgrowth (ELO) MOVPE [14].

Table 1 shows a comparison of the results obtained in this and other studies. The peak temperatures of the defects obtained in this study, which are indicated in the table, were measured at an emission rate of 80 s^{-1}. Two new defects observed after Xe irradiation are indicated by the Arrhenius plots in Fig. 3. The energy levels of these defects were 0.07 and 0.48 eV below the conduction band. The 0.07 eV defect has an apparent capture cross section of 5.1×10^{-20} cm^2. This defect is similar to those reported by Goodman et al. and Polenta et al. [15,16]. They both reported an activation energy of 0.06 eV and an apparent capture cross section of 2×10^{-19} cm^2 and $1–3 \times 10^{-20}$ cm^2 respectively. Goodman et al. modeled the defect by simulating a DLTS spectrum whereas Polenta et al. observed it after 1 MeV electron irradiation. When the GaN sample was measured again after a couple of weeks, the 0.07 eV defect was not observed. This indicates that the defect annealed out at room temperature after some time. This implies that the defect was not stable at room temperature.

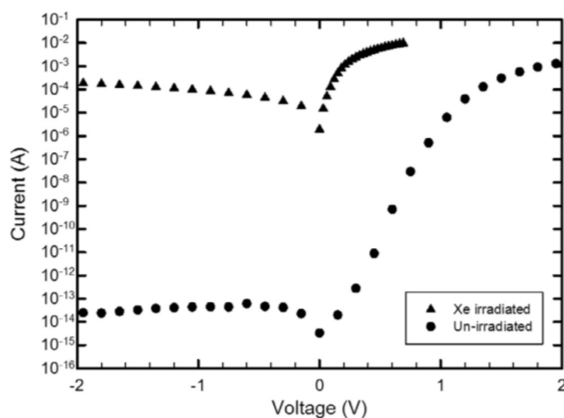

Fig. 1. *I-V* characteristics of un-irradiated and Xe irradiated GaN measured at room temperature.

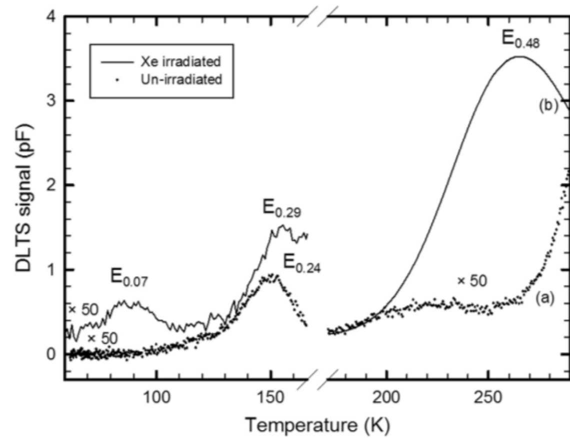

Fig. 2. DLTS spectra of un-irradiated and Xe irradiated GaN. Where indicated, the spectra have been increased by a factor of 50 for clarity. The spectra were recorded using a reverse bias of −2 V, filing pulse of 0 V, filing pulse width of 2 ms and emission rate window of 80 s^{-1}.

The defect with activation energy of 0.48 eV had an apparent capture cross section of 1.5×10^{-15} cm^2. Similar defects were obtained by different research groups. Reddy et al. [17] obtained the E2 defect with an activation energy of 0.49 eV. This defect was induced after thermal annealing. Cho et al. [18] also obtained a similar defect, also labeled E2, and obtained after In doping. There was a change in the activation energy of the 0.24 eV defect after Xe irradiation. The activation energy was increased to 0.29 eV. This change in the activation energy could be attributed to base line effects of the 0.48 eV defect. The as grown 0.58 eV defect was not observed after Xe irradiation. It seems that the defect was suppressed by Xe irradiation.

The SRIM program was utilised to determine the depth profile and the energy loss of the Xe ions in GaN. The projected range of the Xe ions was 11 μm. Since the thickness of the GaN layer is 5 μm, this implies that the ions went through the entire GaN thin film. The electron energy loss, also calculated from SRIM, was 28 keV/nm whilst the nuclear energy loss was 0.13 keV/nm [13]. It is suspected that ion tracks were formed by Xe irradiation in this study. Mansouri et al. reported track formation by 92 MeV Xe irradiation [9]. They suspected that the ion track formation threshold for electronic energy loss is 17 keV/mm.

4. Conclusion

High energy Xe irradiation has been carried out on *n*-type GaN. The reverse current of the diode measured at – 2 V increased by 10 orders of magnitude after irradiation. Two defects were observed after irradiation with activation energies 0.07 and the 0.48 eV below the conduction band. The 0.07 eV defect was similar to defects which have been modeled and measured after electron irradiation. This defect annealed out at room temperature after some time. The 0.48 eV was similar to defects which were induced

Table 1
Defects observed after different processing techniques.

Process	Defect label	Defect level (eV)	Apparent capture cross section (cm^2)	Peak Temperature (K)	Similar defects/Ref.
As grown	$E_{0.24}$	0.24	1.9×10^{-16}	150	[14]
As grown	$E_{0.58}$	0.58	1.2×10^{-15}	323	[14]
Xe irradiation	$E_{0.07}$	0.07	5.1×10^{-20}	86	[15,16]
Xe irradiation	$E_{0.48}$	0.48	1.5×10^{-15}	265	[17,18]
Modelling	ER3b	0.06	2×10^{-19}	87	[15]
Modelling	ED1	0.060	$1–3 \times 10^{-20}$	–	[16]
Thermal annealing	E2	0.49	5.43×10^{-17}	–	[17]
In doping	E2	0.50	4.94×10^{-17}	–	[18]

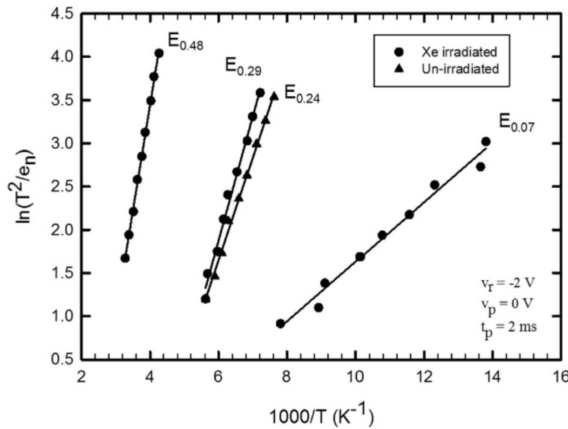

Fig. 3. Arrhenius plot of defects in resistively evaporated Ni/Au diodes on GaN. One sample was subjected to Xe irradiation while the other was a control sample.

by thermal annealing and In doping. The activation enthalpy of the as grown 0.24 eV defect increased to 0.29 eV due to baseline effects. The 0.58 eV defect was not observed after Xe irradiation.

Acknowledgements

The authors would like to acknowledge the financial assistance of the South African National Research Foundation (NRF) under grant number 98961.

References

[1] S. Nakamura, G. Fasol, The Blue Laser Diode, Springer, Berlin, 1997.
[2] A. Ionascut-Nedelcescu, C. Carlone, A. Houdayer, H.J. von Bardeleben, J.L. Cantin, S. Raymond, IEEE T. Sci. Nucl. 49 (2002) 2733.
[3] J. Nord, K. Nordlund, J. Keinonen, Phys. Rev. B 68 (2003) 184104.
[4] M. Schmidt, H. de Meyer, P.J. Janse van Rensburg, W.E. Meyer, F.D. Auret, Phys. Status Solidi B 251 (2014) 211.
[5] Z.-Q. Fang, J.W. Hemsky, D.C. Look, M.P. Mack, Appl. Phys. Lett. 72 (1998) 448.
[6] M. Senthil Kumar, G. Sonia, D. Kanjilal, R. Dhanasekaran, J. Kumar, Nucl. Instrum. Meth. B 207 (2003) 308.
[7] S. Arulkumaran, K. Ranjan, G.I. Ng, J. Kennedy, P.P. Murmu, T.N. Bhat, S. Tripathy, J. Vac. Sci. Technol., B 34 (2016) 042203.
[8] Y. Li, G.I. Ng, S. Arulkumaran, Z.H. Liu, K. Ranjan, W.C. Xing, K.S. Ang, P.P. Murmu, J. Kennedy, Phys. Status Solidi A 214 (2017) 1600555.
[9] S. Mansouri, P. Marie, C. Dufour, G. Nouet, I. Monnet, H. Lebius, Z. Benamara, Y. Al-Douri, Int. J. Nanoelectron Mater. 1 (2008) 101.
[10] S.O. Kucheyev, J.S. Williams, J. Zou, C. Jagadish, G. Li, Nucl. Instrum. Meth. B 178 (2001) 209.
[11] J. Kennedy, P.P. Murmu, E. Manikandan, S.Y. Lee, J. Alloys Compd. 616 (2014) 614.
[12] S. Ruvimov, Z. Liliental-Weber, J. Washburn, K.J. Dux-stad, E.E. Haller, Z.F. Fan, S.N. Mohammed, W. Kim, A.E. Botchkarev, H. Morkoc, Appl. Phys. Lett. 69 (1996) 1556.
[13] J.F. Ziegler, M.D. Ziegler, J.P. Biersack, Nucl. Instrum. Meth. B. 268 (2010) 1818.
[14] F.D. Auret, S.A. Goodman, G. Myburg, W.E. Meyer, J.M. Spaeth, P. Gibart, B. Beaumont, Radiat. Eff. Defects Solids 156 (2001) 255.
[15] S.A. Goodman, F.D. Auret, M.J. Legodi, B. Beaumont, P. Gibart, Appl. Phys. Lett. 78 (2001) 3815.
[16] L. Polenta, Z.Q. Fang, D.C. Look, Appl. Phys. Lett. 76 (2000) 2086.
[17] V.R. Reddy, M.S. Reddy, P.K. Rao, Microelectron. Eng. 87 (2010) 117.
[18] H.K. Cho, C.S. Kim, C.H. Hong, J. Appl. Phys. 94 (2003) 1485.

5.5. SUMMARY OF RESULTS

Table 5.4 Table consisting of all the defects which were induced in GaN in this study

Process	Defect label	Defect level (eV)	Apparent capture cross section (cm^2)	Peak Temperature (K)
Electron beam exposure	$E_{0.12}$	0.12	8.0×10^{-16}	100
Cs implantation	E_{Cs}	0.19	1.1×10^{-15}	119
Xe irradiation	$E_{0.07}$	0.07	5.1×10^{-20}	86
	$E_{0.48}$	0.48	1.5×10^{-15}	265

REFERENCES

[1] G. Myburg and F.D. Auret, Influence of the electron beam evaporation rate of Pt and the semiconductor carrier density on the characteristics of Pt/n-GaAs Schottky contacts, J. Appl. Phys. 71 (1992) 6172.

[2] F.D. Auret, S.A. Goodman, G. Myburg, S.E. Mohney, and J.M. de Lucca, Processing-induced electron traps in n-type GaN, Mat. Sci. Eng., B82 (2001) 102.

[3] F.D. Auret, S.A. Goodman, G. Myburg, F.K. Koschnick, J.-M. Spaeth, B. Beaumont, and P. Gibart, Defect introduction in epitaxially grown n-GaN during electron beam deposition of Ru Schottky contacts, Physica B 273 (1999) 84.

[4] S.M.M. Coelho, F.D. Auret, P.J. Janse van Rensburg, and J.M. Nel, Electrical characterization of defect introduced in n-Ge during electron beam deposition or exposure, J. Appl. Phys. 114 (2013) 173708

Chapter 6

Conclusions

6.1. INTRODUCTION

DLTS was successfully used to characterise electrically active defects in *n*-type GaN. This characterisation was performed after various processing techniques. In each of the studies performed, there were defects which were induced by each processing technique. The conclusions in this chapter will be discussed based on the specific study done for each processing technique. Future work is also outlined in this chapter.

6.2. ELECTRON BEAM EXPOSURE

A defect with energy level of 0.12 eV and apparent capture cross section of 8.0×10^{-16} cm^2 was observed after electron beam exposure. This defect was similar to defects induced by other processing techniques such as electron, proton and gamma particle irradiation. The electron beam exposure induced defect has a lower activation energy compared to the defects used in electron beam deposition. This is due to the energy of the impinging metal atoms

6.3. Cs ION IMPLANTATION

The implantation of Cs ions into GaN resulted in a defect with energy level of 0.19 eV and apparent capture cross section of 1.1×10^{-15} cm^2. This defect is comparable to defects found in other DLTS studies, which had ions such as Xe, Eu, Er and Pr implanted in GaN. Although the defect found in the electron beam exposure was not comparable to electron beam deposition, it was found that Cs ion implantation induced a defect with similar characteristics to a defect induced by electron beam deposition.

6.4. Xe ION IRRADIATION

The irradiation of GaN by Xe ions at energy of 167 eV caused significant damage to the semiconductor. Defects with energy levels of 0.07 and 0.48 eV and apparent capture cross section of 5.1×10^{-20} cm^2 and 1.5×10^{-15} cm^2 were induced respectively. The 0.07 eV defect was not observed after a couple of weeks. This was attributed to annealing at room temperature. The irradiation by Xe ions altered the electrical properties of the Ni/Au Schottky diodes and thus caused a significant increase in the leakage current. The reverse bias voltage was increased by 10 orders of magnitude from 1.1×10^{-14} A to 1.9×10^{-4} A. The as deposited defect with an energy level of 0.58 eV was not observed after Xe irradiation. This defect was suppressed by Xe irradiation.

6.5. SUMMARY

This study investigated defects induced in identical GaN samples by ions with greatly varying energies. Four distinct electrically active defects were observed. Since defects similar to the defects observed were found by other investigators using different ions, it is concluded the defects observed during the investigations were not specific to the ions incident on the materials, and are therefore either intrinsic defects or related to impurities. It therefore seems that the species of defect observed depended on the energy of the incident ions, showing that the energy of the incident ion had a significant effect on the species of defect created.

This information will assist in understanding defects formed in GaN during processes involving interactions with ions, ranging from processing steps during fabrication, to radiation exposure during use. This knowledge will lead to GaN devices with improved quality and reliability.

6.6. FUTURE WORK

Future work will encompass the following:

- Annealing studies to observe the evolution of the defects.
- Investigation of the influence of the defects on the electronic and optoelectronic operation of these devices at different temperatures.
- Characterising defects after varying the fluence of the implanted and irradiated ions.

- Using shorter periods of electron beam exposure to verify the time required to reach defect saturation concentration.
- Verifying the possible ion track formation by Xe^{26+} ion using TEM
- Exposure to high fluence ion implantation with the aim of studying the recrystallization of the damaged surface layer via surface morphology techniques. This recrystallization process could provide a regrown layer with novel defect structures.